VOL. 257 APRIL 1959 No. 4

American Journal of Science

Established in 1818 by Benjamin Silliman

EDITORS
JOHN RODGERS—JOSEPH T. GREGORY

ASSOCIATE EDITORS

GEORGE GAYLORD SIMPSON
NEW YORK, N. Y.

A. F. BUDDINGTON
PRINCETON, N. J.

CARL O. DUNBAR
HENRY MARGENAU
HORACE WINCHELL
EDWARD S. DEEVEY, JR.

MATT WALTON
RICHARD F. FLINT
HAROLD G. CASSIDY
G. EVELYN HUTCHINSON
NEW HAVEN, CONN.

WILMOT H. BRADLEY
WASHINGTON, D. C.

LEASON H. ADAMS
LOS ANGELES, CALIF.

HOWEL WILLIAMS
BERKELEY, CALIF.

C. R. LONGWELL
PALO ALTO, CALIF.

ADOLPH KNOPF
STANFORD, CALIF.

FREDERICK J. ALCOCK
OTTAWA, CANADA

CECIL E. TILLEY
CAMBRIDGE, ENGLAND

STERLING TOWER
YALE UNIVERSITY
NEW HAVEN, CONNECTICUT

Published 10 times a year. Ten dollars a year. One dollar twenty-five cents a copy.
Foreign, ten dollars sixty cents Canada, ten dollars thirty-five cents.

AMERICAN JOURNAL OF SCIENCE

Established in 1818 by Benjamin Silliman

THE FIRST SCIENTIFIC JOURNAL IN THE UNITED STATES

DEVOTED TO THE GEOLOGICAL SCIENCES AND TO RELATED FIELDS

Editors: JOHN RODGERS—JOSEPH T. GREGORY
Managing Editor: BETH A. BROMBERT

Entered as second-class matter at the Post Office at New Haven, Conn., under the Act of March 3, 1879. Published monthly, except July and September, at Sterling Tower, Yale University, New Haven, Conn.

Subscription rate $10 per year ($1.25 a number). Student rate $5 per year (application blanks available on request). Postage prepaid to the United States; 35 cents per year to Canada; 60 cents per year elsewhere.

The JOURNAL completed its *first* series of 50 volumes in 1845, its *second* series of 50 volumes in 1870, its *third* series of 50 volumes in 1895, its *fourth* series of 50 volumes in 1920, its *fifth* series of 36 volumes in 1938. Since 1938 the numbering by series has been discontinued, and volumes are annual and bear the whole numbers as of 1818, that for 1939 being volume 237.

Back numbers and volumes, also cumulative indices of all series, may with few exceptions be obtained from the office of the AMERICAN JOURNAL OF SCIENCE, Sterling Tower, New Haven, Conn. Positive microfilm copies of each complete volume may be purchased by subscribers to the paper edition from *University Microfilms*, 313 N. First St., Ann Arbor, Michigan. Regular subscribers may purchase each past year in microcard form, from *The Microcard Foundation*, Wesleyan University, Middletown, Connecticut.

INSTRUCTIONS TO CONTRIBUTORS

Typescripts of articles submitted should be double-spaced, should follow the recommendations in the pamphlet *Suggestions to Authors*, 5th ed. (see below), and should be preceded by brief abstracts. They should be checked with special care before being submitted, to avoid changes in proof other than printer's errors.

References to literature should be listed alphabetically by authors at the end of the article; all references should be complete. For articles in journals or other serial publications, the reference should give in order: Author's name, year of publication, full title: name of periodical or series, volume number, inclusive pages. For books or other unnumbered publications, it should give: Author's name, years of publication, full title: place of publication, publisher. This form follows the recommendations in the pamphlet "Abbreviations used in publications of the U. S. Geological Survey", which is also the standard used for abbreviating names of periodicals, etc. Citations within an article should be to author and year, with specific pages wherever appropriate.

Plates (photographs), *figures* (line drawings), and *footnotes* should each be numbered consecutively through each article, using arabic numerals. If two photographs form one plate, they are figures 1 and 2 of that plate.

Illustrations should be neat and legible and should include explanations of symbols used. Copy that cannot be reproduced cannot be accepted. Plates and figures should be capable of reduction to not more than 4 by 7 inches, all lettering being at least 1/16th inch high after reduction. When necessary, one large map or table can be accepted, if it will not exceed 7 inches in width after reduction. Line drawings should be in black India ink on white drawing board, tracing cloth, or coordinate paper printed in blue. Photographs should be positive glossy prints. Photostatic and typewritten material cannot be accepted as copy for illustrations.

Reprints. Thirty separate copies of each article will be furnished to the author free of cost and without previous notice from him; these will be without a cover. Additional copies will be furnished at cost, which will of course be greater if the article is accompanied by plates involving unusual expense. Copies will be furnished with a printed cover giving the title, author, volume, page, and year, when specially ordered.

Suggestions to Authors of the Reports of the United States Geological Survey, 5th ed. Washington, D. C., 1958 (Government Printing Office, $1.75).

[American Journal of Science, Vol. 257, April 1959, P. 241-270]

American Journal of Science

APRIL 1959

SOME MINERALOGICAL EQUILIBRIA IN THE SYSTEM K_2O—Al_2O_3—SiO_2—H_2O

J. JULIAN HEMLEY*

Department of Geology, University of California, Berkeley, California

ABSTRACT. An experimental investigation was made at elevated temperatures and pressures of the hydrolysis of K-feldspar to mica + silica and of mica to kaolinite. Values of the equilibrium quotient, m_{KCl}/m_{HCl}, were determined at temperatures ranging from 200° to 550°C. The solution pressure for most of the runs was 15000 psi although determinations were made at both higher and lower pressures. The reactions are exothermic and the equilibria show a marked shift to higher acidities with increasing temperature. The equilibrium curves for the two reactions are essentially parallel. Above about 350°C the assemblage mica-kaolinite changes to mica-pyrophyllite-boehmite, and at still higher temperatures mica-pyrophyllite-andalusite is formed. At 400°C and 15000 psi the equilibrium quotient is $10^{2.7}$ for the assemblage K-feldspar-mica-silica, and $10^{1.3}$ for the assemblage mica-pyrophyllite-boehmite. The experimental equilibrium quotients probably do not differ from the thermodynamic equilibrium constants of the reactions by more than a factor of 5 up to temperatures of 350°C or higher.

The experimentation shows that the most important controls on the fields of stability of these several minerals are the K^+/H^+ activity ratio and the temperature. At a given temperature and with increasing K^+/H^+ ratio the fields of kaolinite, mica and K-feldspar are successively traversed. Similarly, at constant K^+/H^+ ratio with increasing temperature this same sequence is observed. The free energy drive of hydrolysis decreases with increasing temperature. Thus the alteration potential of hydrothermal solution would increase with decreasing temperature provided the rate of migration were sufficiently rapid in comparison with the rate of reaction with the wall rock. Experiments at solution pressures of 5000 and 35000 psi show that the effect of solution pressure on these equilibria is relatively small. An increase in pressure increases the extent of hydrolysis, whereas a decrease in pressure shifts the equilibria in the opposite direction.

The experimental results have particular application to hydrothermal alteration and the genetic interpretation of various alteration mineral patterns.

INTRODUCTION

Detailed examination of many occurrences of rock alteration in ore deposits over the last 20 years has emphasized the need for a greater understanding of the chemistry of rock alteration processes. Advances in the study of sheet-structure silicates during this period have made possible the identification and structural characterization of minerals composing rock alteration suites. A number of geological investigations of rock alteration have utilized and contributed to this fund of information. These studies have revealed systematic features, as well as complexity, in the mineralogy and field patterns of mineral distribution. They have thus brought into focus a great lack of fundamental chemical information on alteration processes and the genetic significance of various alteration patterns.

The term rock alteration as used here has the general meaning associated with it in the geological literature regarding ore deposits. It is characterized

* Present address, U. S. Geological Survey, Denver Federal Center, Denver, Colorado.

chiefly by the development of primarily layer-structure, hydrated minerals from pre-existing rock forming minerals, notably feldspars.

The present study considers equilibria in the system K_2O—Al_2O_3—SiO_2—H_2O. Consideration of these components involves, among other minerals, the stability relations of sericite, the fine-grained potassium-aluminum mica. Sericite is one of the most characteristic alteration minerals associated with hydrothermal sulfide ore deposits. A better understanding of the chemistry of sericite will have broad application to alteration problems in general. Moreover, sericite, as compared to other typical alteration minerals, is most often closely associated spatially and temporally with the ore itself. Information on the chemistry of sericite will therefore relate closely to the problem of the nature of the processes by which ore minerals are deposited.

SOME FIELD RELATIONS

This investigation was the outgrowth of studies of rock alteration in hydrothermal vein deposits in granodiorite-type rocks, and alteration in the porphyry coppers. The geological aspects of the study have been summarized in another paper (Meyer and Hemley, 1957) and are only briefly noted here.

Perhaps the most unambiguous geometrical and temporal relationships between alteration mineral assemblages are observed in certain vein deposits of the type mentioned above, notably those of Butte, Montana. Enveloping the copper, zinc and manganese veins of Butte an alteration envelope made up of two major units is observed. An innermost sericitic envelope is bordered sharply by an outer argillic envelope which in turn grades into fresh granite. The clay mineral content of the argillic envelope consists of a high percentage of kaolin nearer the vein with montmorillonite dominant farther out. The development of the clay zone is the result of the preferential decomposition of plagioclase. K-feldspar and quartz are only slightly affected. In the sericite zone quartz and white mica are the dominant mineral constituents. Clays are absent. K-feldspar in this zone in some environments, such as in the upper levels of a large portion of the Butte district, is completely sericitized. In other instances, notably in some alteration types in porphyry copper deposits, the association of K-feldspar with sericite, as well as with clays, is commonly observed.

These brief summary statements should not be considered an adequate review of all aspects of the rather variable alteration picture under consideration. They do, however, serve to delineate a number of important chemical problems. May the assemblages mica-K-feldspar, mica-kaolin, and K-feldspar-kaolin, each in association with quartz, represent stable associations? If so, what are the parameters which define their stability? If, on the other hand, any of these assemblages are metastable, what kinetic factors are involved in their formation? Investigations of the reactions which give rise to these various mineral associations are requisite to an understanding of the conditions of their formation and to the definition of their respective stability fields. Of immediate interest are the hydrolysis equilibria of K-feldspar and K-mica.

PREVIOUS WORK

Exploratory experiments on the decomposition by feldspar in aqueous

solutions were carried out by Gruner (1944). The studies involved the treatment of feldspar in a large excess of 0.1N HCl at elevated temperatures and pressures. Some experiments were also conducted using chemical mixtures of equivalent feldspar or mica composition. The temperatures of experimentation were 300, 340, 360, and 400°C. Pressures in the bombs were determined by degree of filling.

In using a large excess of acid, the experiments were designed so that the pH at the end of the run was approximately the same as at the beginning. In all instances in which K or Na feldspar alone were treated in the acid solutions pyrophyllite was produced. If aluminum hydroxide and KCl were added to the system, mica was formed at higher temperatures and kaolinite or boehmite at lower temperatures. The transition occurred between 340° and 360°C. If KCl alone were added in the treatment of feldspar no alteration was observed. It was concluded that under these conditions K-feldspar persists metastably. The results of Gruner's work indicate a course of alteration under conditions of constant high acidity at certain conditions of temperature and pressure, but they have little import from the standpoint of alteration under equilibrium or near equilibrium conditions. They therefore have limited application to the definition of K-feldspar or mica stability fields.

Studies of mineral alteration in a leaching environment under conditions of moderate temperature, pressure and acidity were conducted by Norton (1939). These experiments, like those just described, were designed as exploratory tests on mineral alteration rather than as chemical equilibrium studies. The experimental technique involved continuous leaching of finely ground feldspar or other silicate mineral by CO_2-bearing aqueous solutions. Sericite and quartz were reported to have formed from K-feldspar. Mineral identifications as they were reported, however, were not completely satisfactory.

Morey and Chen (1955) conducted similar studies using pure water. The relative rates of solution of mineral components were determined and the residual mineral substances identified.

There has been considerable experimental work on synthesis of clay minerals and mica under hydrothermal conditions. Much of this work, such as that of Noll (1936), has been adequately summarized in a comprehensive review by Morey and Ingerson (1937). An important investigation of mineral stability relations in the system K_2O—Al_2O_3—SiO_2—H_2O was that of Yoder and Eugster (1955) on synthetic and natural muscovite. The studies of Yoder and Eugster, however, were concerned primarily with the thermal decomposition reaction of muscovite. Equilibria such as those involved in the present study were not considered.

On the basis of the work of Gruner and others some investigators have attempted to deduce fields of formation for various alteration minerals under hydrothermal conditions (Folk, 1947; Stringham, 1952). Results of the present work indicate these proposed relations to be substantially incorrect.

EXPERIMENTATION

The foregoing discussions have indicated the need for investigation of the hydrolysis reactions of K-feldspar and K-mica. In view of the lack of appropri-

ate experimental data three fundamental points must be considered: (1) What are the correct net reactions involved? (2) What are the equilibrium constants of the reactions? (3) What is the significance of kinetic factors, reaction rates and mechanisms, in the occurrence of these reactions? The first two of these questions are logically of more immediate or fundamental importance and it is with these problems that the present study is largely concerned.

Procedure

Initial experimentation established the occurrence and reversibility of the reactions,

$$\underset{\text{K-feldspar}}{\tfrac{3}{2}KAlSi_3O_8} + H^+ = \underset{\text{mica}}{\tfrac{1}{2}KAl_2AlSi_3O_{10}(OH)_2} + 3\,SiO_2 + K^+$$

$$\underset{\text{mica}}{KAl_2AlSi_3O_{10}(OH)_2} + H^+ + \tfrac{3}{2}H_2O = \tfrac{3}{2}Al_2Si_2O_5(OH)_4 + K^+$$

These experiments were conducted using dilute HCl-KCl solutions. For example, the spontaneous alteration of K-feldspar to mica plus cristobalite and of mica to kaolinite can be accomplished in solutions of 0.15m HCl-0.5m KCl.[1] These reactions are suggested by geological and chemical considerations, but the decomposition process for K-feldspar previously had not been experimentally realized. It is also conceivable that the decomposition of K-feldspar to mica would not represent an equilibrium process under hydrothermal conditions appropriate to rock alteration. The necessity for demonstrating a given net reaction can hardly be overemphasized.

Following such studies of the nature of the reactions, equilibrium points were fixed more precisely by successive equilibration runs. Such experiments could conceivably be conducted in a number of ways, but with the equipment available to this project the most appropriate method appeared to be the equilibration of an excess of the mineral assemblage under consideration with an aqueous phase, followed by a measurement of the potassium and acid concentration in that phase. Equilibrium was approached from both directions, that is, by leaching and by fixation of potassium. For example, in K-fixation experiments involving the K-feldspar-mica-silica assemblage, K-feldspar was produced from mica plus silica in the presence of aqueous potassium at an acid concentration initially less than the equilibrium acid concentration. K-leaching experiments corresponded to the reverse process.

The experiments were conducted using sealed platinum tubes. One hundred to two hundred milligrams of the appropriate mineral assemblage ($<$200 mesh) were used together with about a milliliter of solution of appropriate normality in HCl and KCl. The tube was placed in a cold-seal rod bomb under external water pressure and the bomb heated to temperature. The use of such vessels in hydrothermal experimentation has been described by Tuttle (1949)

[1] The alteration of K-feldspar to mica + silica (cristobalite) in dilute KCl solutions indicates Gruner's conclusions that feldspar remains unaltered under such conditions to be mistaken. On the basis of some preliminary results of the present study it is suggested that there was alteration of the *finer* grained material in Gruner's charges, but the product was amorphous material not evidenced in his x-ray diffraction patterns.

and others.[2] The total confining pressure for most of the runs was 15000 psi. Temperature was controlled within ±5°C.

At the end of the run, the bomb was quenched rapidly at essentially constant pressure. The quench consisted of immersion in a mercury bath, contained in a large reservoir of ice-water mush. The bomb reached a low internal temperature, probably less than 50°C in 1-1½ minutes, and then about 2 minutes was required for extraction of the sample and measurement of its pH. Since the solutions contained KCl in large excess, the concentration of this material was known. The concentration could of course be calculated in those instances where there was significant change in KCl and HCl concentration in the experiment. The true HCl concentration of the experimental samples was readily obtained by calibration of the response of the pH meter with solutions of known HCl-KCl normality. A Beckman one-drop glass electrode was used. The reproducibility of the readings was ±0.03 pH units.

Both synthetic and natural minerals were used in the experimentation. The same equilibrium results were obtained with each, equilibrium being approached from either direction. Synthetic materials yielded slightly faster reaction rates and were used in a majority of the runs. The synthetic minerals were made hydrothermally from gels of appropriate composition. Reaction time for the runs was from one to three weeks. At lower temperatures experiments of several weeks duration were the rule. Approximately one hundred runs were involved in the experimentation.

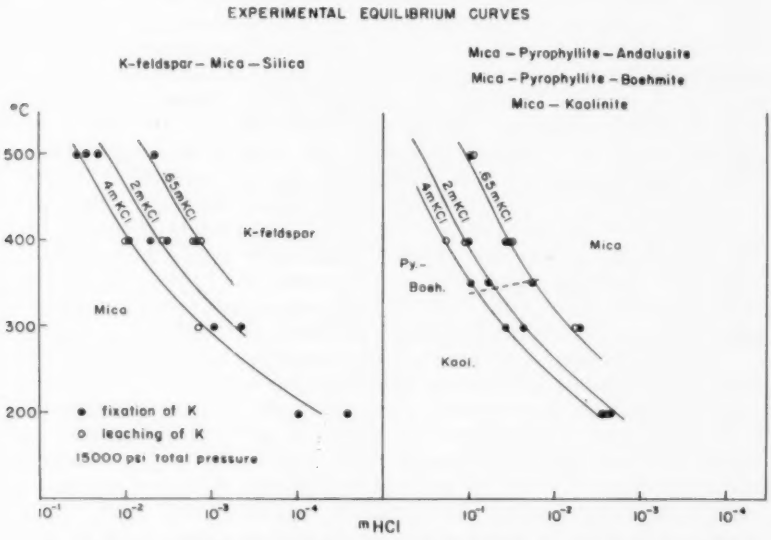

Fig. 1. The experimental equilibrium curves. K-fixation designates the approach to equilibrium from the right on the diagram, K-leaching designates the reverse process.

[2] The writer is grateful for two bombs loaned by George Kennedy as models for the apparatus.

Experimental Results

Stability Fields.—Results of the experimental work are summarized in the equilibrium curves of figure 1. The pressure of the solutions was 15000 psi. The curves delineate the fields of stability of K-feldspar, mica and kaolinite. They are expressions of the critical KCl/HCl ratio for the transition from one field of mineral stability to another at a given temperature. The KCl/HCl ratio is an approximate expression of the equilibrium constant of the reactions, and shows a shift of the equilibrium to more acid conditions at higher temperatures. The KCl/HCl ratio, the temperature and the pressure are therefore the parameters which define stability relations among these mineral assemblages.

The variation of the equilibrium quotient with temperature for the two mineral assemblages, K-feldspar-mica-silica and mica-kaolinite, are given in figure 2. The curves are essentially parallel and separated by an interval of acid concentration corresponding to about 1.5 pH units. The significance of the dashed curve is discussed on a later page. At a given KCl/HCl ratio, then, the stability fields of kaolinite, mica and K-feldspar are successively traversed with increasing temperature. Similarly, at a given temperature the three fields are successively traversed with increasing KCl/HCl ratio.

At higher temperatures the curve corresponding to the mica-kaolinite equilibrium gives way to different relationships. At 350-355°C mica de-

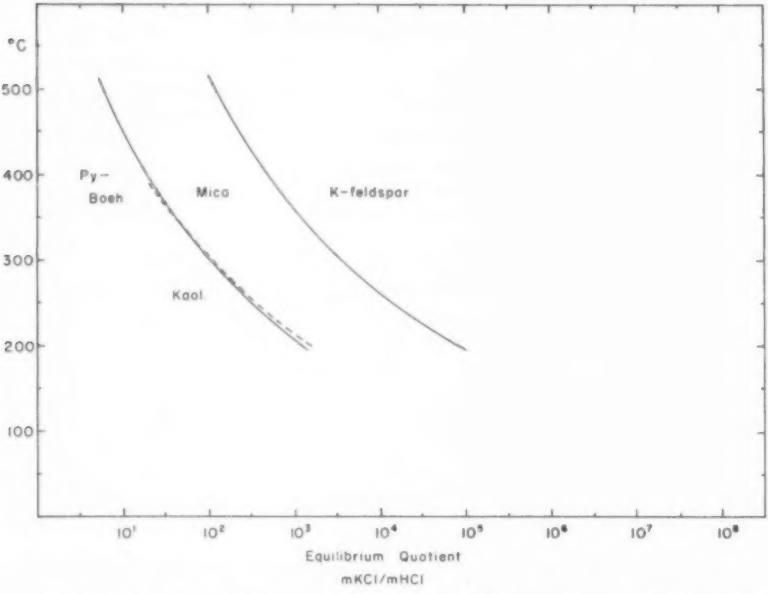

Fig. 2. Plot of the experimental equilibrium quotients versus temperature. The dashed curve is discussed on a later page.

composes to pyrophyllite plus boehmite instead of kaolinite because of the instability of kaolinite above this temperature.

$$\underset{\text{mica}}{KAl_2AlSi_3O_{10}(OH)_2} + H^+ = \frac{3}{4}\underset{\text{pyroph.}}{Al_2Si_4O_{10}(OH)_2} + \frac{3}{4}\underset{\text{boeh.}}{Al_2O_3 \cdot H_2O} + K^+$$

$$\text{or } \underset{\text{kaolin}}{Al_2Si_2O_5(OH)_4} = \frac{1}{2}\underset{\text{pyroph.}}{Al_2Si_4O_{10}(OH)_2} + \frac{1}{2}\underset{\text{boeh.}}{Al_2O_3 \cdot H_2O} + H_2O$$

The point at 352°C on the 0.65m curve shows only minor decomposition of kaolinite whereas on the other curves kaolinite is replaced by pyrophyllite + boehmite. Diaspore rather than boehmite may be the stable alumina hydrate under these conditions (Roy and Osborn, 1954), but this would have very little effect on the energy relations.

At 400°C the assemblage mica-pyrophyllite-boehmite was observed and its equilibrium quotient determined. At somewhat higher temperature the assemblage mica-pyrophyllite-andalusite is developed.

$$\underset{\text{mica}}{KAl_2AlSi_3O_{10}(OH)_2} + H^+ = \frac{1}{2}\underset{\text{pyroph.}}{Al_2Si_4O_{10}(OH)_2} + \underset{\text{andal.}}{Al_2SiO_5} + H_2O + K^+$$

The temperature of formation of this assemblage, as well as the dehydration temperature or upper stability limit of the alumina hydrate, are among considerations that could not be investigated fully in the present study because of limitations of time. The tendency of the monohydrate to persist above its temperature limit of stability has been noted by other investigators (Roy and Roy, 1955). The temperature of formation of the mica-pyrophyllite-andalusite assemblage is at least as low at 450°C. Evidence of the presence of andalusite in some experiments at 420°C suggests that andalusite will form at this temperature under the conditions of the present experimentation if sufficient time is allowed for crystallization. The development of andalusite agrees with the work of Clark, Robertson and Birch (1957) on the stability fields of Al_2SiO_5 polymorphs. The x-ray powder diffraction pattern of the andalusite phase is nearly identical with that of andalusite from Fresno County, California.

As discussed in an earlier paragraph the equilibrium points illustrated in the curves in figure 1 were determined by the degree of approach of potassium leaching and potassium fixation experiments. In K-leaching the approach to equilibrium was from the left on the diagram; for K-fixation it was from the right. For some of the equilibrium values a number of successive experiments were required before the two approaches closed on one another in the time allowed for reaction. In other cases, such results were obtained in one or two runs. The reason for a lag in approach to equilibrum in many instances is presumably grain-coating effects. When the position of the curve becomes approximately known, experiments can of course be run with certain attainment of equilibrum. The values shown in figure 1 represent nearly all of the equilibrium points. Experiments to determine the reactivity of dilute HCl solutions with platinum indicated the reaction to be negligible. An experimental uncertainty in this experimentation of 0.15-0.20 pH units is indicated by typical equilibrium values plotted on the curves.

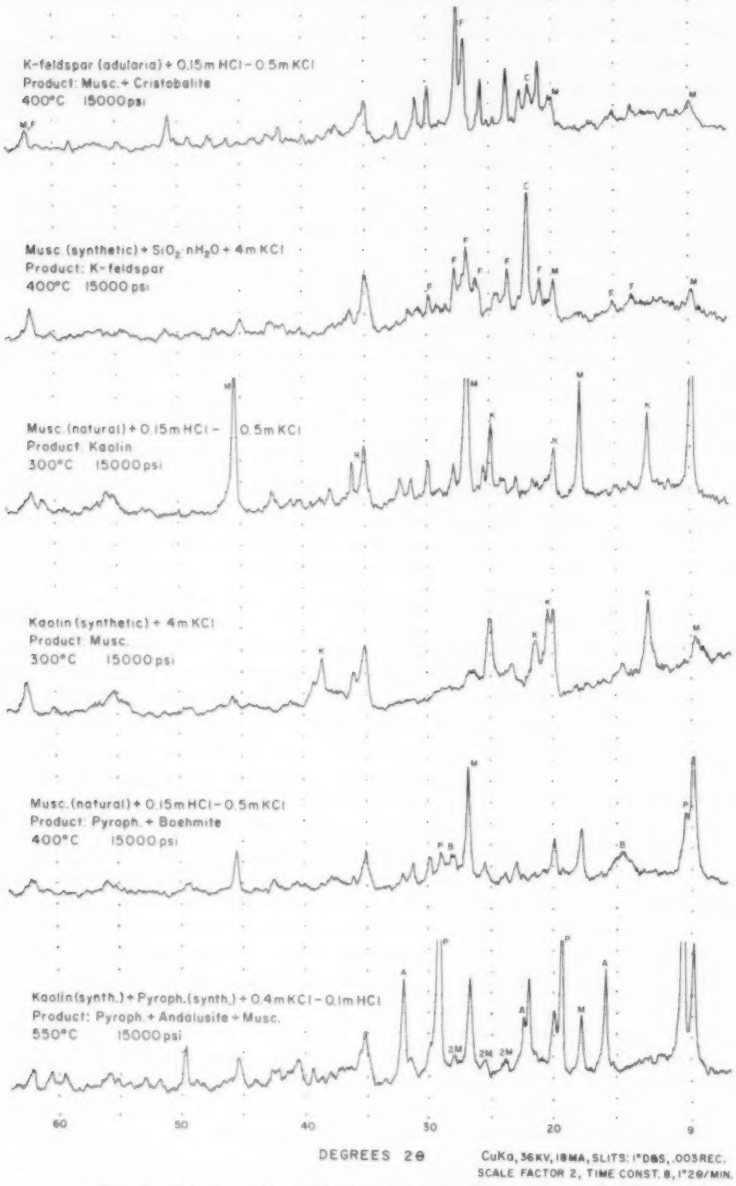

Fig. 3. X-ray powder diffraction patterns of reaction products.

The x-ray diffraction results for a number of the runs are shown in figure 3. Powder diffraction patterns were of course the principal means of mineral identification because of the very fine grained character of the reaction products. The muscovite polytype formed in the experimentation was generally 1Md, the 1-layer disordered structure. The $2M_1$ polytype was indicated in a few runs.

Slow crystallization of silica at low temperatures.—In the K-feldspar-mica-silica assemblage at temperatures below 400°C, considerable trouble was encountered because of the tendency of silica to remain uncrystallized. The result of this was a higher activity of silica in the solutions than that present at equilibrium, with consequent stabilization of K-feldspar at acidities much higher than the equilibrium value. This supersaturation with respect to silica was markedly illustrated by experiments utilizing powdered hydrated silica (reagent silicic acid). At 400°C and above, this material readily crystallized to cristobalite or silica-K, but at 300°C and below, there was no crystallization of a silica mineral. Instead, the reacted solutions, after extraction from the tubes and standing for several days, congealed to a gel.

The problem presented by the slow crystallization of silica required that the equilibrium point in these instances be established primarily by K-fixation using quartz. Even synthetic quartz, however, because of its extremely fine crystallinity and therefore greater solubility was possibly a source of slight error. The points on the K-feldspar-mica-silica curve at 200°C represent synthetic quartz, on the one hand, and natural quartz sized to >10 microns on the other. The sized material was slow in reacting and the result probably does not express complete approach to equilibrium. If the natural material had not been sized it would probably have given a result falling essentially on the curve as drawn. At higher temperatures where silica crystallized readily, the use of either cristobalite or quartz in the experiment yielded the same equilibrium results within experimental error. This would be expected from the small difference in free energy between these two phases.

Hydrolysis on Quenching.—Referring to the experimental curves it is seen that the equilibrium acid concentration in the several reactions is increased by higher temperature, as well as by greater salt concentration. These higher concentrations of salt and acid would be advantageous in minimizing errors that might result from back hydrolysis during quenching. Back hydrolysis reactions would probably have to be largely of surface character in order to occur to a significant extent during the short time interval allowed in quenching. The amount of reaction that could occur would therefore be limited, and under more acid conditions the resulting error would be less significant.

If the equilibrium acidity corresponded to a high pH value, say 4 or 5, only a negligible amount of reaction, essentially 0.0001 meq/ml, would be sufficient to change the pH by a whole unit. On the other hand, in order to change the pH by a whole unit in a solution with an acid concentration corresponding to a pH of 1, the amount of reaction required would be about 0.1 meq/ml. This is a very large amount of reaction, of the order of the total amount of mineral present in the charge. Also, it cannot be argued that higher

acidity would necessarily increase the rate of hydrolysis since increased acidity implies higher salt concentration which would suppress hydrolysis. These statements are born out by observation. In some of the initial experimentation, a slow drift in pH to higher values after quenching was sometimes observed, but only in those solutions with pH values greater than 4 or 5.

The relationship between free energy and rate of reaction is also of significance. From the slope of the curves it is apparent that the greatest free energy drive for hydrolysis would exist at low temperatures, where rates of reaction would be minimum. At high temperature, where rates are high, the tendency for hydrolysis diminishes. It is therefore possible that hydrolysis during quenching would occur to no greater extent at the higher temperatures than it would at temperatures approaching room temperature.

Perhaps it should be pointed out again that it is not the hydrogen ion activity or pH of the system at elevated temperatures and pressures that is quenched and measured. Rather it is the total molar acidity of the system that is quenched, and the measurement of pH at room temperature is the means of establishing that value. Hydrogen ion and potassium ion activities at the higher temperature conditions of the experiments are estimated from thermodynamic considerations.

Pressure Experiments.—In addition to the studies at 15000 psi solution pressure, experiments were also conducted at higher and lower pressures using the 2m KCl solution. The pressure involved is of course essentially water pressure. The results are given in figure 4, plotted in reference to the 15000 psi

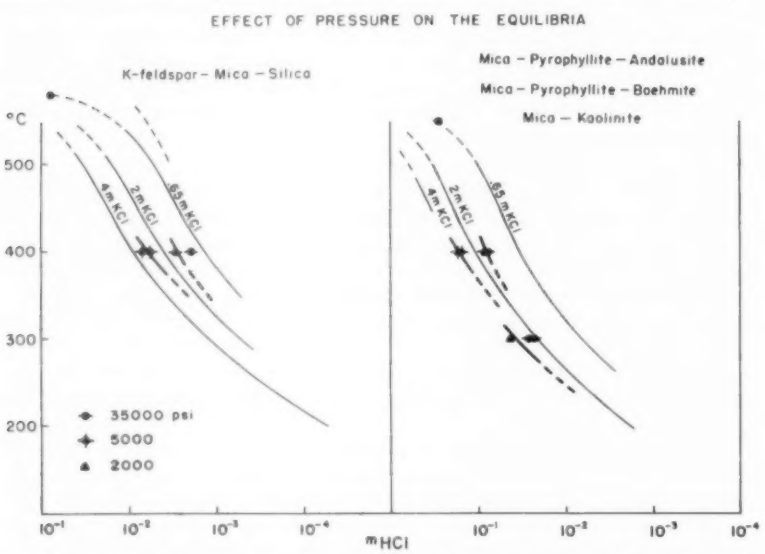

Fig. 4. Displacement of the equilibria with change in pressure. The points in the legend are for 2m KCl plotted in reference to the curves at 15000 psi solution pressure. The values at the highest temperatures are for 0.65m KCl at 15000 psi solution pressure.

curves. The effects of pressure are small, but apparently real. Higher pressures increase alteration, lower pressures result in the precipitation of K-feldspar or mica for the two reactions respectively. It is evident from the data that composition of the aqueous phase and temperature are more important than solution pressure as controls on stability relations. In addition to the experiments at high and low pressures, high temperature points for the 15000 psi curves are also shown in figure 4. At very high temperatures the 15000 psi curves are seen to show a break to higher acidity analogous to that of lower pressure curves at lower temperatures. Thus a sheaf of curves corresponding to different pressures and fanning out at high temperatures could be illustrated. This rapid shift to higher acidity at higher temperatures corresponds to a widening of the K-feldspar field relative to the other two. Alteration of K-feldspar would occur with diminished intensity with increasing temperature, and at very high temperature feldspar would be stable at very high acid concentrations.

Experiments with Excess Silica.—The role of silica in the displacement of the mica-kaolinite equilibrium curve was also investigated. The results are shown in figure 5. At 300°C there was no effect on the position of the equilib-

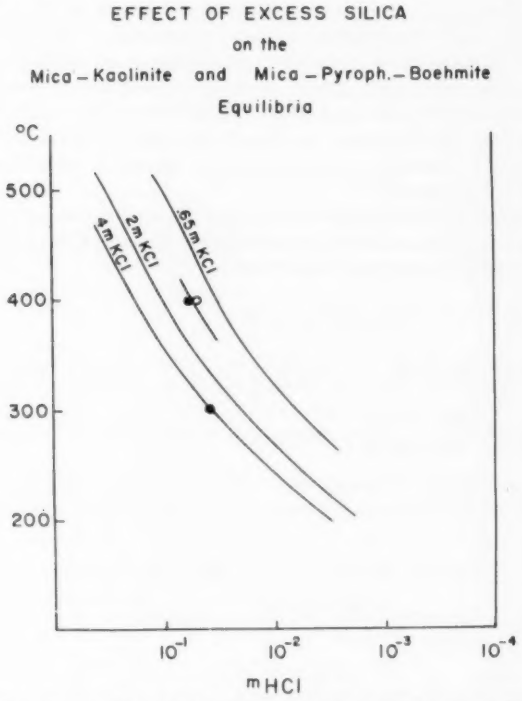

Fig. 5. Experiments with added silica. The points at 400°C are for 2m KCl and the value at 300°C is for 4m KCl. These are plotted in reference to the curves at 15000 psi solution pressure and silica deficiency.

rium, even with the use of highly reactive silicic acid as the source of silica. This indicates that mica-kaolinite-quartz is a stable assemblage under these conditions. At 400°C, using either cristobalite or silicic acid, there was a small, but distinct shift in the equilibrium point. This corresponds to the silication of the high alumina phase, boehmite. Here the equilibrium assemblage with excess silica is mica-pyrophyllite-cristobalite. Experiments with quartz rather than cristobalite were not carried out. The reaction at 400°C would occur with somewhat smaller free energy.

At high temperatures the assemblage mica-aluminosilicate-quartz would become stable with the breakdown of pyrophyllite. This reaction was not demonstrated in the experimentation, although one run at 550°C apparently produced some cristobalite, as well as the mica-andalusite-pyrophyllite assemblage, from kaolinite plus pyrophyllite starting materials. However, the cristobalite may have been metastably produced in the rapid decomposition of kaolinite at this high temperature.

DISCUSSION OF RESULTS

Evaluation of the experimental results involves consideration of possible errors of experimentation and problems involved in the estimation of equilibrium constants and other thermodynamic parameters of the reactions. Only approximate values of these quantities can be obtained in this system because of the lack of pertinent data at elevated temperatures and pressures, but some thermodynamic conclusions are nevertheless desirable. With such information mineral stability relations can be framed in more general terms and the several equilibria can be more quantitatively related to other chemical reactions of geological interest.

The molar KCl/HCl quotient is an approximate expression of the equilibrium constants of the several reactions studied. For the K-feldspar-mica-silica and mica-pyrophyllite-boehmite reactions:

$$\tfrac{3}{2}KAlSi_3O_8 + H^+ = \tfrac{1}{2}KAl_2AlSi_3O_{10}(OH)_2 + 3\,SiO_2 + K^+$$

$$KAl_2AlSi_3O_{10}(OH)_2 + H^+ = \tfrac{3}{4}Al_2Si_4O_{10}(OH)_2 + \tfrac{3}{4}Al_2O_3\cdot H_2O + K^+$$

$K = \dfrac{a\pm_{KCl}}{a\pm_{HCl}} = \dfrac{M_{KCl}\,\gamma\pm_{KCl}}{M_{HCl}\,\gamma\pm_{HCl}}$, where $\gamma\pm$ is the mean activity coefficient of the electrolyte.[3] Values of the experimental equilibrium quotients are illustrated in table 1. They are surprisingly constant in view of experimental difficulties.

TABLE 1

Equilibrium Quotients at 400°C & 15000 psi

	K-feld.-Mica-SiO_2	Mica-Pyroph.-Boeh.
4m KCl	$10^{0.00}/10^{-2.05} = 10^{2.05}$	$10^{0.00}/10^{-0.73} = 10^{1.33}$
2m KCl	$10^{0.30}/10^{-2.40} = 10^{2.70}$	$10^{0.30}/10^{-0.98} = 10^{1.28}$
0.65m KCl	$10^{-0.19}/10^{-2.80} = 10^{2.70}$	$10^{-0.19}/10^{1.40} = 10^{1.30}$

[3] The molal concentration unit indicated is consistent with the further discussion of the relations given on page 254.

Experimental Errors

The consistency of the values shown for the experimental equilibrium quotients imply that the values are correct to a fairly high degree of accuracy, and that the activity coefficient ratios remain essentially constant with moderately large changes in electrolyte concentration. If the ratios were not constant and if gross experimental errors were involved in the measurements, for example errors as large or larger than the differences in salt concentrations involved, it would be required that these errors operate in precisely such a way as to bring the equilibrium quotients into close agreement. Although this is a possibility it is clearly the less plausible view. Such arguments cannot be considered proof of a high degree of accuracy of the experimental results, but they do constitute a strong indication that the experimental uncertainty is small. As observed earlier, an uncertainty of no more than $10^{\pm 0.2}$ was indicated in the reproducibility of points on the equilibrium curves. Errors arising from problems in quenching mentioned earlier, which should be the major source of uncertainty, would thus appear to be essentially of this magnitude.

The accuracy of the experimental results can be examined using other experimental techniques. For example, a small amount of mineral charge might be equilibrated with a large excess of solutions of given K^+/H^+ ratio, and the ratio observed at constant temperature and pressure at which the products of the reaction change. Also, for the K-feldspar-mica-silica assemblage mica and feldspar can be equilibrated in the manner of the present investigation, but without the presence of silica. Fixation of potash does not then take place and the acid concentration cannot increase above the initial concentration in the charge. Hydrolysis toward higher pH is the only change that may occur. Such studies made on the K-feldspar-mica-silica assemblage using 4m KCl at 400°C indicated that the maximum quenching error to be expected is about 0.5 pH units. The actual error would probably be considerably less. This agrees with conclusions already expressed above.

Activity Coefficients

Practically no information is available in the chemical literature on the activity coefficients of electrolytes at elevated temperatures and pressures. Calculation of equilibrium constants must therefore depend upon extrapolation of activity coefficients to the higher temperature pressure conditions of the experiments.

Temperature Extrapolation.—This point will be discussed, first from the standpoint of activity coefficients of the ions based on thermal data at room temperature, followed by consideration of the degree of dissociation of the electrolytes at elevated temperatures and pressures. The overall activity coefficient will include both of these effects.

The temperature dependence of the activity coefficient is given by the relation:

$$\left(\frac{\partial \ln \gamma \pm}{\partial T}\right)_{P,M} = -\frac{\bar{H} - \bar{H}^\circ}{2RT^2} = -\frac{\bar{L}}{2RT^2}$$

$\bar{H}$ is the partial molal enthalpy of the solute, $\bar{H}^\circ$ is the partial molal enthalpy

at infinite dilution, and $\bar{L}$ is termed the relative partial molal enthalpy of the solute. The mean activity coefficient $\gamma\pm$ refers to the ions in molal concentration units. The solutions used in the experimentation were made up on a molar or volumetric basis, but for the purposes of these approximate calculations, and considering that it is concentration ratios that are involved, these can be taken as molal values.

Partial molal quantities for KCl and HCl are known at 25°C and have been tabulated by Harned and Owen (1958). Because partial molal heat capacities of these electrolytes are unknown at higher temperatures and pressures extrapolation, of the relative partial molal enthalpy must be based upon heat capacity values at low temperature. The relative partial molal enthalpy then becomes

$$\bar{L} = \bar{L}_{298^\circ} + \Delta\bar{C}p_{298^\circ}\,(T - 298)$$

where $\Delta\bar{C}p$ is the relative partial molal heat capacity. Incorporating this into the above equation, and assuming $\Delta\bar{C}p$ constant, we obtain the relation:

$$\log \gamma\pm = \frac{\bar{L}_{298^\circ} - \Delta\bar{C}p_{298^\circ}\,(298)}{(2)\,(2.303)\,RT} - \frac{\Delta\bar{C}p \log T}{2R} + I$$

From knowledge of the activity coefficient and relative enthalpy and heat capacity values at some reference temperature such as 298° K the constant I can be evaluated.

Calculations of activity coefficients using this relation are based on the assumption that the relative partial molal heat capacity $\Delta\bar{C}p$ remains constant with increase in temperature. In cases where $\Delta\bar{C}p$ is large, however, this implies a considerable increase in $\bar{L}$ and decrease in the activity coefficients at higher temperatures. For 2M KCl $\bar{L}$ = 446 cal/mole and $\Delta\bar{C}p$ = 23.8 cal/mole/deg. at 25°C. At 100°C, $\bar{L}$ becomes 1790 cal/mole, and continues to increase to very large values at higher temperatures. The quantity $\bar{L}$ is a heat of dilution with sign changed. Thus if enthalpy changes are to be limited to realistic values $\Delta\bar{C}p$ must decrease with temperature. Lewis and Randall (1923, p. 107) have discussed these points and have suggested that at considerably higher temperatures $\Delta\bar{C}p = 0$ is a better basis of approximation than the assumption of a constant $\Delta\bar{C}p$. The actual trend of the activity coefficients would probably follow some intermediate course between values based on $\Delta\bar{C}p$ constant and $\Delta\bar{C}p = 0$.

The properties of mixed electrolytes rather than individual electrolytes must be considered in a discussion of the experimental solutions. Not only activity coefficients but also relative molal enthalpy and heat capacity values of electrolytes in electrolyte mixtures are found to be a function of the total concentration or ionic strength of the solution. The result is that the activity coefficient of a minor component in a mixture of electrolytes tends to follow that of the major component.

Mixtures of KCl and HCl at controlled ionic strength have been studied

in some detail. An important observation is that at a given concentration of KCl, $\gamma_{\pm HCl}$ is independent of HCl concentration at low acid concentrations. Thus the range of experimental pH measurements for a given KCl concentration would all involve the same activity coefficient of HCl. The activity coefficient ratios for the extrapolated activity coefficients are brought much closer to unity when the mixed electrolyte, dilute HCl in more concentrated solutions of KCl, is considered. This behavior helps explain the approximate constancy with change in salt concentration of the equilibrium quotients in the experimental solutions.

Extrapolated values from 25°C of the mean activity coefficients of KCl and HCl are given in table 2. For the mixed electrolyte the mean activity coefficients for 0.01M HCl in 2M KCl are presented in table 3. These values were calculated from experimental data available from 0° to 50°C (Harned and Owen, 1958). Such data is also given for KCl solutions. For the mean activity coefficient ratio, the values for 2M KCl/0.01M HCl represent a fair average for the experimentation as a whole. These values are presented in table 4.

TABLE 2

Mean Activity Coefficients

$\Delta\bar{C}p$ = constant

	HCl			KCl		
	0.1M	0.01M	0.001M	4M	2M	0.7M
100°	0.754	0.883	0.982	0.570	0.520	0.579
200°	0.697	0.850	0.975	0.347	0.372	0.461
300°	0.646	0.823	0.966	0.204	0.238	0.352
400°	0.600	0.794	0.960	0.096	0.151	0.261
$\bar{L}$*	202	71	22.6	−782	−446	−85
$\Delta\bar{C}p$	2.9	1.4	0.3	33.6	23.8	14.0
			$\Delta\bar{C}p$ = 0			
100°	0.764	0.890	0.961	0.661	0.662	0.637
200°	0.743	0.879	0.957	0.740	0.664	0.644
300°	0.730	0.875	0.956	0.794	0.691	0.650
400°	0.720	0.871	0.956	0.836	0.713	0.653

* cal/mole

TABLE 3

Mean Activity Coefficients of HCl

0.01M HCl in 2M KCl

	from 25°C		from 50°C	
	$\Delta\bar{C}p$ = const.	$\Delta\bar{C}p$ = 0	$\Delta\bar{C}p$ = const.	$\Delta\bar{C}p$ = 0
100°	0.68	0.71	0.62	0.66
200°	0.51	0.66	0.32	0.56
300°	0.40	0.63	0.16	0.51
400°	0.30	0.61	0.08	0.47

$\bar{L}_{25°}$ = 1120, $\Delta\bar{C}_{p25°}$ = 11 $\quad$ $\bar{L}_{50°}$ = 540, $\Delta\bar{C}p_{\ 50°}$ = 34

TABLE 4

Mean Activity Coefficient Ratios
KCl/HCl, 0.01M HCl in 2M KCl

	from 25°C		from 50°C	
	$\Delta\bar{C}p = \text{const.}$	$\Delta\bar{C}p = 0$	$\Delta\bar{C}p = \text{const.}$	$\Delta\bar{C}p = 0$
100°	0.77	0.87	0.80	0.84
200°	0.73	1.0	1.0	0.95
300°	0.60	1.1	1.3	1.0
400°	0.50	1.2	1.4	1.1

Pressure Effect.—In the above calculations the effect of pressure on the activity coefficients of HCl and KCl was neglected. The pressure variation is given by:

$$\left(\frac{\partial \ln \gamma\pm}{\partial P}\right)_{T,M} = \frac{\bar{v} - \bar{v}^\circ}{2RT}$$

where $\bar{v}^\circ$ is the partial molal volume of the solute in the standard state. The conventional standard state would be a hypothetical solution of unit activity at 1 atm. pressure, which obeys the limiting law for infinite dilution. It is apparent that the effect of pressure on activity coefficients should be relatively small. This is fortunate since no data are available at the elevated temperature and pressure conditions of the present experiments for partial volumes and partial compressibilities of electrolytes. It should be noted that the pressure variation of the activity coefficient is not measured by the difference between the partial molal volume of the solute in solution at 1000 atm. versus its partial molal volume in the standard state at 1 atm. Rather it is a function of the change in the difference between the two volumes at 1000 atm. and 1 atm. respectively. As with temperature, changes in activity coefficients of HCl and KCl with pressure would parallel one another and tend to cancel. The overall effect of pressure on these equilibria is a function of activity coefficients, molar volumes and partial molal volumes of the reactant and product materials. Although difficult to assess, the uncertainty here is probably considerably less than that involved in the temperature extrapolations.

At lower temperatures, 200° and 300°C, the effect of pressure on activity coefficients would tend to be similar to the effect at room temperature as illustrated in the table below (from Harned and Owen, p. 507).

atm	0.1M HCl	1M KCl
1	0.797	0.605
1000	0.802	0.637

The change at 25°C is negligible, but it is noteworthy that the increase in $\gamma\pm$ HCl is considerably less than that of $\gamma\pm$KCl. Thus, if the same relationship held in the mixed electrolytes the effect of pressure on the activity coefficients would be to shift the equilibrium quotient to smaller values.

EMF Data.—Information on the activity coefficients of pure dilute HCl solutions at higher temperatures and moderate pressures has been presented

by Lietzke (1955). Lietzke calculated $\gamma\pm$ values for 0.017M HCl up to 200°C by the methods of partial molal heat content and the Debye-Hückel theory. These two methods agree to within 0.6 percent up to 200°C. Lietzke used these values to calculate a theoretical EMF of the hydrogen-silver chloride electrode.

$$\tfrac{1}{2}H_2 + AgCl = H^+ + Cl^- + Ag$$

$$E = E^\circ - \frac{RT}{F} \ln \frac{(M\,\gamma\pm)^2}{f^{1/2}_{H_2}}$$

These EMF values were then compared with experimental values of other investigators. The experimental potentials were lower than the theoretical values by only a few millivolts up to about 150°C. Above 175°C the discrepancy increased, and at 200°C and 42 atm. the theoretical potential was 0.489 V, the experimental 0.469 V. Above this temperature both potentials fall off rapidly because of rapid decrease in the partial fugacity of H_2. Higher pressure of course increases the potential at any temperature, the maximum pressure used being approximately 42 atm.

The discrepancy at 200°C would correspond to a difference in the observed and theoretical activity coefficients of only about 5 percent. It is in the wrong direction to be attributed to a decreasing activity coefficient of HCl. The work of Lietzke is therefore evidence that HCl remains a strong electrolyte at these moderately high temperature pressure conditions. This would support the assumption that the activity coefficient values listed in tables 2 and 3 are approximately correct. In the mixed electrolytes HCl would have the greater uncertainty because of the rapidity with which the activity coefficients of HCl are decreasing with temperature at low temperatures in these solutions.

Solubility Data.—Some further insight into the activity coefficients of KCl solutions is afforded by the work of Keevil (1942) on vapor pressures and solubilities in the KCl-H_2O system at elevated temperatures and pressures. The halides of sodium and potassium fall into the class of compounds whose solubility curves are continuous to the melting point of the salt. Very great aqueous solubilities are therefore realized, provided the external pressure is maintained greater than the vapor pressure.

The activity coefficient for the saturated solution can be calculated. The free energy of fusion at any temperature and the free energy of solution can be equated since their sum must be zero.

$$\begin{array}{lll} KCl_{(s)} = KCl_{(liq.)} & \Delta F^\circ \text{ (fusion)} \\ KCl_{(liq.)} = KCl_{(soln)} & \Delta F = RT \ln a \\ \hline KCl_{(s)} = KCl_{(soln)} & \Delta F = 0 \end{array}$$

$$\Delta F^\circ = \Delta Ho - \Delta Cp\, T \ln + IT = -RT \ln a$$

$$\text{and } \Delta H(\text{fusion}) = \Delta Ho + \Delta CpT.$$

The constants ΔHo and I can be evaluated at the melting point (1043°K) from the heat of fusion, and the difference in heat capacity of solid and liquid KCl. Activities may then be computed, and the activity coefficients corresponding to the solubility data of Keevil obtained.

For better comparison with the extrapolated activity coefficient values shown in tables 2 and 3, activity coefficients derived from Keevil's data may be computed on the basis of a moles/1000g. of solution standard state rather than the pure liquid standard state. The total free energy change is then given by $\Delta F^\circ + RT \ln \frac{1^2}{m^2_{KCl\ (pure\ liq)}} + RT \ln m^2 \gamma\pm^2 = 0$, where the second term involves the change in standard state and the third term refers to Keevil's solutions. Using the thermal data of Kelley (1949), the mean activity coefficient of KCl at 400°C is then 0.72. At 500°C it is 0.81. Although the standard state now used is not the same as that of the extrapolated activity coefficients, a hypothetical 1 molal solution obeying the limiting law for infinite dilution, these two standard state fugacities and corresponding activity coefficients will not differ greatly from one another if the solutions are not far from ideal. Also, both will be close to unity. The value of 0.72 at 400°C tends to indicate such behavior.

Finally it will be noted that the activity coefficients given by Keevil's data refer to the saturated solution at the saturation vapor pressure (e.g. 125 atm. at 400°C). At 15000 psi the solubility should be somewhat higher and the activity coefficient somewhat lower. Also, it is possible that at much lower concentrations activity coefficients would be somewhat smaller since $\gamma\pm$ values typically pass through a minimum at some moderately low concentration and then rise to higher values.

These computations constitute an approximate check on the accuracy of the extrapolated activity coefficients given in table 2. It is apparent from these results that the values in table 2 imply a mean activity coefficient of KCl that is certainly of the correct order of magnitude. Furthermore, although the absolute values of the activity coefficients of KCl and HCl are subject to considerable uncertainty, the uncertainty in the ratio of the activity coefficients would be much smaller. The values should compare fairly closely to those indicated in table 4, due to the behavior of the mixed electrolytes.

Conductance Data.—The strength of HCl and KCl as electrolytes at high temperatures and pressures has been evaluated by Frank (1956). Conductances, Λ, were determined at temperatures from 250° to 750°C and at pressures up to 2500 atm. Using the method of Shedlovsky, Frank evaluated Λ_o, the limiting equivalent conductance in dilute solution. The degree of dissociation of the electrolyte is represented by the relation $\alpha = \frac{\Lambda}{\Lambda_o}$. The equilibrium dissociation constant $K = \frac{\alpha^2 c\, \gamma\pm^2}{1-\alpha}$, where c is the concentration. The activity coefficients for the dilute solutions involved in such studies can be estimated from the Debye-Hückel equation. Dissociation constants obtained by Frank are given in table 5.

The most important control on the strength of the electrolytes is the steam density. At densities greater than 0.8 g/cm^3 at 400°C, for example, α for KCl, HCl and KOH gradually approach unity, but at lower densities α decreases rapidly, HCl being affected to the greatest extent. At constant steam density

α decreases slowly with increasing temperature. At low temperatures densities are high and α is essentially unity. These findings indicate that HCl, KCl and KOH remain quite strong electrolytes at elevated temperatures and pressures provided the water density remains high. These general results are consistent with the work of Lietzke in the lower range of temperatures.

Possible values for the mean activity coefficient of 2M KCl and 0.01M HCl at 400°C would be 0.3 and 0.1 respectively. These are taken from the data presented in tables 2 and 3, which, as already noted, are substantiated by the experimental studies that have been discussed. The effect of non-dissociation on these extrapolated values can be computed from the ionization constants in table 5. Assume the activity coefficients of the undissociated species to be 1.

$$K_{KCl} = \frac{aK^+ \, aCl^-}{mKCl - \dfrac{aK^+}{0.3}} = 3.1 \cdot 10^{-2}$$

$aK^+ \cong aCl^- \cong 0.20$

$$K_{HCl} = \frac{aH^+ \, aCl^-}{mKCl - \dfrac{aH^+}{0.1}} = 7.0 \cdot 10^{-3}$$

$aH^+ = 2.58 \times 10^{-4}$

$$\frac{a^{\pm}KCl}{a^{\pm}HCl} = \frac{aK^+ \, aCl^-}{aH^+ \, aCl^-} = 10^{2.89}$$

The total mean activity coefficient ratio is $\dfrac{10^{2.89}}{10^{2.30}} = 10^{0.59}$, whereas the extrapolated ratio is $10^{0.48}$

TABLE 5

Dissociation Constants

	KCl density g/cm³					
°C	0.3	0.4	0.5	0.6	0.7	0.8.
400				$21 \cdot 10^{-3}$	$3.1 \cdot 10^{-2}$	
450	$36 \cdot 10^{-4}$	$4.6 \cdot 10^{-4}$	$2.75 \cdot 10^{-3}$			
500				$6.0 \cdot 10^{-3}$	$12 \cdot 10^{-3}$	$1.4 \cdot 10^{-2}$
550	$10.3 \cdot 10^{-4}$	$2.3 \cdot 10^{-4}$	$1.5 \cdot 10^{-3}$			
600				$2.9 \cdot 10^{-3}$	$4.3 \cdot 10^{-3}$	
650	$6.3 \cdot 10^{-4}$	$1.44 \cdot 10^{-4}$	$1.00 \cdot 10^{-3}$			
700						
750	$3.7 \cdot 10^{-4}$	$1.2 \cdot 10^{-4}$				
	HCl					
400	$4.0 \cdot 10^{-4}$	$2.2 \cdot 10^{-5}$	$11 \cdot 10^{-5}$	$7.2 \cdot 10^{-4}$	$7.0 \cdot 10^{-3}$	$2.0 \cdot 10^{-1}$
500	$2.7 \cdot 10^{-4}$	$1.4 \cdot 10^{-5}$	$6.3 \cdot 10^{-5}$	$3.2 \cdot 10^{-4}$	$2.9 \cdot 10^{-3}$	$2.7 \cdot 10^{-2}$
600	$1.8 \cdot 10^{-4}$	$0.6 \cdot 10^{-5}$	$2.9 \cdot 10^{-5}$	$1.2 \cdot 10^{-4}$	$1.0 \cdot 10^{-3}$	
700	$0.7 \cdot 10^{-4}$	$0.3 \cdot 10^{-5}$	$1.4 \cdot 10^{-5}$			
	KOH					
400	$9.0 \cdot 10^{-5}$	$6.2 \cdot 10^{-4}$	$2.7 \cdot 10^{-3}$	$7.7 \cdot 10^{-3}$	$1.5 \cdot 10^{-2}$	$4.5 \cdot 10^{-2}$
500	$1.9 \cdot 10^{-5}$	$2.8 \cdot 10^{-4}$	$1.9 \cdot 10^{-3}$	$6.4 \cdot 10^{-3}$	$1.5 \cdot 10^{-2}$	$3.4 \cdot 10^{-2}$
600	$0.8 \cdot 10^{-5}$	$1.7 \cdot 10^{-3}$	$1.3 \cdot 10^{-3}$	$5.5 \cdot 10^{-3}$	$1.3 \cdot 10^{-2}$	
700	$0.4 \cdot 10^{-5}$	$1.2 \cdot 10^{-4}$	$1.0 \cdot 10^{-3}$			

after Frank

The above computations serve to illustrate the extent to which non-dissociation of the electrolytes might contribute to the overall activity coefficient ratio. The effect would be significant at 400°C, but would become relatively less important at lower temperatures.

Conclusions.—In summary, on the basis of the preceding discussions it appears that the experimental equilibrium quotients would deviate from true equilibrium constants of the reactions by no more than a factor of 5 up to temperatures of 350°C and possibly higher. Activity coefficient ratios given in table 4 suggest an uncertainty no greater than a factor of 2, but these values may not be reliable to that extent. Because of the relatively rapid change in the mean activity coefficients of HCl from 25° to 50°C there is considerable uncertainty involved in the extrapolation. Electrode potential measurements to only 100° to 150°C would probably do much to eliminate this uncertainty.

Pressure Experiments

In figure 4 are indicated the results of experiments in which the pressure was varied from 15000 psi for the 2M KCl solution. The points are plotted in reference to the 15000 psi curves. The effect on the equilibrium quotient is small.

The free energy change occasioned by a change in pressure is given by the relation $\int \Delta V dp$, where ΔV is the net volume change of the reactants and products. From this the shift in the equilibrium quotient can be deduced. The partial molal volumes of the mixed electrolytes are probably very similar. For the individual electrolytes the difference in partial volumes of 0.01M HCl and 2M KCl at 25°C is about 13 cc, and in the mixture this difference should become even smaller. Also, the density of the experimental solutions at 400°C and 1000 atm. would be quite large, slightly greater than 0.7 g/cm^3, and large changes in partial molal volumes would not be expected. For the solids the volume change can be estimated from the known densities of the natural minerals, bearing in mind that the densities of the imperfectly crystalline synthetic material is probably somewhat less than ideal. For the K-feldspar-mica-silica hydrolysis reaction the molar volume change is about −20 cc/mole H^+. The shift in the equilibrium quotient would be about $10^{0.18}$ for a pressure increase of 1000 atm. This is approximately the observed change. This suggests that differences in partial molal volumes and changes in the activity coefficient ratio for the mixed electrolytes are small, although some compensating changes in activity coefficients and molar and partial molal volumes might also occur.

A change to lower pressure produces a somewhat greater observed effect. This is consistent with the pattern of the dissociation constants noted in table 5.

The effect of pressure on activity coefficients of HCl and KCl at low temperatures was noted on a previous page. Although the effect is small, the activity coefficient of KCl is increased considerably more than that of HCl. Similarly, it will be observed that the high pressure points on the kaolinite-mica curve at 300°C tend to shift the curve slightly to the left. If this effect is real it is a further indication that extrapolation of activity coefficient ratios to at least 300°C involves little error.

A marked displacement of the 15000 psi curve at high temperatures is also shown in figure 4. Although this shift to higher acidity illustrates the same temperature effect as that evident in the lower pressure curves at lower temperature, the process is probably somewhat different. The rapid rate of change probably results from passing into a two phase critical region. Partition of more HCl in the lighter phase, with correspondingly lower activity coefficient, produces the observed effect.

Experiments with Excess Silica

The influence of added silica on the mica-kaolinite and mica-pyrophyllite-boehmite equilibria is illustrated in figure 5. The point at 300°C shows no effect on the equilibrium quotient. Silica apparently takes no part in the net reaction, which indicates that kaolinite plus quartz would be a stable assemblage at this temperature. The absence of reaction between kaolinite and quartz at 300°C, and at temperatures in excess of 350°C, in experiments of 4 months duration at 15000 psi water pressure is additional evidence of such a stability relation.

At 400°C boehmite is silicated to pyrophyllite, which shifts the equilibrium quotient to a new value corresponding to the assemblage mica-pyrophyllite-cristobalite. The displacement is a measure of the free energy of the reaction

$$Al_2O_3 \cdot H_2O + 4SiO_{2\,(Cr)} = Al_2Si_4O_{10}(OH)_2$$

The $\Delta F^\circ = -925$ cal/mole, with a large uncertainty because of the small displacement. If the experiments had been continued at higher temperature there would presumably have been similar silication of andalusite to pyrophyllite.

At higher temperatures the assemblage mica-aluminosilicate-quartz would become stable with the breakdown of pyrophyllite. The decomposition of pyrophyllite occurs at 575°C at 15000 psi water pressure (Roy and Osborn, 1954) (Kennedy, 1955). The product is mullite or mullite-sillimanite solid solution. At still higher temperatures, the assemblage K-feldspar-aluminosilicate-quartz becomes stable with the thermal decomposition of mica, as shown by Yoder and Eugster (1955).

Activity of Water

The foregoing discussion has been concerned only with those equilibria in which water takes no part in the net reaction. But in the decomposition of mica to kaolinite:

$$K = \frac{a\pm_{KCl}}{a\pm_{HCl}\ a^{3/2}{}_{H_2O}} = \frac{M_{KCl}\ \gamma\pm_{KCl}}{M_{HCl}\ M^{3/2}{}_{H_2O}\ \gamma\pm_{HCl}\ \gamma^{3/2}{}_{H_2O}}$$

Although the experimental solutions were moderately concentrated with respect to KCl in the sense of molar concentration, the mole fraction of water was nevertheless greatly preponderant over that of KCl. (e.g. $N_{KCl} \cong 0.07$ in 4m KCl). This of course means that deviation from ideality on the part of the solvent water would be relatively much smaller than that of the solute, and it is for this reason that activities and activity coefficients of solvents, even in fairly concentrated solutions, are not far from unity.

An approximate measure of the departure of a_{H_2O} from unity is obtained in terms of general thermodynamic considerations. The standard free energy of the mica-kaolinite reaction corresponds to the free energy change when water is in its standard state, at unity activity. The experimental solutions at 15000 psi consisted of a single homogeneous phase of liquid character, and therefore the liquid state would be the logical choice for the standard state. By convention the standard state would be pure liquid water at 1 atmosphere pressure and the respective temperature. In other words, the standard state would be a hypothetical state of pure, super-heated liquid water at 1 atmosphere pressure. The change in activity of water in the solutions can be viewed as a combination of two processes: The change in free energy when pure water goes from 1 atm. to 1000 atm. plus the change in free energy at 1000 atm. when pure water goes to water in the electrolyte solution. For the first process ΔF is given by $\int vdp$, where v is a function of p

$$\Delta F = RT \ln a_{H_2O}\,(^{\text{pure}}_{\text{1000 atm}}) = RT \ln \frac{f}{f^\circ} = \int_1^{1000} vdp$$

The change in molar volume v would not be great for *liquid* water in the two states. This can be seen in the P-V-T data of compressed water (Dorsey, 1940). Assuming an average specific volume of 2, which is certainly too large a value, for the pressure interval 1 to 1000 atm. at 300°C $a_{H_2O} = \frac{f}{f^\circ} = 2.2$. Thus by virtue of the increase in pressure, the fugacity would be increased by a factor of no more than 2 over the standard state fugacity. In the second process:

$$\Delta F = RT \ln a_{H_2O}\,(^{\text{soln}}_{\text{1000 atm}}) = RT \ln \frac{f_{H_2O\ (\text{soln})}}{f_{H_2O\ (\text{pure})}}$$

The sum of these free energies would then correspond to the activity of water in the solution at 1000 atm. referred to the proper standard state.

$$\Delta F = RT \ln a_{H_2O}\,(^{\text{soln}}_{\text{1000 atm}}) = RT \ln \frac{f_{H_2O\ (\text{soln})}}{f^\circ_{H_2O}}$$

The decrease in fugacity or activity occasioned by the transport of water from the pure state to the solution would be small. From these considerations it would be expected that the activity of water in the experimental solutions would be less than 2, and possibly slightly less than 1 in the more concentrated solutions.

The above discussion could have been based upon any standard state for water. Plausible alternatives would have been pure gaseous water at 1 atm. pressure or water at 1000 atm. pressure. If the gas standard state were chosen, the activity change from H_2O (g, 1 atm.) to H_2O (g, 1000 atm.) could be calculated from known fugacity coefficients of water (Holser, 1954).

Consideration of a_{H_2O} helps explain the difference in curvature of the equilibrium constant curves below 350°C. Figure 2 is a plot of the K values

in which the a_{H_2O} for the mica-kaolinite reaction is assumed to be 1. The latter curve appears to be essentially the metastable extension of the mica-pyrophyllite-boehmite curve below 350°C, and suggests that the true curve should have a break in slope and trend somewhat to the right. Holser's data indicate that the fugacity of water at 200°C and 1000 atm. is only 21, as compared to 109 at 300°C. Thus, when relatively smaller activities of water are substituted into the expression for the equilibrium constant at lower temperatures, the constant is increased and the curve shifted relatively to the right. At the transition temperature, unless the activity of water happened to be unity, the two curves would be somewhat displaced from one another. The dashed curve illustrated would correspond to $a_{H_2O} = 0.87$ at 200°C and $a_{H_2O} = 1$ at 350°C. Exact parallelism of the curves would not be expected, since that would imply identical heats of reaction.

Free Energy and Heat of Reaction

Values for the standard heats of reaction for the results at 15000 psi are given by the curves shown in figure 6. These are derived from the relation

$$\left(\frac{\partial \ln K}{\partial T}\right)_{P,M} = \frac{\Delta H^\circ}{RT^2}$$

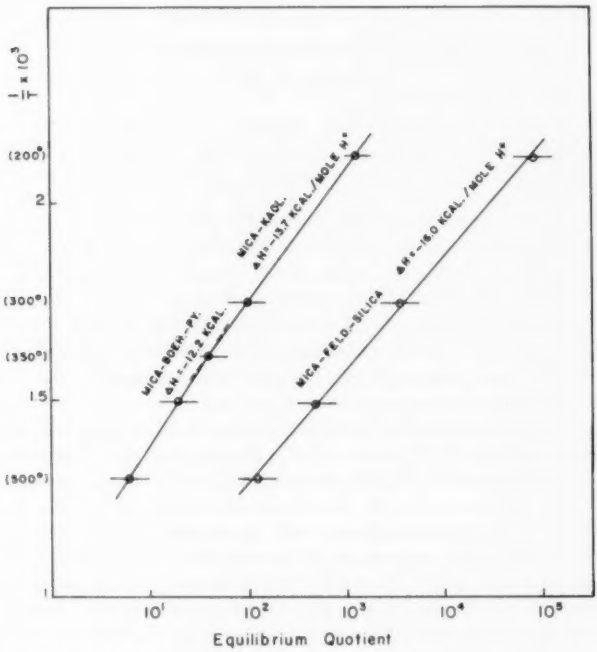

Fig. 6. Plot of the equilibrium quotient versus the reciprocal of the absolute temperature.

The heats of reaction are exothermic, as would be expected for hydration or hydrolysis reactions. The units are kcal/mole H^+. These results are based on the assumption that the equilibrium quotient is a close approximation of the equilibrium constant of the reactions as already discussed. The uncertainty indicated would correspond to an experimental reproducibility of $10^{\pm 0.2}$ in the equilibrium constant.

Although the mica-kaolinite curve is plotted on the assumption of $a_{H_2O} = 1$, a small break in slope is indicated at the kaolinite decomposition temperature. A more pronounced change in slope, which for example would correspond to the dashed curve of figure 2, is probably correct. This would imply a more negative heat of reaction.

Standard free energies of reaction are tabulated in table 6 as given by the relation

$$\Delta F^\circ = -RT \ln K$$

The free energy drive for hydrolysis decreases with increase in temperature. The standard entropy change is obtained from the free energy and enthalpy values. Average values of –11.3 and –14.8 cal/mole/deg. are indicated for the hydrolysis of K-feldspar and mica respectively. The dashed mica-kaolinite curve would correspond to a more negative entropy of reaction.

TABLE 6

Standard Free Energy of Reaction
kcal/mole H^+

	200°	300°	400°	500°
K-feld.-Mica-SiO_2	–10.6 ± 0.43	–9.30 ± 0.52	–8.31 ± 0.61	–7.42 ± 0.71
Mica-Kaolin; etc.	–6.70 ± 0.43	–5.24 ± 0.52	–4.00 ± 0.61	–2.83 ± 0.71

At 25°C the standard entropy change for the hydrolysis reactions can be estimated by procedures such as those described by Latimer (1952). The values obtained, however, are rather uncertain in the case of the present reactions involving hydrated silicate minerals. A point that might be mentioned is that the standard entropy change for these reactions at room temperature is positive. This positive change in entropy becomes negative at higher temperatures. This is accomplished by the relative increase in $\Delta\bar{C}p$ for HCl in the mixed electrolyte as the temperature increases.

Thermodynamic relations between K-feldspar, mica and kaolinite at 25°C have been considered by Garrels (1957). On the basis of field relations and hydrolysis experiments on K-feldspar and mica, equilibrium constants of $10^{7.5}$ and $10^{6.5}$ were proposed for the hydrolysis of K-feldspar and K-mica respectively. These are minimum values, with an estimated uncertainty of about $10^{0.7}$ in the equilibrium constant or 1 kilocalorie in the standard free energy of reaction per mole of H^+. It can be seen in figure 2, or in an extrapolation of the curves for the heat of reaction,[4] that the mica-kaolinite curve would extrapolate to approximately the value proposed by Garrels. The K-feldspar hydrolysis curve would extend to a value somewhat higher than that given by Garrels. The discrepancy in this instance suggests an error of about 2 kilo-

calories in Garrels' values. The agreement between Garrels' values and the results of the present experimentation is satisfactory.

Measurements of activity coefficients at moderately low temperature-pressure conditions are very much needed. They would be of great value inasmuch as the rate of change in the thermodynamic properties of these electrolyte solutions is rapid in this low temperature range.

Phase Relations

Mineral Phases.—These relations in the system K_2O—Al_2O_3—SiO_2—H_2O are simply stated. In the hydrolysis of K-feldspar to mica plus silica the minimum number of components is 4. These may be taken as K-feldspar, mica, silica, water or K_2O, Al_2O_3, SiO_2, and H_2O. Applying the phase rule, the variance $w = 4-4+2 = 2$. At a given temperature, the system will be at equilibrium over a range of pressures, or at a given pressure over a range of temperatures. If the temperature and pressure are fixed the system will attain equilibrium at a unique K^+/H^+ ratio and unique concentration of KOH. If chloride is added to the system a new component is introduced. This will increase the variance to 3. Here, in order to define the composition of the aqueous phase the concentration of either KCl, HCl, or total chloride must be specified, even though the K^+/H^+ ratio will be the same as in the previous case at a given temperature and pressure.

The same type of analysis applies to all of the assemblages encountered in this study. For mica-kaolinite-water only 3 phases exist, which would imply a variance of 3. Here, however, the number of independently variable oxide components can be reduced to 3 because of the restriction of the same ratio of Si/Al in the mica and kaolinite. Addition of acid increases the number of components in the same manner as discussed above. In the thermal decomposition of muscovite to K-feldspar plus corundum, on the other hand, the system has a variance of only 1. A univariant dehydration curve describes this type of reaction, but the curve is not unique if added electrolytes are present.

The activities of Al_2O_3 and SiO_2, as well as those of the other components, are fixed at a given pressure, temperature and total chloride concentration. Addition of alumina to the K-feldspar-mica-silica assemblage, for example, would only produce more mica at the constant K^+/H^+ ratio. If added to the mica-kaolinite reaction it would simply precipitate as excess alumina. In this connection it is of interest that in the hydrolysis of mica to kaolinite in the more saline solutions a small amount of boehmite appears with kaolinite in the reaction product. This superimposed reaction results from greater solubility of silica under these conditions, but it does not affect the equilibrium constant for the reaction under consideration.

A point of special interest is the question of equilibrium between assemblages at the thermal breakdown of kaolinite to pyrophyllite plus boehmite. Here 5 phases would be in equilibrium and $4-5+2 = 1$. At a given pressure there would be only one temperature, the thermodynamic decomposition temperature of kaolinite, at which all of the phases could exist in equilibrium. In

[4] These do not extrapolate as straight lines, but must steepen in slope at lower temperatures consistent with the entropy change already noted.

this instance the activity of water is particularly important, for it determines the decomposition temperature of kaolinite at any given salt concentration. Increasing the concentration of dissolved electrolyte decreases the activity of water and lowers the decomposition temperature.

The temperature of decomposition of kaolinite at 15000 psi pure water pressure was not established in the present study. Conclusions as to the decomposition temperature of kaolinite in the electrolyte solutions are based on the points at 352°±5°C shown in figure 1. These results incidentally, are consistent with the experimental results of Gruner (1944). The decomposition temperatures of kaolinite in the 2m and 4m KCl solutions are indicated only diagramatically and may be somewhat lower, especially in the 4m KCl solution. Roy and Osborn (1954) and Sand (1956) found that kaolinite decomposes at 400-405°C at 15000 psi water pressure. The product, a material which does not occur in nature, was named hydralsite by Roy and Osborn. Pyrophyllite also was generally present. Hydralsite was not observed in the present experimentation using electrolyte solutions.

KCl—H_2O System.—Phase relations in the KCl—H_2O system are important to the experimentation. These are described in other papers. Keevil (1942) determined the solubility curve and saturation vapor pressures in the system KCl—H_2O up to 600°C. A paper by Copeland, Silverman and Benson (1953) on the system NaCl—H_2O describes phase relations at low concentrations in the supercritical region.

Effect of Composition

This experimental work has been concerned exclusively with the evaluation of certain mineralogical equilibria in which pure solid phases in the system K_2O—Al_2O_3—SiO_2—H_2O are involved. If, as would occur in nature, other components are present that would enter the reaction, equilibria would be correspondingly changed. For instance, a small amount of Na in the K-feldspar would result in a correspondingly small change in the equilibrium constant for hydrolysis to mica, and any change in the composition of the resulting mica would have a similar effect. The magnitude of an equilibrium constant expresses the free energy change of a reaction, and therefore any change in the free energies of formation of any of the reactant and product phases must affect its value. For the hydrolysis of K-feldspar to mica + silica the equilibrium expression now becomes $\frac{a_{\text{mica}}\, a_{K^+}}{a_{\text{K-feldspar}}\, a_{H^+}}$. With only small changes in the composition of the solids the equilibrium constant would be but little affected.

GEOLOGICAL APPLICATIONS

In the applications of the experimental results to geological problems the ratio of the activity of aqueous potassium to the activity of acid in the hydrolysis reactions for K-feldspar and mica will be referred to simply as the K^+/H^+ ratio. From the standpoint of the effect of solution composition on stability relations this quantity is the important thermodynamic consideration, regardless of what species of acids or potassium compounds may actually be

present in the natural system. The equilibrium K^+/H^+ values are, of course, independent of the H^+ activity of the solution, its acid or basic character. The geologic applications of the present experimentation have been, for the most part, stated or implied in discussions on previous pages of the several equilibria and equilibrium curves. Only a review of some of the salient points is appropriate here.

Hydrothermal Processes

In the experimental curves of figure 2 it is observed that the equilibrium K^+/H^+ ratios trend toward higher acidities at higher temperatures. This slope means that the potential of hydrothermal solution to alter its wall rock as it ascends from environments of higher temperature would not necessarily diminish as its temperature falls. In fact, that ability would increase if the rate of migration were sufficiently rapid in comparison with the rate of reaction with the wall rock. In order to avoid confusion one should distinguish two different vantage points of analysis (Meyer, 1950), that which transpires at any given point in the vein or system with the passage of time, and that which takes place in an increment of solution as it rises from depth to higher levels. Considering first the solution, three competing processes would operate, (1) as the temperature falls the reactive potential of the solutions would increase due to the negative slope of the equilibrium curves and, at higher temperatures, the increase in dissociation of the acid components, (2) increased reaction with the wall rocks would tend to compensate for the increased reactivity of the solutions, (3) lower temperature would result in lower rates of reaction. The net effect would be a complex combination of these processes. It is at once apparent that the total amount of alteration in a hydrothermal system would be small at points representing the two extremes of very high and very low temperature, with maximum alteration somewhere in between. At any intermediate point conditions would change with time. In detail this change would be a function of many factors such as rates of reaction, fluid flow, heat transfer and diffusion, even assuming for the moment constant composition of solutions at "source". The over-all effect, however, would be increased reaction with the wall rock with falling temperature which would tend to maintain the K^+/H^+ ratio at an equilibrum value. Continuous leaching and steadily increasing chemical insulation in the walls along the preceding path, on the other hand, would tend to produce a gradual decrease in the ratio. But a smaller ratio again means greater reactivity of the solutions. In this way the system would constantly seek to establish equilibrium at every point along its path, in accordance in fact with the principle of Le Chatelier.

The above mentioned process of progressive chemical insulation might be accompanied by a similar thermal effect. A rising temperature at any level would tend to counteract any increased reactive potential of the solutions. Similarly, from the pressure experiments it is apparent that decreasing pressure would tend to compensate for the effects of decreasing temperature. In figure 4 the displacements of the equilibrium curves by pressure show that an increase in pressure increases the extent of hydrolysis whereas a decrease in pressure shifts the equilibria in the opposite direction. If pressure effects were

dominant at any point, as would very likely be the case for surface or near-surface processes, the result would be deposition rather than alteration. This, then, is a logical source of the adularia observed in some hot springs and "shallow" precious metal vein deposits.

The experimental results have considerable application in the interpretation of alteration zoning and the development of various alteration patterns. These problems, however, have been more fully discussed in another paper (Meyer and Hemley, 1957).

Metamorphism

Some implications of the experimental results to rock metamorphism might also be noted. Metamorphic and hydrothermal effects are, of course, gradational. The same chemical stability relations apply to mineral genesis in either instance.

The appearance of the assemblage muscovite-chlorite or muscovite-biotite, often together with albite-epidote, is one of the first changes to occur in the development of low grade regional metamorphism. If this transition is considered the lower limit of the Greenschist facies, it is clear that its position would be a function of the K^+/H^+ ratio of the environmental solutions as well as the pressure-temperature conditions. At higher K^+/H^+ ratios the facies boundary would shift to lower temperatures.

At higher temperatures these equilibrium ratios or constants are likewise an intrinsic part of the mineralogical equilibria. In the Amphibolite facies, for example, two important general groups of assemblages containing excess silica may be designated. These are defined as containing an excess and a deficiency respectively of K_2O (Turner and Verhoogen, 1951, p. 448). In the former, K-feldspar co-exists with muscovite, whereas in the latter andalusite or andalusite plus muscovite is observed. This relationship is consistent with the equilibrium curves of figures 1 and 2. The muscovite-andalusite and muscovite-K-feldspar curves are separated, with the feldspar incompatible with andalusite. The metamorphic processes responsible for the development of these two metamorphic assemblages, were therefore characterized by different K^+/H^+ ratios. Thus, in addition to the difference in K_2O content of the rocks as they now appear, the andalusite bearing assemblage could be described as the result of processes operating in a lower range of K^+/H^+ values. The converse would be true of the other assemblage. In this way the investigation of chemical equilibria of the type considered in the present study would be helpful in the analysis and interpretation of various metamorphic problems.

FUTURE WORK

There are a great many possibilties for continued research along these lines. These would include fundamental studies of electrolyte solutions at elevated temperatures and pressures, expansion of the experimental system to include more components, and kinetic studies on alteration reactions.

Mineralogical equilibria with $Na_2O—CaO—Al_2O_3—SiO_2—H_2O$ and $K_2O—MgO—Al_2O_3—SiO_2—H_2O$ as components of the alteration system are currently being studied. The alteration and stability of plagioclase of varied

composition as a function of pressure, temperatures and chemical environment is of course a problem of major geological importance. Similarly, equilibria between possible alteration products such as montmorillonite, paragonite, and zeolites are of interest. In the alteration system containing MgO—K_2O, stability relations involving phases such as phlogopite, chlorite, and serpentine are analogous problems that need to be investigated.

ACKNOWLEDGMENTS

Financial assistance for this investigation was rendered by the National Science Foundation (Grant No. 568, Meyer) and by the American Research Institute. The work was conducted in association with Professor Charles Meyer of the Department of Geology, University of California. I am deeply grateful to Professor Meyer and to the Department of Geology for the opportunity to undertake this study and for their assistance in innumerable ways throughout the course of the work. Sincere appreciation is expressed to Professor Leo Brewer of the Department of Chemistry, University of California. The interest and assistance of Professor Brewer contributed greatly to the investigation. I would also like to thank John Verhoogen and R. M. Garrels, and also Professor R. H. Powell of the Department of Chemistry, University of California, for many valuable comments and criticisms. Equipment for the study was made by Mr. Stanley Chebul of the Department of Geology, University of California, using the shop facilities of the Division of Mineral Technology.

REFERENCES

Copeland, C. S., Silverman, J., Benson, S. W., 1953, The system NaCl—H_2O at supercritical temperatures: Jour. Chem. Physics, v. 21, p. 12-16.

Clark, S. P., Jr., Robertson, E. C., and Birch, Francis, 1957, Experimental determination of kyanite-sillimanite equilibrium relations at high temperatures and pressures: Am. Jour. Sci., v. 255, p. 628-640.

Dorsey, E. E., 1940, The properties of ordinary water substance: Am. Chem. Soc. Monograph Series: New York, Reinhold Publ. Corp.

Folk, R. L., 1947, The alteration of feldspar and its products as studied in the laboratory: Am. Jour. Sci., v. 245, p. 388-394.

Frank, E. U., 1956, Hochverdichteter wasserdamf, I. Electrolytische leitfahigkeit in KCl—H_2O losungen bis 750°C: Z. Physik. Chem., v. 8, p. 92-106.

II. Ion dissoziation von KCl in H_2O bis 750°C., ibid, p. 107-126.

III. Ion dissoziation von HCl, KOH und H_2O in uberkritischem wasser, ibid, p. 192-206 .

Garrels, R. M., 1957, Some free energy values from geologic relations: Am. Mineralogist, v. 42, p. 780-791.

Gruner, J. W., 1944, Hydrothermal alteration of feldspars in acid solutions between 300° and 400°C: Econ. Geol., v. 39, p. 578-589.

Harned, H. S., and Owen, B. B., 1958, The physical chemistry of electrolytic solutions, 3d ed.: New York, Reinhold Publ. Corp.

Holser, W., 1954, The fugacity of water at high temperature and pressure: Jour. Phys. Chem., v. 58, p. 316-318.

Keevil, N. B., 1942, Vapor pressures of aqueous solutions at high temperatures: Jour. Am. Chem. Soc., v. 64, p. 841-850.

Kelley, K. K., 1949, Contributions to data on theoretical metallurgy: U. S. Bureau Mines Bull. 476.

Kennedy, G. C., 1955, Pyrophyllite-sillimanite-mullite equilibrium relations to 20000 bars and 800°C, (abstract): Geol. Soc. America Bull., v. 66, p. 1584.

Latimer, Wendell, M., 1952, Oxidation potentials, 2d ed.: New York, Prentice-Hall, Inc.

Lewis, G. N., and Randall, M., 1923, Thermodynamics and the free energy of chemical substances: New York, McGraw-Hill Book Company, Inc.

Lietzke, M. H., 1955, The hydrogen-silver chloride electrode system at high temperatures: Jour. Am. Chem. Soc., v. 77, p. 1344-1346.

Meyer, Charles, 1950, Hydrothermal wall rock alteration at Butte, Montana: Ph.D. thesis, Harvard University.

Meyer, Charles, and Hemley, J., 1959, Alteration in some granodiorites: London, Pergamon Press, Sixth National Clay Conference Proc.

Morey, G. W., and Chen, W. T., 1955, The action of hot water on some feldspars: Am. Mineralogist, v. 40, p. 996-1000.

Morey, G. W., and Ingerson, E., 1937, The pneumalolytic and hydrothermal alteration and synthesis of silicates: Econ. Geol., v. 32, p. 607-761.

Noll, W., 1936, Uber die bildungsbedingungen von kaolin, montmorillonit, sericit, pöryphyllit und analcim: Mineralog. u. Petrog. Mitt., v. 48, p. 210-247.

Norton, F. G., 1939, Hydrothermal formation of clay minerals in the laboratory: Am. Mineralogist, v. 24, p. 1-17.

Roy, D. M., and Roy, R., 1955, Synthesis and stability of minerals in the system MgO—Al_2O_3—SiO_2—H_2O: Am. Mineralogist, v. 40, p. 147-178.

Roy, R., and Osborn, E. F., 1954, The system Al_2O_3—SiO_2—H_2O: Am. Mineralogist, v. 39, p. 853-885.

Sand, L. B., Roy, R., and Osborn, E. F., 1957, Stability relations of some minerals in the Na_2O—Al_2O_3—SiO_2—H_2O system: Econ. Geol., v. 52, p. 169-179.

Stringham, Bronson, 1952, Fields of formation of some common hydrothermal alteration minerals: Econ. Geol., v. 47, p. 661-664.

Turner, F. J., and Verhoogen, J., 1951, Igneous and metamorphic petrology: New York, McGraw-Hill Book Company, Inc.

Tuttle, O. F., 1949, Two pressure vessels for silicate water studies: Geol. Soc. America Bull., v. 60, p. 1727-1729.

Yoder, H. S., and Eugster, H. P., 1955, Synthetic and natural muscovites: Geochim. et Cosmochim. Acta, v. 8, p. 225-280.

[American Journal of Science, Vol. 257, April 1959, P. 271-275]

THE MAGNETIC FIELD IN A PRIMARY METEORITE BODY

JOHN F. LOVERING

Dept. of Geophysics, Australian National University, Canberra, Australia

ABSTRACT. The magnetic properties and mineralogical composition of the Moore County eucrite indicate that, while situated within about 10 km of the surface of the silicate mantle of a primary meteorite body, this meteorite cooled through the Curie temperature of its magnetic constituents (about 560°C) *while in a magnetic field*. If this field associated with the primary body was generated within a fluid metallic core, then at this time temperatures within the core must have been greater than about 1700°C. Furthermore the inclination of the direction of magnetization with the horizontal plane of crystal layering observed in the meteorite suggests that the Moore County eucrite formed close to either the 10°N or 10°S magnetic latitude of the primary body.

INTRODUCTION

The most promising explanations of the Earth's magnetic field invoke the action of hydrodynamical motions within its conducting fluid core (Hide, 1956). As it appears that iron meteorites formed by the solidification of an originally fluid metallic core within a primary meteorite body (Lovering, 1957a) it is not unlikely that a magnetic field was also associated with the primary body.

A preliminary study was made of the magnetic properties of various primary meteorites to see if any evidence could be found of the existence of a magnetic field in the primary body. Those primary meteorites containing a considerable proportion of iron-nickel metallic phases (i.e. iron meteorites and pallasites) were all found to have relatively low remanent magnetic intensities (table 1) comparable to those acquired by nickel-iron alloys in the Earth's field. These meteorites have also been shown to be magnetically "soft" (F. D. Stacey, personal communication) so that their observed remanent magnetic intensities were probably acquired in the terrestrial field after they had fallen on the Earth's surface.

Certain achondritic stony meteorites (i.e. the eucrites or basaltic achondrites) have apparently crystallized in the outer regions of the silicate mantle of the primary body. These meteorites have compositions and textures very similar to those of certain terrestrial basic igneous rocks, such as basalts and particularly dolerites, whose magnetic properties are widely used to determine terrestrial palaeomagnetic fields. Probably the most intensively studied of these achondrites is the Moore County eucrite (Hess and Henderson, 1949) and it was this meteorite which was selected for the present study.

REMANENT MAGNETIZATION OF THE MOORE COUNTY EUCRITE

A fragment of the Moore County eucrite was found to have a remanent magnetization with an intensity (table 1) similar to that of the lowest values observed for Cenozoic basic igneous rocks which have cooled through their Curie temperatures in the Earth's magnetic field. The magnetic constituents of the Moore County eucrite make up less than 2.5 percent of the meteorite and a preliminary thermomagnetic study indicates that there are two main components contributing to its remanent magnetization. The magnetically most important phase is magnetite with a Curie temperature of about 560°C while there are minor metallic phases which are probably demagnetized or only weakly magnetic by analogy with the iron meteorites.

The most likely way in which the Moore County eucrite could have ac-

TABLE 1
Remanent Magnetic Intensities of Some Primary Meteorites

Type	Name	Classification	Nickel content of Metal Phase* (%)	Remanent Magnetic Intensity (10^{-5}c.g.s. per cc.)
Iron Meteorites	Mount Stirling	Coarse octahedrite	6.93	16.1
	Kyancutta	Medium octahedrite	8.28	22.0
	Mungindi No. 2	Fine octahedrite	12.36	60.3
	Santa Catherina	Nickel-rich ataxite	33.60**	439.0
Stony-Iron Meteorites	Bendock	Pallasite (metal phase only)	9.20	70.5
Stony (Achondritic) Meteorites	Moore County	Eucrite	—	5.0

* Lovering, et al. (1957). ** This work.

quired its observed remanent magnetization is by cooling through the Curie temperature of its constituent magnetite (560°C) while situated in a magnetic field and presumably while still forming part of the outer mantle of the primary body. An important corollary is that while the metal core of the primary body was at some temperature above that of the lowest melting point iron-nickel alloy within the core [i.e. greater than about 1700°C, assuming maximum core pressures of about 10^4 to 10^5 atmospheres (Lovering, 1957b)] and thus still at least partially fluid and capable of field producing motions, the outer silicate mantle had crystallized and cooled to a temperature of below 560°C. This conclusion provides important data concerning the cooling history of the primary body as well as its internal temperature distribution. However it does not agree with the conclusions of a study of the Moore County eucrite by Hess and Henderson (1949). They found that the lowest temperature reached by the meteorite in the mantle of the primary body and immediately prior to its disruption was about 1135 ± 65°C. This figure was based on two observations; firstly, the limited (about 11 percent) inversion of the pigeonitic pyroxene to hypersthene and secondly the occurrence of tridymite in the Moore County. However it is well established that the presence of impurity ions can buttress the tridymite lattice and prevent its transformation to quartz when the temperature is lowered (Eitel, 1954). Since the tridymite in the Moore County meteorite is interstitial and evidently the last of the essential constituents to crystallize, it may well contain a relatively high content of impurity ions. In point of fact Hess and Henderson (1949) have reported that the tridymite in the Moore County meteorite is crowded with minute inclusions, indicating a high impurity content in the silica. Thus the presence of tridymite in the Moore County eucrite gives no unequivocal data concerning the cooling history of the meteorite. However it does tell us something of the pressures operating on this meteorite in the mantle of the primary body. It has been calculated from thermodynamic data (Mosesman and Pitzer, 1941)[1] that the stability field

[1] An experimentally derived pressure-temperature diagram for SiO_2 has recently been published by O. F. Tuttle and N. L. Bowen (1958) which is considerably different from the diagram derived by Mosesman and Pitzer (1941) on the basis of thermodynamic calculations. The experimental diagram indicates that tridymite is stable up to pressures of about 7900 atmospheres rather than 650 atmospheres given by the theoretical calculations. Tuttle and Bowen conclude that at present it is not possible to decide which diagram is correct but on the basis of their experimental results it would appear that the Moore County eucrite may have formed at depths of up to 40 km in the mantle of a primary meteorite body.

of tridymite disappears at pressures above 650 atmospheres. Above this pressure liquid silica crystallizes to cristobalite and above 1, 160 atmospheres cristobalite is no longer stable and only quartz crystallizes. If the primary meteorite body had interior pressures of between 10^4 and 10^5 atmospheres (Lovering, 1957b) then a pressure of 650 atmospheres would correspond to a depth of about 10 km in the mantle of such a body. The existence of tridymite in the Moore County eucrite suggests that this meteorite formed within about 10 km of the surface of the primary body, provided that impurities have little effect on the pressure above which tridymite is unstable.

The evidence of the apparently restricted inversion of the pigeonite in the Moore County eucrite is still considered by Dr. H. H. Hess (personal communication) to be indicative of rapid chilling from a temperature of about 1135°C after it became a meteorite. Brown (1957) has studied the pyroxenes of the Skaergaard intrusion and has shown how uninverted and partially inverted pigeonite need not have been due to rapid cooling of the magma, but rather to the sluggishness of the inversion of the intermediate and ferri-ferrous pigeonites at a stage when an appreciable time interval separates the temperatures of crystallization and inversion. The Moore County eucrite has already been shown to have formed in the outer regions of the mantle of the primary body and its partially inverted pigeonite has a composition $Ca_5\ Mg_{47.5}\ Fe_{47.5}$ (Hess and Henderson, 1949). From Brown's conclusions it would not seem at all unlikely that the pigeonite of the Moore County eucrite could have remained only partially inverted even after cooling to temperatures below 500°C before the primary body was disrupted.

SITE OF CRYSTALLIZATION OF THE MOORE COUNTY EUCRITE

Hess and Henderson (1949) have reported that the pyroxene and plagioclase crystals in the Moore County eucrite show a distinct planar dimensional orientation. They found a tendency towards a weak linear orientation of the c-axes of the pyroxenes in this plane and from these observations concluded that the fabric of this meteorite suggests it was formed by the settling of plagioclase and pyroxene crystals to the floor of a magma chamber where they accumulated in nearly horizontal layers. Consequently in the Moore County eucrite the plane of layering of the crystals approximates a plane perpendicular to the radius of the primary body at the site of crystallization of the meteorite. If it is assumed that the magnetic field in the upper mantle of the primary body was dipolar, like the Earth's field, then the angle between this plane and the direction of magnetization in the meteorite will be the magnetic inclination of the field at this place and can be used to calculate the magnetic latitude of the site of crystallization of the meteorite.

The direction of magnetization of a slice cut from the Moore County eucrite was determined by a well established procedure (Collinson, et al., 1957) and then the same slice was made into a thin section so that the orientation of the place of crystal layering could be determined relative to the direction of magnetization. The orientation of the c-axes of 34 pyroxenes was determined on the universal stage and the results are plotted stereographically in figure 1. The c-axes of the pyroxenes lie in a plane at 90° to the plane of the thin sec- percent are {100} sections and 11 percent {001} sections. However the most important observation is thate the poles of almost all the sections lie in the plane of layering LL′ given by the pyroxenes, confirming a planar dimensional

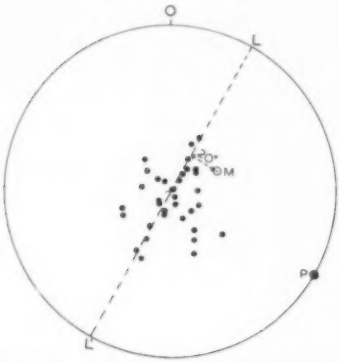

Fig. 1. Stereographic projection of c-axes of 34 pyroxenes relative to the plane of the thin section. (Inclination of direction of magnetization M to the plane of layering LL′ with pole P is 20°)

orientation of the pyroxene and plagioclase crystals in the Moore County eucrite. A minor point of interest is the observation that the preponderance of {010} sections in the thin section studied indicates a tendency towards a lineation of the plagioclase crystals. Hess and Henderson (1949) observed a similar weak lineation of the longest axes (i.e. the c-axes) of the pyroxenes. They also tion. This plane of layering would appear to correspond to that found by Hess and Henderson (1949) although our section seems to have been cut at about 90° to the plane of their section.

In figure 2, the orientation of 35 plagioclase crystals in the thin section has been plotted, from which it appears that 66 percent are {010} sections, 23 found that the b- and c-axial directions in the plagioclase crystals were elongated so that most of the crystals were lying with their {100} faces in the plane of layering. The orientations found in the present study are in accord with this conclusion.

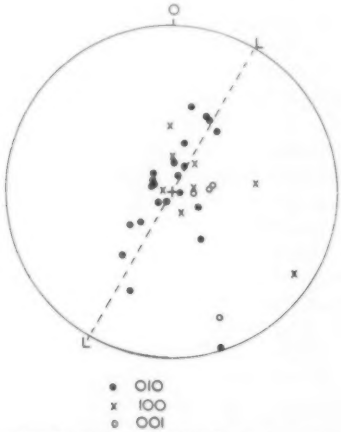

Fig. 2. Poles of the {010}, {100}, and {001} plagioclase faces plotted on the plane of the thin section. (LL′ is the plane of layering of the c-axes of the pyroxene defined in figure 1)

The direction of magnetization (M) in the thin section has been plotted in figure 1 and is inclined at an angle of about 20° to the plane of crystal layering in the section, giving a "geomagnetic" latitude of either 10°N or 10°S for the site of crystallization of the Moore County eucrite in the primary body.

CONCLUSION

The remanent magnetization observed in the Moore County eucrite suggests that while the meteorite formed part of the outer silicate mantle of the primary meteorite body it cooled through the Curie temperature of its most important magnetic constituent magnetite (560°C) under the influence of a magnetic field. Furthermore the Moore County eucrite would have cooled below this temperature (i.e. 560°C) while the metal core of the primary body was still at least partly fluid and capable of generating a magnetic field. From these conclusions it can be estimated that the temperature within the core at this time must have been at least 1700°C.

The site of crystallization of the Moore County eucrite within the outer silicate mantle of the primary body can be estimated in two ways. Firstly, the existence of tridymite in the meteorite suggests that it probably crystallized within about 10 km of the surface of the body. Secondly, the inclination of the direction of magnetization in the eucrite to its plane of crystal layering (i.e. the horizontal plane at the site) suggests that the meteorite formed close to either the 10°N or the 10°S magnetic latitude of the primary body.

ACKNOWLEDGMENTS

The assistance is gratefully acknowledged of Mrs. Kerry Lovering in determining the crystal orientations and of E. Irving and R. Green in measuring the magnetic properties of the meteorites. L. G. Parry determined the magnetic constituents of the Moore County as part of a joint programme to investigate the magnetic constituents of meteorites. Dr. H. H. Hess and Dr. E. P. Henderson very kindly critically read the manuscript and Dr. Henderson also provided the fragment of the Moore County eucrite used in this work.

REFERENCES

Brown, G. M., 1957, Pyroxenes from the early and middle stages of fractionation of the Skaergaard intrusion East Greenland: Mineralog. Mag., v. 31, p. 511-543.

Collinson, D. W., Creer, K. M., Irving, E., and Runcorn, S. K., 1957, Palaeomagnetic investigations in Great Britain I. The measurement of the permanent magnetization of rocks: Roy. Soc. London Phil. Trans., ser. A, v. 250, p. 73-82.

Eitel, W., 1954, The physical chemistry of the silicates: Chicago, Univ. of Chicago Press.

Hess, H. H., and Henderson, E. P., 1949, The Moore Co. Meteorite: A further study with comment on its primordial environment: Am. Mineralogist, v. 34, p. 494-507.

Hide, R., 1956, The hydrodynamics of the Earth's core *in* Physics and Chemistry of the Earth, v. 1: London, Pergamon Press, p. 94-137.

Lovering, J. F., 1957a, Differentiation in the iron-nickel core of a parent meteorite body: Geochim. et Cosmochim. Acta, v. 12, p. 238-252.

———, 1957b, Pressures and temperatures within a typical parent meteorite body: Geochim. et Cosmochim. Acta, v. 12, p. 253-261.

Lovering, J. F., Nichiporuk, W., Chodos, A., and Brown, H., 1957, The distribution of gallium, germanium, cobalt, chromium, and copper in iron and stony-iron meteorites in relation to nickel content and structure: Geochim. et Cosmochim. Acta, v. 11, p. 263-278.

Mosesman, M. A., and Pitzer, K. S., 1941, Thermodynamic properties of the crystalline forms of silica: Am. Chem. Soc. Jour., v. 63, p. 2348-2356.

Tuttle, O. F., and Bowen, N. L., 1958, Origin of granite in the light of experimental studies in the system $NaAlSi_3O_8$—$KAlSi_3O_8$—SiO_2—H_2O: Geol. Soc. America, Mem. 74, 153 p.

[American Journal of Science, Vol. 257, April 1959, P. 276-286]

PETROFABRIC STUDY OF CONESTOGA LIMESTONE FROM HANOVER, PENNSYLVANIA*

RICHARD P. NICKELSEN and GERARDO W. GROSS

Pennsylvania State University, University Park, Pa.

ABSTRACT. The study applies established techniques of calcite petrofabric analysis to a low-grade metamorphic, sandy-textured, carbonate rock. Prominent features of the fabric are overall monoclinic symmetry, postcrystalline late phase orthorhombic symmetry, and *ac* girdles perpendicular to megascopic fold axes. The fabric results from differently oriented episodes of orthorhombic movement the axes of which rotated through the rock during deformation. Compression axes causing late phase deformation are in the *ac* plane in zones approximately bisected by the normal to slaty cleavage.

INTRODUCTION

Experimental deformation of single crystals and aggregates of crystals of calcite has provided much data about the mechanical behavior of calcite under stress (Turner and Ch'ih, 1951; Borg and Turner, 1953). New methods of calcite petrofabric analysis and interpretation of fabric of naturally deformed marbles have resulted (Turner, 1953; McIntyre and Turner, 1953). The present work was done to: 1. extend these methods of analysis and interpretation to rocks of a different area that are of lower metamorphic grade than those previously studied; 2. describe and interpret the fabric of the Conestoga limestone. The Conestoga limestone was particularly suitable for this study because: 1. megascopic structures such as slaty cleavage, and bedding are well-developed at the outcrop and provide optimum conditions for correlating field and microscope data (fig. 1); 2. the rock is a coarse-grained calcarenite with calcite grains large enough for easy optical measurement (fig. 2). Most other limestones sampled in the Great Valley and western Piedmont proved too fine-grained for universal stage work.

ACKNOWLEDGMENTS

Kenneth E. Weaver, who mapped the Hanover area (1955), familiarized the writers with the regional geology and showed them the outcrop sampled. Dr. P. D. Krynine discussed the petrography of the rock with the writers and offered a number of helpful comments. Professor F. J. Turner kindly read and criticized a preliminary draft of this manuscript. Suggestions from graduate students who studied other specimens from the same locality in a course at Pennsylvania State University are also acknowledged.

LOCATION AND DESCRIPTION OF OUTCROP

The outcrop of Conestoga limestone sampled is 1.1 miles N 52 E of Hanover, Pennsylvania in a small abandoned quarry. It is the only outcrop in an 8 square mile area mapped as Conestoga limestone by Weaver (1955). The rock is a limestone conglomerate (boulders to 1 foot in diameter) with sandy beds and matrix of coarse-grained quartz and calcite. Other writers (Wise, 1953) described conglomerate near the base of the Conestoga limestone. This is the probable stratigraphic position of this conglomerate.

* College of Mineral Industries Contribution Number 58-45.

Fig. 1. Outcrop showing slaty cleavage (parallel to pencil) and bedding.

Southeast dipping bedding (S_1) is intersected by more steeply dipping slaty cleavage (S_2) (fig. 1). Pebbles and boulders of limestone are flattened in the slaty cleavage and elongated down the dip of the cleavage in the *a* fabric direction. Phyllites in the area contain a mineral assemblage characteristic of the green schist facies of metamorphism.

PETROGRAPHIC DESCRIPTION

Specimens for this study were selected from the calcarenite matrix and beds. Thin sections were cut in the fabric *ac* plane, perpendicular to intersections of bedding and slaty cleavage. In this plane all grains are elongated parallel to the trace of slaty cleavage, the *ab* fabric plane, and flattened normal to the cleavage (fig. 2). Long dimensions of grains measured .5 to 2.5 mm. Quartz was studied in both *ac* and *bc* cuts. The mean ratio of long axes (fabric *a*) to short axes (fabric *c*) in 50 grains was 3:1 for both calcite and quartz. In a *bc* cut the ratio of long axes (fabric *b*) to short axes (fabric *c*) was 1.9:1 and 2.2:1 for calcite and quartz respectively.

Essential components of the rock are quartz grains (38 percent), grains of fine to coarse crystalline calcite (40 percent), and aggregate grains of microcrystalline calcite (22 percent). Quartz is slightly strained, replaced at all boundaries by crystalline calcite, and contains deformation lamellae in 50 percent of the grains observed. Crystalline calcite is clear, fractured into slivers parallel to slaty cleavage and cut by one or more sets of deformation lamellae (see below). This material was originally clastic, sand-sized crystalline calcite (e.g. fossil fragments) and clear calcite cement. Aggregate grains of micro-

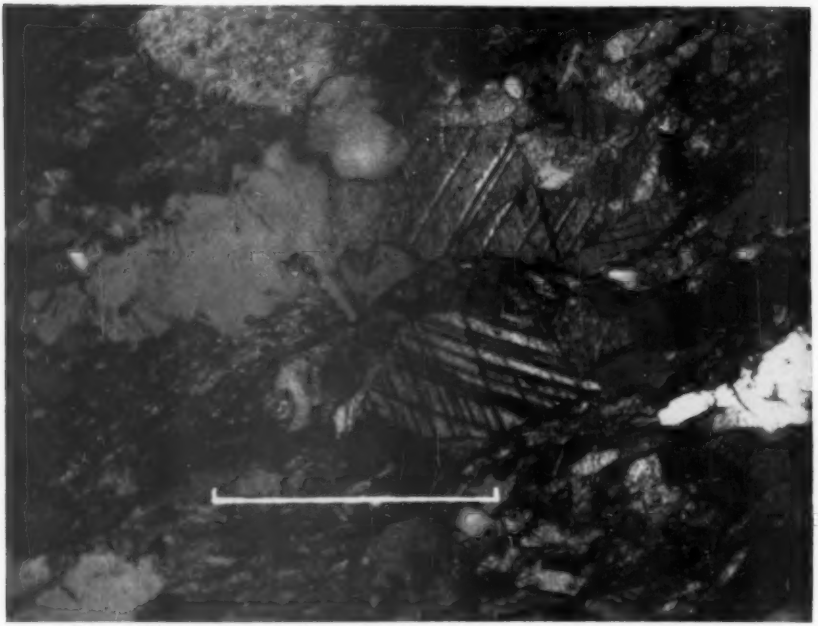

Fig. 2. Photomicrograph showing quartz, sand-sized crystalline calcite grains with deformation twins, and sand-sized aggregate grains of micro-crystalline calcite (NW and SW corners). Slaty cleavage is oriented NE-SW. White line represents 0.5 mm.

crystalline (.001 to .1 mm) calcite are sand-sized clastic fragments of very fine-grained lime mud.

METHOD OF PETROFABRIC STUDY

Measurement of orientation data in thin sections from two specimens (S-3 and S-18) was done on a Leitz 4-axis Universal Stage. Data were plotted on a Schmidt-Lambert equal area projection net of 20 cm diameter.

Using procedures described by Turner (1949, p. 595-602) the following data were measured in each calcite grain:

1. Orientation of the optic axis = c crystallographic axis [0001].
2. Orientation of poles of all sets of visible deformation lamellae. In these specimens they were all found to be lamellae parallel to $\{01\bar{1}2\}$ = e.

The following plots were made from the measured data:

1. Orientation of direction and sense of gliding in each $\{01\bar{1}2\}$ lamella. Glide line = [e:r] or $(01\bar{1}2) : (10\bar{1}1)$.
2. Orientation of the edge [e:e′] between any two $\{01\bar{1}2\}$ lamellae in one grain.
3. Axes of compression and tension most favorably oriented to have formed each $\{01\bar{1}2\}$ twin. These directions are inclined at 45° to the glide line [e:r], oriented so that gliding along the twin plane *e* would

occur in the sense required to produce twinning. (Turner, 1953, p. 282.)

It is important to differentiate {01$\bar{1}$2} lamellae into descriptive classes that are comparable with lamellae produced in experimental work (Turner, 1953; McIntyre and Turner, 1953; Borg and Turner, 1953, p. 1344-1346). When viewed in vertical position some lamellae of {01$\bar{1}$2} orientation appear as fine, dark lines that are not broad enough at 300 × magnification to show symmetrical differences in extinction with the parent grain. These are termed *nontwinned lamellae*. Other lamellae are clearly recognized as twins and are called *twinned lamellae*. Calcite grains studied have: no lamellae of any kind, one set of either nontwinned or twinned lamellae, 2 sets of either twinned lamellae or nontwinned lamellae, one set of twinned and one set of non-twinned lamellae. Table 1 shows the frequency of occurrence of the above classes. Although thin sections of only one orientation were studied, virtually all lamellae were seen because c-axes lie near the plane of the section.

TABLE 1

Percent Occurrence of Twinned or Nontwinned {01$\bar{1}$2} Lamellae Sets in Two Specimens Conestoga Limestone

Type and number of sets of lamellae in each grain	Spec. S-3	Spec. S-18
No lamellae of any kind	8	11
1 set, nontwinned lamellae	10	30.5
2 sets, nontwinned lamellae	1	10
1 set, twinned lamellae	43	30.5
2 sets, twinned lamellae	9	5.5
1 set twinned, 1 set nontwinned lamellae	29	12.5
	100%	100.0%

DESCRIPTION OF DIAGRAMS

Each writer analyzed one specimen independently and figures 3-12 show stereographic plots of data. Orientation of the plane of thin section is shown by the central strike and dip symbol in each diagram. Field orientation of the northwest end of the strike line is given by azimuth where 0° = N, 90° = E, 180° = S, 270° = W. Angles of dip from 1-90° represent planes dipping toward the observer and angles over 90° indicate planes dipping away from the observer (Cloos and Hietanen, 1941, p. 37). Traces of bedding (S_1) and slaty cleavage (S_2) and positions of *a*, *b*, and *c* fabric axes are shown.

Both specimens show a well developed *ac* girdle of calcite *c*-crystallographic axes (figs. 3 and 4) and of {01$\bar{1}$2} deformation lamellae (figs. 5 and 6). S-18 shows better concentrations of both c-axes and deformation lamellae than S-3. C-axis maxima occur near the trace of the bedding and also at a large angle to the traces of bedding and cleavage. In both specimens, deformation lamellae maxima occur in pairs approximately bisected by the normal to slaty cleavage (S_2). In S-18 an additional lamellae maximum is located in the bedding (S_1). Figures 7 and 8 show central maxima for [e:e′] edges. That these maxima are close to the fabric *b* axis is at least partially a consequence of the *ac* girdle of

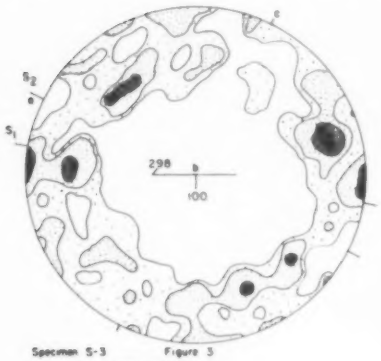

Specimen S-3 Figure 3
100 c-axes, contours-6,4,2,1 %

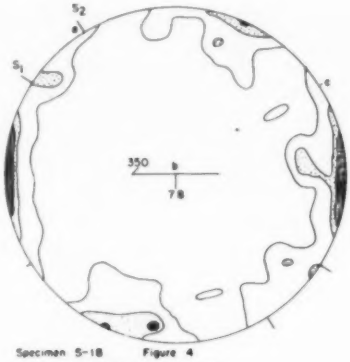

Specimen S-18 Figure 4
71 c-axes, contours- 9.8,7,4.2,1.4 %

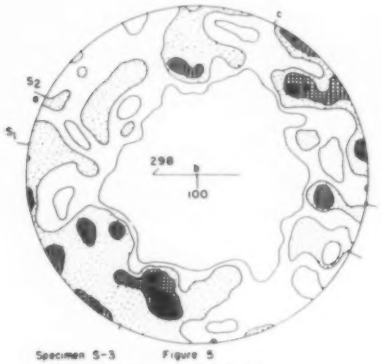

Specimen S-3 Figure 5
133 lamellae, contours- 4.5,3,1.5, 7 %

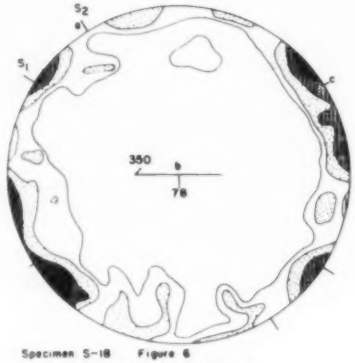

Specimen S-18 Figure 6
84 lamellae, contours- 7.2, 4.7, 2.4, 1.2 %

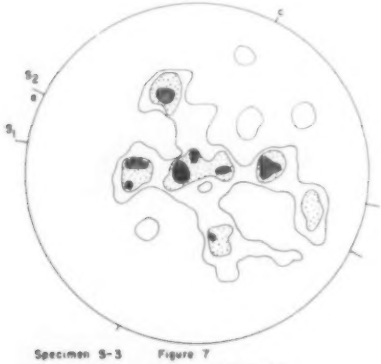

Specimen S-3 Figure 7
37 e:e' edges, contours- 10.8, 8, 5.4, 2.6 %

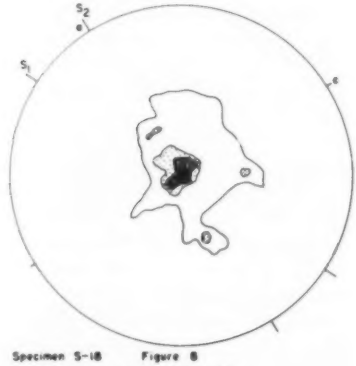

Specimen S-18 Figure 8
18 e:e' edges, contours- 22, 16, 11, 5 %

Figs. 3-8. Calcite c-axes, deformation lamellae and e:e′ edges. Note: Figures 3-14 are lower hemisphere projections of fabric data. Contours represent percent concentration of data in 1% areas.

c-axes and deformation lamellae. The more concentrated [e:e′] edge maximum of S-18 (fig. 8) is correlated with a narrow *ac* band of lamellae poles (fig. 6) while the more disperse [e:e′] edge diagram of S-3 (fig. 7) is correlated with a wide *ac* band of lamellae poles (fig. 5).

Figure 9 is a plot of 9 grains in which two twinned sets of deformation lamellae were observed in specimen S-3. There is a strong grouping of c-axes of these grains in the zone perpendicular to the direction of applied compres-

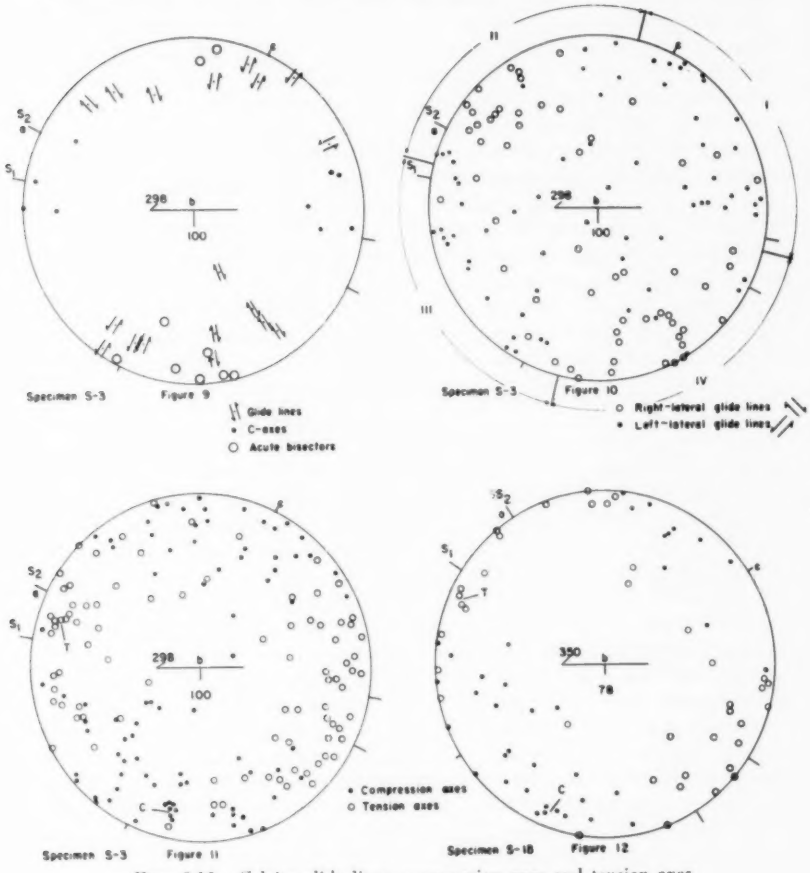

Figs. 9-12. Calcite glide lines, compression axes and tension axes.

sion shown in figure 11. Following Turner (1953, fig. 7) a plot of the bisector of the acute angle between glide lines [e:r] of adjacent twinned lamellae is also shown on figure 9. These bisectors lie close to the mean direction of applied compression shown in figure 11. Glide lines and sense of movement along them

are plotted in figure 9, where it is apparent that the mean compression direction (fig. 11) and grouping of bisectors separate zones of right lateral and left lateral twin gliding. Glide line orientation and relative slip direction along the glide line for all {01$\bar{1}$2} lamellae (both twinned and nontwinned) are shown in figure 10. Relative slip along glide lines has been classified as right lateral or left lateral with respect to the plane of the section, and the percent concentration of right lateral and left lateral gliding in two opposite quadrants bounded by diameters passing through mean compression and tension positions (fig. 11) has been computed. In quadrants II and IV, 79 percent of the right lateral and 31 percent of the left lateral glide lines occur, while in quadrants I and III, 69 percent of the left lateral and 21 percent of the right lateral glide lines occur (fig. 10).

The stress that would be most effective in causing twin gliding on each of the twinned lamellae in the two specimens is plotted in figures 11 and 12 as mutually perpendicular compression and tension axes, according to the method of Turner (1953, p. 282). Both diagrams show a broad zone of compression axes in a partial *ac* girdle symmetrically distributed about the normals to bedding and cleavage. Tension axes are most concentrated near the periphery in a narrower zone cut by the traces of cleavage and bedding. In figure 11 compression axes approach the center of the diagram from both peripheral concentrations suggesting a weak *bc* girdle. Maximum areas of concentration of compression and tension axes are marked C and T on both diagrams.

INTERPRETATION OF DIAGRAMS

Both indirect componental movements (recrystallization under stress) and direct componental movements (intragranular gliding, rupture and shear of grains, and rotation of grains) were probably effective in shaping the present fabric. The efficacy of each throughout the early stages of deformation can only be estimated; the role of posterystalline, direct componental movements near the end of deformation is shown by petrofabric analysis. Calcite lattice orientation developed before the posterystalline, direct componental movements which are recorded in the diagrams of deformation lamellae and glide lines. Lattice orientation may be the result of early sedimentary or diagenetic orientation, recrystallization under stress, or early direct componental movements, evidences of which have been destroyed by post-tectonic recrystallization. The possibility that the major part of the calcite lattice orientation is the result of sedimentary or diagenetic processes is ruled out by the marked relation between fabric axes and c-crystallographic axis orientation. Sedimentary or early diagenetic orientation may be responsible for the c-axis maximum in both figures 3 and 4 near the trace of bedding (S_1). Sander (1951, p. 38, 154) states that paradiagenetic calcite grows with c-axis parallel to bedding in Alpine Trassic limestones. The girdle of c-axes in the bedding produced by such growth could have been destroyed by later deformation except where the primary bedding girdle intersects the *ac* fabric girdle, thus giving rise to the maximum in the trace of bedding.

In strong experimental deformation the c-axes of calcite are brought into an apparently stable orientation at an angle of 10°-30° to the compression axis. (Turner, et al., 1956, p. 1284). This is the result of direct componental

movements without recrystallization. It has also been shown that syntectonic experimental recrystallization at 400° to 600° C. tends to align the c-axes of calcite parallel to the compression axis. (Griggs, et al., 1958, p. 48).

In S-3 and S-18 compression axes sweeping through the rock perpendicular to fabric *b* and passing through a number of different orientations at different times could explain the distribution of c-axes of calcite in an *ac* girdle (figs. 3 and 4).

Alternatively, radial compression perpendicular to fabric *b* may have caused the *ac* girdle of c-axes. MacDonald (1957) has predicted on thermodynamic grounds that radial compression should form a girdle of calcite axes in the plane of compression. However, the presence of maxima within the *ac* girdle seems to indicate a number of different episodes of compression in different orientations as suggested above. The effect of recrystallization under stress in producing preferred orientation of calcite lattices is not known.

Postcrystalline, late stage, deformation of the rock has produced deformation lamellae that may be interpreted dynamically. That this late deformation has had little effect upon pre-existing orientation of c-axes of calcite is shown in figure 9. C-axes of 9 grains showing 2 equally developed sets of twinned lamellae lie in a belt nearly perpendicular to the mean compression axis shown in figure 11. Obviously the original lattice orientation was the main factor controlling intensity of twin gliding. Other data shows that c-axes of grains with no deformation lamellae of any kind are all located in the direction of compression, a position where twin gliding on any of the potential {01$\bar{1}$2} twin glide planes would be impossible.

Although Turner and Ch'ih (1951, p. 902) have shown that concentrations of [e:e′] edges parallel axes of extension in experimentally deformed marbles, central maxima of [e:e′] edges in figures 7 and 8 do not necessarily warrant this interpretation. A peripheral girdle of c-axes would be expected to give rise to a central maximum of [e:e′] edges since c $\wedge$ e:e′ $\cong$ 70°. Close correlation between width of *ac* girdles of deformation lamellae poles and c-axes and spread of *b* maxima of [e:e′] edges when comparing figures 3, 5 and 7 and 4, 6 and 8 suggests that the degree of preferred calcite lattice orientation of the earlier fabric is largely responsible for [e:e′] edge concentrations.

Concentration of compression axes in a broad zone approximately perpendicular to cleavage (S_2) (figs. 11 and 12) agrees very well with observed flattening of grains, pebbles, and boulders in outcrop. Grouping of right lateral and left lateral glide lines show (fig. 10) the sense of movement that would be expected for the compression and tension axes plotted in figure 11. It is difficult to illustrate in a 2-dimensional figure the system of 3-dimensional movement along glide lines, but since glide lines most commonly plot near the periphery of the diagram the writers believe that most twin gliding had a large component of movement in the *ac* fabric plane. The distribution of compression and tension axes (fig. 11), the distribution of right lateral and left lateral glide lines (fig. 10) and the distribution of double sets of strongly twinned lamellae (fig. 9) have an orthorhombic symmetry which is superimposed upon the dominant monoclinic symmetry of c-axes and all deformation lamellae.

SYMMETRY AND INTERPRETATION OF FABRIC

Sander's (1950, part I, p. 81-83) basic assumption that symmetry of fabric of a deformed rock reflects the symmetry of movements which have produced the fabric has been confirmed by experimental deformation of marble, metal aggregates and clay aggregates (Turner, 1957, p. 11-16). A monoclinic symmetry of c-axes and all deformation lamellae is shown in figures 3, 4, 5 and 6. The symmetry plane is *ac* and *b* is the axis of symmetry. The symmetry, strong b-axes, and accompanying *ac* girdles mark both specimens as b = B tectonites (Turner and Verhoogen, 1951, p. 548) except that no megascopic lineation *b* is recognized. B-tectonites are classically interpreted to result from either deformation on s-surfaces of shear intersecting in B or flexure folding and rotation about B, in which case there are no intersecting (h01) s-planes.

In the specimens studied, monoclinic symmetry of c-axes is the product of early stages of rock formation and deformation. As orientation of deformation lamellae hinges upon c-axis orientation the monoclinic symmetry of the plot of all deformation lamellae is indirectly also a product of early stages, although the actual formation of lamellae occurred during late phase, postcrystalline direct componental deformation. Orthorhombic symmetry is apparent in diagrams of selected twinned deformation lamellae (fig. 9), directions of slip along all glide lines (fig. 10) and compression and tension axes of twinned deformation lamellae (figs. 11 and 12), all results of late phase, postcrystalline, direct componental deformation. It is concluded that the monoclinic symmetry of the fabric is the product of successive phases of orthorhombic symmetry and movement that swept through the rock to different orientations during its history of deformation. The last orthorhombic phase is preserved in unrecrystallized deformation lamellae whereas evidence of earlier phases has been obliterated by post-tectonic recrystallization.

The above discussion has dealt with distortion in the *ac* fabric plane only and *bc* thin sections would have to be studied to discover distortion parallel to fabric *b*. For the following reasons, however, it is believed that distortion parallel to *b* has not been great:

1. Macroscopic elongation of grains parallel to *a*, down the dip of the cleavage is visible in outcrop and hand specimen. Shortening parallel to *b* is considerably smaller.
2. Most glide lines (fig. 10) fall near the *ac* plane and movement along them has a large component in the *ac* plane.
3. Compression axes in at least specimen S-3 (fig. 11) approach the center of the diagram in a discontinuous *bc* girdle, ruling out the possibility of extension in *b*. However, as suggested above, *b* could be a secondary axis of compression giving rise to the observed shortening in *b*.

Cloos (1947, p. 888) has shown in the South Mountain fold to the west that deformation in *b* is variable from place to place but generally small when compared to deformation in *ac*.

DESCRIPTION OF QUARTZ DIAGRAMS (figs. 13 and 14)

Quartz in specimen S-3 was studied in two mutually perpendicular thin sections parallel to *ac* and *bc*. C-axes and available deformation lamellae were measured in one hundred grains in each slide and data from the *bc* thin section were rotated into the *ac* plane for presentation. While in calcite virtually

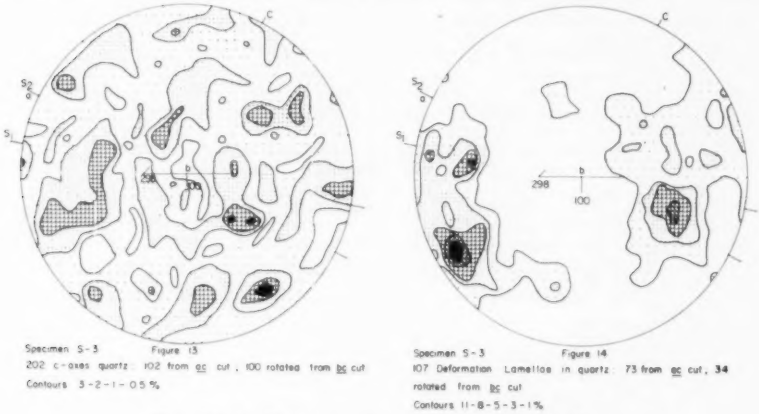

Figs. 13-14. Quartz c-axes and deformation lamellae.

all deformation lamellae were visible in the *ac* thin section, such is not the case for the less strongly oriented quartz. By studying two perpendicular thin sections all possible quartz deformation lamellae could be observed.

Quartz c-axes show no definable pattern of preferred orientation and it is suggested that the cushioning action of surrounding calcite has prevented development of clear orientation. Cloos and Hietanen (1941, p. 65 and diagrams D-37 and D-38) demonstrate that quartz surrounded by other minerals commonly shows a poor orientation.

Deformation lamellae in quartz are located in two well defined areas of concentration corresponding to maxima for calcite deformation lamellae. Areas of minimum concentration for calcite and quartz deformation lamellae also correspond. In the experience of the writers it is common to find better concentrations of quartz deformation lamellae than of c-axes. No fixed crystallographic relation of c-axes and deformation lamellae was found; the angle between c-axes and the perpendicular to deformation lamellae varies from 0-90° with a maximum between 10-40°. Interpretation of these relationships will have to await experimental work on quartz deformation. Thus far quartz deformation lamellae have not been produced in laboratory experiments.

SUMMARY AND CONCLUSIONS

Petrofabric analysis of calcite in a low-grade metamorphic rock with well-preserved sedimentary structures and textures has revealed surprisingly good preferred orientation of c-axes, deformation lamellae, slip along glide lines, and compression and tension axes. Petrofabric techniques of Turner (1953)

and others are definitely applicable to rocks of this metamorphic grade and offer excellent opportunities for the study of coarse-grained carbonate rocks of the Great Valley and western Piedmont. The monoclinic symmetry of c-axes and deformation lamellae in the Conestoga limestone is a cumulative effect of many orthorhombic episodes of movement, differently oriented with respect to present fabric *a* and *c* but always perpendicular to *b*. The last phase of orthorhombic, postcrystalline, direct componental deformation is recorded in deformation lamellae analyzed in the present petrofabric study.

References

Borg, I., and Turner, F. J., 1953, Deformation of Yule Marble, Part VI: Geol. Soc. America Bull., v. 64, p. 1343-1352.

Cloos, E., and Hietanen, A., 1941, Geology of the "Martic Overthrust" and the Glenarm Series in Pennsylvania and Maryland: Geol. Soc. America, Special Paper, v. 35, p. 1-205.

Cloos, E., 1947, Oolite deformation in the South Mountain Fold, Maryland: Geol. Soc. America Bull., v. 58, p. 483-918.

Griggs, D. T., Turner, F. J., Heard, H. C., and Paterson, M. S., 1958, Recrystallization in Calcite Crystals and Aggregates: Am. Geophys. Union, 29th Annual Meeting, Program Abstracts, p. 48.

MacDonald, J. F., 1957, Orientation of anisotropic minerals in a stress field (Abstract): Geol. Soc. America Bull., v. 68, p. 1762.

McIntyre, D. B., and Turner, F. J., 1953, Petrofabric analysis of marbles from Spathspey and Strathavon: Geol: Mag., v. 90, p. 225-240.

Sander, Bruno, 1950, Einführung in die Gefügekunde der geologischen Körper, v. 1 & 2: Wien, Julius Springer.

Sander, Bruno, 1951, Contributions to the study of depositional fabrics, rhythmically deposited triassic limestones and dolomites: Tulsa, Am. Assoc. of Petroleum Geologists, 207 p.

Turner, F. J., 1949, Preferred orientation of calcite in Yule Marble: Am. Jour. Sci., v. 247, p. 593-621.

———, 1953, Nature and dynamic interpretation of deformation lamellae in calcite of three marbles: Am. Jour. Sci., v. 251, p. 276-298.

———, 1957, Lineation, symmetry and movement in monoclinic tectonite fabrics: Geol. Soc. America Bull., v. 68, p. 1-18.

Turner, F. J., and Ch'ih, C. S., 1951, Deformation of Yule Marble, Part III: Observed fabric changes due to deformation at 10,000 atmospheres: Geol. Soc. America Bull., v. 62, p. 887-906.

Turner, F. J., Griggs, D. T., Clark, R. H., and Dixon, R. H., 1956, Deformation of Yule Marble, Part VII: Geol. Soc. America Bull., v. 67, p. 1259-1294.

Weaver, K. E., 1955, The geology of the Hanover area, York County, Pa., unpublished Ph.D. thesis: The Johns Hopkins University, Baltimore, Md.

Wise, D. U., 1953, A structural approach to the stratigraphy of the Conestaga limestone: Pa. Acad. Sci. Proc., v. 27, p. 169-173.

[American Journal of Science, Vol. 257, April 1959, P. 287-296]

THE SYSTEM Na_2CO_3—$NaHCO_3$—CO_2—H_2O AT TEMPERATURES UP TO 200°

A. J. ELLIS

Dominion Laboratory, D.S.I.R., Wellington, New Zealand

ABSTRACT. The equilibrium conditions in the system above were obtained by a differential vapor pressure method and the results up to 200° are reported.

From measurements of the differences in vapor pressure between pure water and a salt solution it is possible in principle to obtain activity coefficients for the ions in solution. The vapor pressures of sodium chloride and sodium carbonate solutions up to 200° are given, but it was not possible to obtain results of sufficient accuracy to derive activity coefficients.

INTRODUCTION

Information on the system Na_2CO_3—$NaHCO_3$—CO_2—H_2O is required in understanding many problems which involve carbonate deposition in nature.

Results giving the equilibrium conditions were reported by Walker, Bray, and Johnston (1927) at 25° and 37°, and more recently by Mai and Babb (1955) at temperatures up to 65°C. Both workers used a wide range of concentrations, and the agreement between the two sets of results is satisfactory.

A sensitive method of measuring small differences in the vapor pressures over two liquids is often required in the investigation of two phase aqueous solutions at high temperatures (e.g. equilibria involving a second gas, accurate determination of the vapor pressure of salt solutions). Results from the present investigation showed that the mercury-in-glass manometer could be used to record small pressure differences up to at least 250°. The limiting factor in measuring small differences in water vapor pressure is the minimum temperature difference that can be maintained between the two containers. The behavior of a suitable differential pressure apparatus was tested on the carbonate system and in determining the vapor pressure of salt solutions.

THEORY

In this paper carbonic acid refers to the molecule H_2CO_3 and not to the mixture ($H_2O + CO_2$) often called by this name. At 25°, 0.259 percent of the total carbon dioxide in a pure water solution consists of H_2CO_3 (Wissbrun, French, and Patterson, 1954).

For the liquid-vapor equilibrium of carbon dioxide the following equation holds.

$$(CO_2) = B.\ f_{co_2} \qquad (1)$$

where B is an inverse Henry's Law coefficient, (CO_2) is the activity of molecular carbon dioxide in solution, and f_{co_2} its fugacity in the vapor. In this paper rounded brackets indicate activities of species, and square brackets concentrations.

For the first and second ionization constants of carbonic acid at constant temperature and pressure the following relationships exist.

$$(H^+)\,(HCO_3'')\,/\,(H_2CO_3) = K_1 \qquad (2)$$

$$(H^+)\,(CO_3'')\,/\,(HCO_3') = K_2 \qquad (3)$$

The hydration of carbon dioxide in solution to carbonic acid is given by

the equilibrium constant

$$K_s = (H_2CO_3)/f_{H_2O} \cdot (CO_2) \qquad (4)$$

where f_{H_2O} is the fugacity of water vapor. For the ionic reaction

$$2HCO_3'(\text{soln.}) \rightarrow CO_3''(\text{soln.}) + H_2O(\text{gas}) + CO_2(\text{gas})$$

the equilibrium constant K is equivalent to

$$K = (CO_3'') \cdot f_{H_2O} \cdot f_{CO_2} / (HCO_3')^2$$

By substitution from equation (1) to (4) it can be shown that

$$K = K_2/K_1 \cdot B \cdot K_s$$

The quantities determined directly from the experiments are the concentrations of sodium carbonate and bicarbonate in solution and the partial pressures of water and carbon dioxide.

Let $[Na_2CO_3] \cdot p_{CO_2} \cdot p_{H_2O}/[NaHCO_3]^2 = k$,

$$(HCO_3') = \gamma_1 [NaHCO_3],$$

and $$(CO_3'') = \gamma_2 [Na_2CO_3] .$$

γ_1 and γ_2 are the respective ion activity coefficients for the HCO_3' and CO_3'' ions. k may then be related to K.

$$k = K \cdot \gamma_1^2/\gamma_2 \cdot \alpha_1 \cdot \alpha_2 = \frac{K_2}{K_1 \cdot K_s \cdot B} \cdot \frac{\gamma_1^2}{\gamma_2 \cdot \alpha_1 \cdot \alpha_2}$$

α_1 and α_2 are the fugacity coefficients of CO_2 and H_2O in the vapor phase.

The apparent acid dissociation constant of the mixture ($CO_2 + H_2O$) is labelled K_1'.

$$\begin{aligned} K_1' &= (H^+)\ (HCO_3')/(H_2CO_3 + CO_2) \\ &= (H^+)\ (HCO_3')/(CO_2)\,(1 + K_s \cdot f_{H_2O}) \\ &= K_1 \cdot K_s \cdot f_{H_2O}/(1 + K_s \cdot f_{H_2O}) \\ &\cong K_1 \cdot K_s \cdot f_{H_2O} \end{aligned}$$

The error involved in the last approximation is equal to the percentage of total carbon dioxide present in solution as carbonic acid. This is unlikely to be greater than 1 percent in the temperature range examined.

THE PRESENT EXPERIMENTAL METHOD

The present study of the system Na_2CO_3—$NaHCO_3$—CO_2—H_2O, was made by a differential pressure technique. Figure 1 is a diagrammatic outline of the apparatus. In a 3 inch stainless steel block two holes were drilled; the large one had a volume of approximately 105 cc and the other one held approximately 5 cc. In the experiments the small chamber contained pure water, and the large one a carbonate solution of known initial composition. The difference in pressure, as indicated by a thick-walled glass manometer, was equal to the partial pressure of carbon dioxide above the carbonate solution less the lowering of water vapor pressure by the salts in solution. The glass manometer was shielded by heavy metal gauze in case of an explosion.

The technique was as follows: the high pressure lines (capillary stainless steel tubing) were removed from the top of the glass-metal connection and connected to dead-end pieces. The bombs and all the lines at this stage were completely dry. Known quantities of sodium bicarbonate and carbonate were placed in the large chamber, and both heads placed on the bomb.

With all valves open the system was quickly evacuated to better than 1

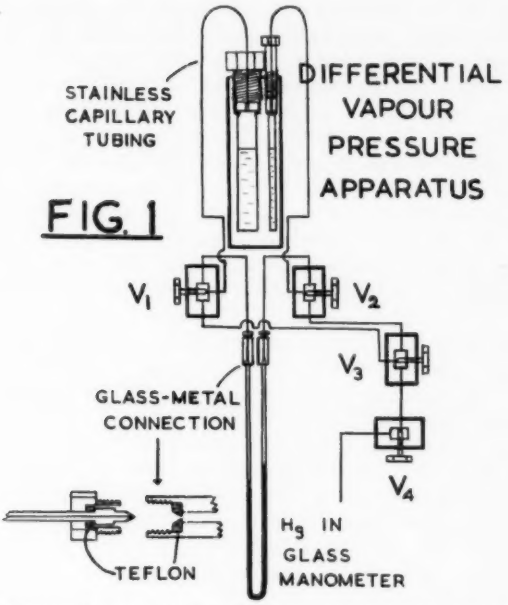

Fig. 1. Apparatus for measuring small differences between the vapor pressure of two solutions.

mm vacuum by a rotary oil pump. This was found not to affect appreciably the dry $NaHCO_3$. The evacuation was through valve 4 which was also connected to a source of degassed water through a T piece.

The degassed water was prepared by boiling water under reflux for 2-3 hours under a partial vacuum in an apparatus of the type described by Law (1949). With valve 2 closed, approximately 70 cc of water was let into the large chamber and valve 1 closed. Valve 2 was temporarily opened to admit a few cc of water into the small chamber. At this stage all the lines were filled with degassed water at atmospheric pressure. The manometer was always filled with water from the mercury surface up to the top of the glass-metal connection. With the latter overflowing with water the lines were again connected to it with valves 3 and 4 closed.

The bomb was heated in an 18 inch diameter 10 gallon bath of oil which was surrounded by a foot thickness packing of diatomaceous earth. A thermostat controlled the temperature to about $\pm$ 0.1° and the bath was vigorously stirred. The fact that the two chambers were in the one massive piece of metal damped out temperature variations in the bath. With pure water in both cavities the differences in pressure registered at 200° were of the order of $\pm$ 0.3 cm. As at 200° the change of vapor pressure is about 24 cm for a degree temperature difference, the difference in temperature between the two chambers was less than 0.01°.

After the apparatus had been at the temperature of observation for about an hour, valves 1 and 2 were opened and the values of Δp read on the manometer until they remained constant. This usually required less than an hour. With a little experience the manometer could be pre-set to about the value of Δp expected so that there was no appreciable transfer of water into either the solution or the small chamber when the mercury moved.

The weight of solution in the bomb was measured after the experiments and the concentrations estimated. In the calculations, corrections were made for the water transferred by changes in the mercury level, the water in the vapor space, the depression of the water vapor pressure by the salt in solution, the carbonate in the bicarbonate used, and the change in the original carbonate-bicarbonate ratio by the reaction to form carbon dioxide in the vapor and liquid.

The only correction which was very appreciable was the depression of the water vapor pressure by the salts in solution. Values for this correction were taken from experiments reported below with the assumption that the osmotic effect of NaCl equalled that of $NaHCO_3$.

The lines from the bomb were arranged symmetrically about the manometer and the heads of the two chambers were at the same level. The values of Δp were corrected to pressures in centimetres of mercury by taking the effective density of the manometer liquid as 12.55 g/cc.

RESULTS

Three series of experiments were completed at ionic strengths equal to 0.2, 0.5, and 1.0. A typical experimental result is calculated in detail.

Ionic strength (μ) = 1		T = 162°C
Bomb volume 105.4 cc	The $NaHCO_3$ used contained 0.0034 moles Na_2CO_3/mole $NaHCO_3$.	
Na_2CO_3 added		= 0.01063 moles
$NaHCO_3$ added		= 0.0385 moles
Weight of water in solution		= 67.9 g
v.p. pure water, 162°		= 487.7 cm Hg
Correction for salts		= 11.6 cm Hg
v.p. water over solution		= 476.1 cm Hg
Δp		= 12.9 cm Hg
Partial pressure of CO_2 (p_{CO_2})		= 24.5 cm Hg
Volume of solution (162°)		= 76.6 cc
Volume of gas		= 28.8 cc
Total moles of CO_2 in system		= 0.00048
Corrected moles $NaHCO_3$		= 0.03755
Corrected mole Na_2CO_3		= 0.01111
$NaHCO_3$ concentration $[NaHCO_3] = 0.553$ moles/1000 g water		
Na_2CO_3 concentration $[Na_2CO_3] = 0.162$ moles/1000 g water		
$k = p_{H_2O} \cdot p_{CO_2} \cdot [Na_2CO_3]/[NaHCO_3]^2$		= 1.08 at.^{2} kg.mole^{-1}

The total quantity of carbon dioxide in the system was calculated from the partial pressure of the gas, the volumes of gas and liquid, and the solubility of carbon dioxide reported in the first paper of this series (Ellis, 1959).

TABLE 1

T°C	Wt.H_2O (g)	P_{H_2O} corrected (cm Hg)	ΔP (cm Hg)	P_{CO_2} (cm Hg)	Moles CO_2 in system $\times 10^4$	Corrected $NaHCO_3$ moles per 1000g H_2O $\times 10$	Corrected Na_2CO_3 moles per 1000g H_2O $\times 10^2$	Volume Soln. T° (cc)	k (at.^{2} kg. moles^{-1})
	$\mu = 0.2$								
133.5	72.6	237.1	3.9	5.0	1.0	1.32	2.11	78.4	0.24
162.5	72.6	488.8	5.2	7.4	1.4	1.31	2.16	80.7	0.79
190.5	72.6	948.0	5.2	9.2	1.5	1.31	2.18	83.3	1.91
126	72.8	178.6	9.8	10.7	2.3	1.57	1.33	78.0	0.18
163	72.8	497.4	11.6	14.2	2.7	1.56	1.39	81.0	0.69
193	72.8	999.4	13.7	19.0	3.2	1.55	1.46	83.8	2.00
119	70.8	143.6	2.5	3.2	0.7	1.22	2.61	75.4	0.18
147	70.8	327.9	3.3	4.8	1.0	1.23	2.66	77.3	0.48
172	70.8	620.8	2.6	5.2	1.0	1.21	2.66	79.4	1.02
194	70.8	1022.4	2.3	6.4	1.1	1.23	2.67	81.4	2.00
	$\mu = 0.5$								
125.5	49.8	158.1	25.2	27.9	6.6	3.83	4.44	53.9	0.231
165	49.8	518.3	25.6	32.9	8.0	3.78	4.72	56.6	0.98
120	49.8	146.6	20.5	22.8	5.5	3.88	4.21	53.5	0.162
180	49.8	742.5	28.0	37.5	8.8	3.75	4.87	56.9	1.69
124	58.5	166.6	10.9	13.1	3.3	2.88	4.95	62.6	0.226
163.5	58.5	499.8	8.1	14.6	3.3	2.88	4.95	65.1	0.754
180	58.5	743.5	12.0	20.5	4.4	2.84	5.14	66.3	1.68
127	66.5	182.3	38.4	41.2	9.1	4.36	3.62	72.4	0.247
158	66.5	434.0	45.6	52.1	10.5	4.32	3.83	74.7	0.79
197	66.5	1079.6	47.0	61.9	11.1	4.30	3.92	78.0	2.45
125	75.3	170.0	4.1	6.2	1.3	2.41	7.61	80.8	0.239
162	75.3	484.9	2.0	7.6	1.4	2.38	7.62	83.8	0.85
190	75.3	939.2	2.1	9.5	1.5	2.38	7.64	86.4	2.08
	$\mu = 1$								
124	83.6	164.0	45.8	50.6	9.3	6.38	7.20	90.7	0.254
157	83.6	417.5	53.3	65.1	10.0	6.38	7.28	93.5	0.842
187	83.6	859.0	59.8	81.7	11.7	6.33	7.49	96.7	2.27
125.5	69.3	172.8	12.8	16.8	3.7	5.45	15.9	75.2	0.269
160.5	69.3	458.2	14.0	25.4	4.9	5.42	16.2	77.9	1.11
191	69.3	941.0	10.9	31.9	5.5	5.40	17.0	80.6	3.03
126.5	67.9	177.5	11.5	15.6	3.4	5.57	16.2	73.9	0.25
162	67.9	476.1	12.9	24.5	4.8	5.53	16.4	76.6	1.08
192	67.9	961.7	11.3	32.7	5.8	5.52	16.5	79.2	3.30
126.5	71.3	177.7	27.5	32.6	6.9	6.68	13.1	77.3	0.294
163	71.3	487.1	35.1	48.0	8.9	6.62	13.4	80.3	1.24
192	71.3	959.8	37.1	60.4	10.2	6.59	13.6	82.0	3.14
127	67.4	180.2	20.7	25.6	5.7	6.48	15.6	73.5	0.296
165	67.4	513.0	24.9	37.5	7.3	6.43	15.8	76.4	1.27
195	67.4	1025.8	25.5	48.6	8.6	6.39	16.0	79.2	3.38

The results from the experiments are given in table 1 and the values of log k are plotted against $1/T^\circ$ K in figure 2.

It was shown that $K = k.\ \gamma_2.\alpha_1.\alpha_2/\gamma_1^2$

where K is the thermodynamic equilibrium constant for the reaction

$$2HCO_3' \text{ (soln.)} \rightarrow CO_3'' \text{ (soln.)} + H_2O\text{(gas)} + CO_2\text{(gas)}$$

At constant pressure and composition

$$\frac{\partial \ln K}{\partial T} = \frac{\partial \ln k}{\partial T} + \frac{\partial \ln(\gamma_2.\alpha_1.\alpha_2/\gamma_1^2)}{\partial t}$$

$$\Delta H^\circ = \Delta H + \Delta h$$

where ΔH° is the standard increment in heat content for the reaction and Δh incorporates the overall change in relative partial molal heat contents of ions

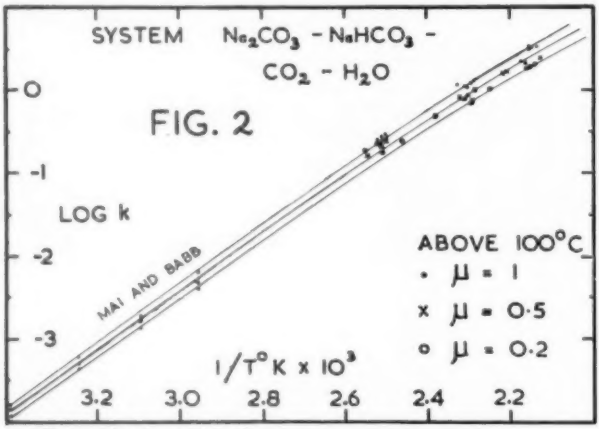

Fig. 2. The results obtained for k at various temperatures ($k = [Na_2CO_3].\ p_{CO_2}.\ p_{H_2O}/[NaHCO_3]^2$).

in solution and gases in the vapor. Table 2 gives values of ΔH obtained from the experiments.

TABLE 2

T°C	25	50	100	150	200
$\Delta H(\mu = 1)$	16400	16400	15800	14600	13000 cals./mole
$\Delta H(\mu = 0.2)$	15900	15900	15500	14200	12500 cals./mole
ΔH_{H_2O}(vapzn.)	10480	10230	9697	9074	8348 cals./mole
$\Delta H^*(\mu = 0.2)$	5700	5670	5800	5130	4150 cals./mole

ΔH_{H_2O} (vapzn.) is the latent heat of vaporization for pure water (Keenan and Keyes, 1936), and assuming that this heat of vaporization is the same for a solution of ionic strength $\mu = 0.2$, $\Delta H^* = \Delta H - \Delta H_{H_2O}$ (vapzn.) is the experimental increment in heat content if the reference state of water is taken as the liquid rather than the gas.

For the reaction

$$2NaHCO_3\text{(soln.)} \rightarrow Na_2CO_3\text{(soln.)} + H_2O(1) + CO_2(g)$$

ΔCp^* is very small at temperatures below 100° (ΔH^* is constant within ex-

perimental error). At higher temperatures ΔH for vaporization of CO_2 from solution decreases rapidly (see first paper of this series) and this will be a major factor in the decrease of ΔH^*.

If as an approximation in the equation

$$k = \frac{K_2}{K_1.K_s.B} \cdot \frac{\gamma_1^2}{\gamma_2.\alpha_1.\alpha_2}$$, it is assumed that the fugacity coefficients α_1 and α_2 are unity, and that $K_1' = K_1.K_2.f_{H_2O}$,

$$\text{then } k = \frac{K_2.p_{H_2O}.\ \gamma_1^2}{K_1'.B.\ \gamma_2} = k' \cdot \frac{\gamma_1^2}{\gamma_2}$$

Approximate values of k' are calculated in table 3 from known experimental data (K_1' up to 50°, Harned and Davis, 1943; K_2 up to 50°, Harned and Scholes, 1941; and up to 90°, Cuta and Stráfelda, 1954). Values of K_1' and K_2 are extrapolated to higher temperatures by means of equations of the type used by Pitzer (1937). Values of B were obtained from the solubility results reported earlier.

Mean ionic activity coefficients $\gamma_\pm$ determined by experiment are related to the individual ion activity coefficients by the equation

$$\gamma_\pm^{n+m} = \gamma^n{}_+ \cdot \gamma^m{}_-$$ (Harned and Owen, 1950, p. 10)

where n and m are the number of positive and negative ions respectively produced by a salt.

TABLE 3

T°C	$K_2 \times 10^{11}$	$K_1' \times 10^7$	$B \times 10^2$ (mol. at.$^{-1}$kg^{-1})	p_{H_2O} (at.)	k'	k (μ=1.0)	γ_1^2/γ_2 (μ=1.0)
25	4.69	4.45	3.43	0.0313	9.6×10^{-5}	2.6×10^{-4}	2.7
50	6.73	5.16	1.89	0.1217	8.4×10^{-4}	2.1×10^{-3}	2.5
100	7.3	5.8	1.18	1.00	1.1×10^{-2}	6.3×10^{-2}	5.7
150	5.6	4.7	1.14	4.70	4.4×10^{-2}	0.74	17
200	3.8	2.8	1.27	15.3	0.16	4.3	27

Therefore

$$\frac{\gamma_1^2}{\gamma_2} = \frac{\gamma_\pm^4 \text{ (NaHCO}_3\text{ soln.)}}{\gamma_\pm^3 \text{ (Na}_2\text{CO}_3\text{ soln.)}}$$

$$\cong \frac{\gamma_\pm^4 \text{ (NaCl soln.)}}{\gamma_\pm^3 \text{ (Na}_2\text{CO}_3\text{ soln.)}}$$

Values of $\gamma_\pm$ are reported by Harned and Owen (1950) p. 557, for NaCl solutions up to 100°, and for Na_2CO_3 solutions up to 95° by Taylor (1955). For solutions in the series $\mu = 1.0$, $[Na_2CO_3]$ and $[NaHCO_3]$ equal approximately 0.1 m and 0.75 m respectively. Values of the ratio,

$$\gamma_\pm^4 \text{ (NaCl soln.)} \ / \ \gamma_\pm^3 \text{ (Na}_2\text{CO}_3\text{ soln.)} \cong \gamma_1^2/\gamma_2,$$

at these concentrations are given in table 4.

TABLE 4

T°C	25	50	75	100	125
$\gamma\pm$ (0.75m NaCl)	0.666	0.665	0.643	0.626	0.600
$\gamma\pm$ (0.1m Na_2CO_3)	0.465	0.524	0.505	0.430	0.30
Calc. Ratio γ_1^2/γ_2	1.95	1.4	1.3	1.9	4.8

The calculated values of γ_1^2/γ_2 in table 4 are intended only as a qualitative illustration and cannot be expected to equal the experimental values in table 3. The mean activity coefficients for 0.1m Na_2CO_3 in a 0.75m $NaHCO_3$ solution, will be different, and probably lower than $\gamma_\pm$ (Na_2CO_3) in a pure 0.1m solution.

However, the figures show that the rapid increase in γ_1^2/γ_2 at higher temperatures is caused mainly by the decrease in the mean activity coefficient of sodium carbonate. This would indicate that this substance is only slightly dissociated in high temperature water. Its decrease in solubility to almost zero at the critical temperature of water is therefore not unexpected.

VAPOR PRESSURES OF NaCl and Na_2CO_3 SOLUTIONS

The water vapor pressures over solutions of sodium chloride and sodium carbonate were determined up to 200° using the differential pressure apparatus.

The procedure used was to dry and evacuate the bomb and lines, and with valve 1 closed, to allow degassed water to enter the small chamber. Valve 2 and valve 4 were then closed. The solution to be studied was also degassed in the reflux apparatus and approximately 70 cc of degassed solution was allowed to enter the large chamber through valve 1, valve 3 and valve 4. All valves were then closed and the manometer connections made as before. The manometer was pre-set to the approximate level expected in the experiment.

The concentration and weight of the solution was obtained after the experiment, and where appropriate, corrections were made as before. The practical osmotic coefficient ϕ is defined by the equation

$$\mu_{H_2O} = \mu^o_{H_2O} - \phi RT \frac{t.m}{55.51}$$

or $\ln a_{H_2O} = -\phi\ t.m/55.51$ (Harned and Owen, 1950, p. 13). The activity of water $a_{H_2O} = f_{H_2O} / f^o_{H_2O}$ where f_{H_2O} and $f^o_{H_2O}$ are the fugacities of water over the solution, and over pure water. If it is assumed that the fugacity ratio can be replaced by $p_{H_2O} / p^o_{H_2O}$, i.e., the fugacity coefficients are the same

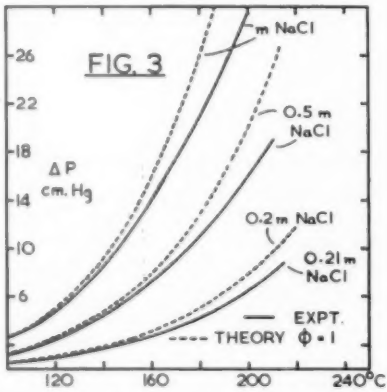

Fig. 3. The difference between the vapor pressure of sodium chloride solutions, and pure water at various temperatures.

for water vapor over the solution and over pure water, then

$$\phi = \frac{55.51}{t.m} \ln \frac{p_{H_2O}}{p^{\circ}_{H_2O}}$$

where t is the number of ions formed by the salt, m its molality, p_{H_2O} the water vapor pressure over the solution, and $p^{\circ}_{H_2O}$ that over pure water.

The results of the determinations are given in figures 3 and 4. Lines for various concentrations, obtained by giving ϕ a value of unity, are also shown.

Harned and Owen (1950, p. 363) tabulate osmotic coefficients for sodium chloride solutions up to 100°. Table 5 gives some of their values for ϕ and the values obtained with sodium chloride in this work above 100°.

Within experimental error the present results follow on smoothly from the previous values.

TABLE 5

Values of ϕ for NaCl Solutions

T°C / m	60	80	100	120	140	160	180	200
0.2	0.9210	0.9178	0.9135	—	—	—	0.82	0.80
0.5	0.9234	0.9195	0.9145	0.91	0.91	0.88	0.82	0.77
1.0	0.9442	0.9402	0.9345	0.91	0.88	0.86	0.785	0.705

It was planned originally to obtain mean activity coefficients for ions of various salts from the vapor pressure measurements by the standard process (Taylor, 1955) of applying an integrated form of the Gibbs-Duhem equation.

$$\log \frac{\gamma_{\pm}\ (m)}{\gamma_{\pm}\ (m_r)} = -\int_{a_1,\ \text{at}\ m_r}^{a_1,\ \text{at}\ m} \frac{55.51}{t.m}\, d \log a_1 - \log m/m_r$$

where m_r is a reference molality at low salt concentrations below which values of the activity coefficients can be extrapolated to infinite dilutions by the Debye-Hückel theory, and a_1 is the activity of water.

To derive useful values for $\gamma_{\pm}$ (m) it would be necessary to obtain values

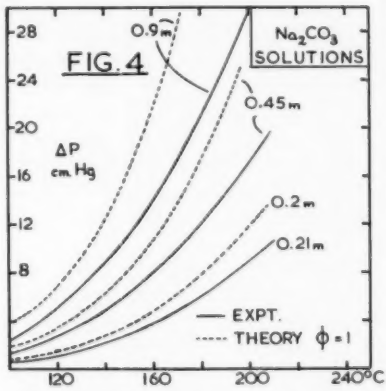

Fig. 4. The difference between the vapor pressure of sodium carbonate solutions, and pure water at various temperatures.

of Δp for solutions down to about 0.1m with an accuracy of the order of 1 percent. It is unlikely that the present results are better than $\pm$ 3mm in Δp over most of the range. Even at 200° this would amount to an error of almost $\pm$ 10 percent in activity coefficients at concentrations of 0.1m.

The results are therefore left in terms of pressure differences and osmotic coefficients, and as such should be useful in calculating water vapor pressures over hydrothermal solutions.

ACKNOWLEDGMENTS

The author would like to thank Prof. H. N. Parton and Dr. W. S. Fyfe for their comments on this work, and Mr. V. G. Tyrell and Mr. L. F. Wylie for constructing the apparatus. He is also indebted to the New Zealand Department of Scientific and Industrial Research for the opportunity of doing this work at the Chemistry Department of the University of Otago.

REFERENCES

Cuta, F., and Stráfelda, F., 1954, The second dissociation constant of carbonic acid between 60 and 90°: Chem. Listy, v. 48, p. 1308-1313.

Ellis, A. J., 1959, The solubility of carbon dioxide in water at high temperatures: Am. Jour. Sci., v. 257, p. 217-234.

Harned, H. S., and Davis, R., 1943, The ionization constant of H_2CO_3 in water and the solubility of CO_2 in water and aqueous solutions from 0-50°: Am. Chem. Soc. Jour., v. 65, p. 2030-2037.

Harned, H. S., and Owen, B. B., 1950, The physical chemistry of electrolyte solutions, 2nd ed.: New York, Reinhold.

Harned, H. S., and Scholes, S. R., 1941, The ionization constant of HCO'_3 from 0 to 50°: Am. Chem. Soc. Jour., v. 63, p. 1706-1709.

Keenan, J. H., and Keyes, F. G., 1936, Thermodynamic properties of steam: New York, John Wiley & Sons.

Law, J. T., 1949, The solubility of gases in water-methanol mixtures, and derived thermodynamic properties: PhD. Thesis, University of New Zealand.

Mai, K. L., and Babb, A. L., 1955, Vapour-liquid equilibria by radioactive tracer techniques: Indust. Eng. Chem., v. 47, p. 1749-1757.

Pitzer, K. S., 1937, The variation of ionization constants with temperature, and the entropy change with ionization: Am. Chem. Soc. Jour., v. 59, p. 2365-2371.

Taylor, C. E., 1955, Thermodynamics of sodium carbonate in solution: Jour. Phys. Chem., v. 59, p. 653-657.

Walker, A. C., Bray, U. B., and Johnston, J., 1927, Equilibrium in solutions of alkali carbonates: Am. Chem. Soc. Jour., v. 49, p. 1235-1256.

Wissbrun, K. F., French, D. M., and Patterson, A., 1954: The true ionization constant of carbonic acid in aqueous solution from 5 to 45°: Jour. Phys. Chem., v. 58, p. 693-695.

[American Journal of Science, Vol. 257, April 1959, P. 297-315]

PHASE EQUILIBRIA IN THE SYSTEM MANGANESE OXIDE—SiO_2 IN AIR*

ARNULF MUAN

Dept. of Metallurgy, Pennsylvania State University,
University Park, Pennsylvania

ABSTRACT. Phase relations in the system manganese oxide—SiO_2 in air have been investigated in the temperature range 990-1571°C, using the quenching technique. The data obtained permit the construction of a phase diagram showing stability relations in the liquidus temperature region as well as at subsolidus temperatures. For sake of simplicity the phase relations are illustrated in the form of a projection into a chosen join through the ternary system. The resulting diagram has the *appearance* of a binary system, with "binary invariant" situations as follows: a peritectic exists at 1230°C, with cubic Mn_3O_4, tephroite ($2MnO \cdot SiO_2$) and liquid coexisting in equilibrium with a gas phase of O_2 partial pressure equal to 0.21 atm. At 1206°C tephroite, $MnO \cdot SiO_2$ solid solution (rhodonite), liquid and gas are present together in what appears as an eutectic situation. Tridymite (SiO_2), $MnO \cdot SiO_2$(ss), liquid and gas exist together in equilibrium in an apparently peritectic situation at 1272°C, and cristobalite together with 2 liquids and gas are the equilibrium phases at approximately 1700°C. In the subsolidus region the following apparently invariant situations have been determined: at 1204°C cubic Mn_3O_4, tephroite and $MnO \cdot SiO_2$(ss) coexist in equilibrium with a gas phase of O_2 partial pressure equal to 0.21 atm. Tetragonal Mn_3O_4, a phase probably analogous to the mineral braunite (Mn_2O_3(ss)), and $MnO \cdot SiO_2$(ss) are in equilibrium with this gas at 1168°C, while at 1048°C Mn_2O_3(ss), $MnO \cdot SiO_2$(ss) and tridymite are the stable phases in air. In addition, "invariant" situations also result from the tridymite-cristobalite inversion at approximately 1470°C and the inversion from tetragonal to cubic Mn_3O_4 at approximately 1160°C.

INTRODUCTION

Phase equilibrium studies are generally recognized as being necessary first steps in any investigation aimed at improving our knowledge of heterogeneous reactions. Accurate measurements of chemical properties in such systems can be interpreted intelligently only if the system is well defined with respect to the phases present.

Oxide systems have been the center of interest of research workers in many different fields. Geochemists and petrologists have gathered a tremendous amount of phase equilibrium data which have enabled them to infer conditions governing the formation and existence of many minerals and rocks. Their studies have dealt mainly with combinations of oxides of noble gas type ions such as for instance SiO_2, Al_2O_3, CaO, MgO, Na_2O, K_2O, while data on most oxides of transition elements, such as for instance manganese oxides, are relatively scarce. This situation undoubtedly exists partly because the latter systems are more difficult to study experimentally, but also because transition elements in their natural occurrences frequently are present as sulfides rather than as oxides.

Oxides also play a very important role as one or more of the phases present in many high temperature industrial processes. Ceramists deal essentially with oxide materials, and their efforts have contributed significantly to our knowledge of oxide chemistry. It is natural that ceramists are interested primarily in the chemically very stable oxides of noble gas type ions, such as

* Contribution No. 58-10 from College of Mineral Industries, The Pennsylvania State University, University Park, Pennsylvania.

SiO_2, Al_2O_3, CaO, MgO, Na_2O, K_2O, in other words the same oxides as are studied by geochemists. In the field of metallurgy, however, one is mainly concerned with the extraction of metals from oxide raw materials, and hence oxides of *low* stability are the center of interest, such as for instance iron oxides and manganese oxides. The metallurgist cannot, however, overlook the importance of systems made up from among the more stable oxides, which form the constituents of the slag phase and also are used in the refractory linings of the furnaces.

The most important oxide by far among those of transition elements is iron oxide. Systems containing iron oxide as a component have been studied and restudied by metallurgists, geochemists and ceramists alike over the last 50 years. By comparison, very few studies have been made of systems where oxides of other transition elements are present. Among those of next importance both technologically as well as geologically is manganese oxide.

While data on the system Mn—O are gradually accumulating in another phase of our research efforts (Hahn and Muan, in press), the present work represents a first step in our investigation of the system Mn—Si—O. Because manganese occurs in different states of oxidation, the O_2 partial pressure of the gas phase must be controlled carefully in any investigation of a system where manganese oxides are present. We have chosen to start our study of manganese oxide—SiO_2 equilibria by investigating the system in air, that is at a constant O_2 partial pressure of 0.21 atm. In choosing this approach we are actually working along the irregularly curved 0.21 atm. O_2 isobaric section through the system Mn—Si—O. Equilibria along this section may be represented in a simplified manner by projecting the points representing compositions of condensed phases into a chosen join. We will present the results in terms of the components Mn_3O_4 and SiO_2. The resulting diagram has the appearance of a binary system. Apparently invariant situations in this system are actually intersections between the 0.21 atm. isobaric surface and univariant lines in the system Mn—Si—O. Along such liquidus univariant lines two crystalline phases, liquid and gas coexist in equilibrium, whereas a subsolidus univariant situation is characterized by the coexistence in equilibrium of three crystalline phases and a gas phase.

Previous Work

Although manganese silicates have attracted considerable attention among geochemists as well as metallurgists, no systematic study of phase relations in the system manganese oxide—SiO_2 in air has been reported in the literature.

The one end member in the system, SiO_2, of course has been the subject of numerous phase investigations over the past few decades, starting with the now classic work in 1913 by Fenner. In spite of all efforts since that time, doubt still exists as to certain of the important characteristics of this substance, particularly with respect to the stability relations of the tridymite phase. An impression of the present status of our knowledge of this system can be obtained by reading recent papers by Sosman (1955), Flörke (1956), Eitel (1957), Hill and Roy (1958).

The system Mn—O, unfortunately, has not been studied experimentally in

any great detail. Scattered equilibrium data and calorimetric data are available in the literature, from which Coughlin (1954) has tabulated the standard free energies of formation of the various manganese oxides as a function of temperature. Most of the values listed in these tables were obtained by addition and subtraction of large numbers, each of which is subject to considerable margins of error. Hence the stability relations of the manganese oxides depicted by Coughlin's tables are uncertain and should be considered only as rough approximations. Hahn and Muan (in press) have studied recently limited parts of the Mn—O system, particularly the equilibria between Mn_2O_3 and Mn_3O_4 and between Mn_3O_4 and MnO. Their data show that Mn_3O_4 is the stable crystalline phase of manganese oxide in air above 877°C and up to the melting temperature of 1567°C. At temperatures slightly below 877°C Mn_2O_3 is the stable phase in air. It is well known that Mn_3O_4 exists in two different stable modifications, one high temperature cubic form with spinel structure and one low temperature tetragonal form. The exact temperature at which these two modifications coexist in equilibrium is still not certain. A discussion of the problem appears in a recent publication by Van Hook and Keith (1958). They indicate that the most likely inversion temperature is approximately 1160°C. The oxide Mn_2O_3, likewise, has two established polymorphic forms, the α-Mn_2O_3 with "C"-type cubic structure (Zachariasen, 1928; Pauling and Shappell, 1930) and the γ-Mn_2O_3 with distorted spinel structure (Dubois, 1935). The latter modification, however, is unstable relative to the former and will not appear in our phase equilibrium diagram.

Some of the previous experimental phase equilibrium studies of mixtures of manganese oxide and silica have suffered from insufficient control of the O_2 partial pressure of the gas phase in equilibrium with the condensed phases. This is probably one of the reasons why such a confusing variety of phase diagrams for the system "manganese oxide—silica" have appeared in the literature (Doerinckel, 1911; Glaser, 1926; Herty, 1930; White, Howat and Hay, 1934). A diagram for the system manganese oxide—SiO_2 under controlled, strongly reducing, conditions was published in 1958 by Glasser, who used CO_2/H_2 mixtures in order to define more precisely the O_2 partial pressure of the gas phase.

A large number of descriptions of naturally occurring manganese minerals with a bearing on the present study are found in mineralogy textbooks (see for instance Dana's System of Mineralogy, 1944) and numerous publications. Papers of particular interest are those describing the mineralogy and geology of the Långban deposits in Sweden (Magnusson, 1924; Flink, 1926; Palache, 1929).

Experimental Method

General Procedure.—The phase relations were determined by the quenching method. Preheated mixtures of manganese oxide and silica were held in platinum containers in air at constant temperature until equilibrium was reached among crystalline, liquid and gas phases. The samples were then quenched rapidly to room temperature. Phases present were identified by x-ray and microscopic methods, and compositions of liquids at liquidus temperatures were determined by wet chemical analysis.

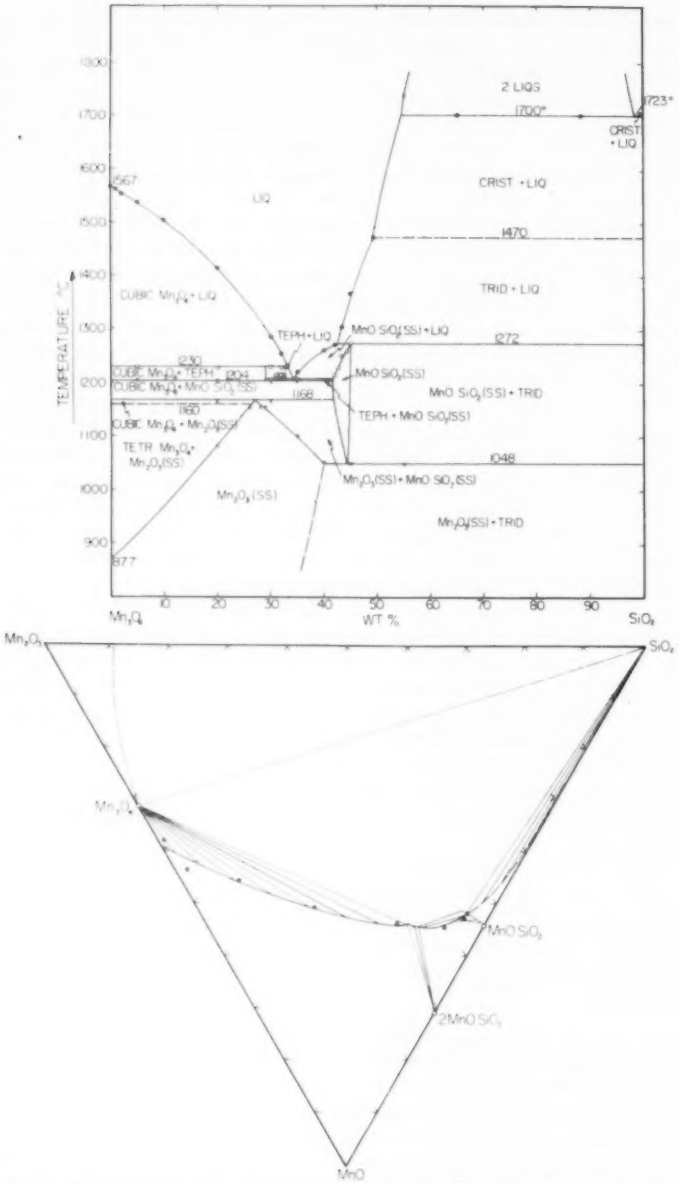

Fig. 1. Diagrams presented in order to show phase relations in the system manganese oxide—SiO_2 in air. The upper diagram has the appearance of a binary system, with

Materials.—Oxides of highest purity available commercially served as starting materials. The source of silica was c.p. silicic acid which was dehydrated by heating at 1300°C for 12 hours. The source of manganese oxide was "Baker Analyzed" grade manganese dioxide, MnO_2. Samples weighing 10 g were made up by mixing these materials in required proportions and mechanically grinding the mixture. Each mixture was then heated slowly to melting either in air atmosphere in a globar furnace, or in a gas-air combustion furnace in case of higher melting mixtures. The heating of the starting materials had to be carried out with utmost caution in slow steps from low temperature up to the liquidus region because the successive decomposition of higher to lower manganese oxides took place very violently. Particularly troublesome in this respect was the temperature region in which the first liquids form. These preheated and quenched mixtures, after grinding to minus 60 mesh, were used for the equilibration runs for determination of liquidus temperatures.

The same mixtures were usually used for determination of boundary curves also in the subsolidus temperature region. As a check on attainment of true equilibrium a few runs in this region were made with two different starting materials prepared by prolonged heating of the mixtures, one at temperatures slightly above and one at a temperature slightly below that of the boundary curve.

Furnaces and Temperature Control.—Vertical tube furnaces with windings of platinum or 80 platinum-20 wt. % rhodium were used for most of the quenching experiments. A modified Roberts and Morey (1930) strip furnace, using strip resistors of a 60 platinum-40 wt. % rhodium alloy, was used for a few quench runs at temperatures above 1600°C.

Temperatures in the vertical tube furnaces were measured before and after each run with a platinum 90–platinum-10 wt. % rhodium thermocouple frequently calibrated at melting points defined as follows: Au, 1063°C; $CaMgSi_2O_6$, 1391.5°C; $CaSiO_3$, 1544°C. Literature values for temperatures on the Geophysical Laboratory scale are used without correction up to 1550°C, the upper limit of the original scale. Temperatures above 1550°C are adjusted to the 1948 International Scale using the correction data tabulated by Corruccini (1949) and by Sosman (1952). Furnace temperature was controlled by a second thermocouple inserted close to the heating element and connected through compensating lead wires to a Celectray controller. The temperature

Mn_3O_4 and SiO_2 chosen as components. This part of the figure shows phases present as a function of temperature and manganese oxide to silica ratios of the mixtures. Heavy lines are boundary curves. These are dashed in regions where experimental data are less reliable or lacking. Solid dots, solid triangle, open circles and crosses represent experimentally determined points on liquidus, 2 liquid, solidus and subsolidus boundary curves, respectively, based on data contained in table 1. The lower, triangular diagram shows true compositions of liquid and crystalline phases expressed in terms of the chosen components MnO, Mn_2O_3 and SiO_2. Solid dots represent experimentally determined compositions of liquids at liquidus temperatures, and the heavy curve is the 0.21 atm. liquidus isobar drawn through these points. Light straight lines indicate approximate locations of conjugation lines connecting points representing compositions of liquids with points representing composition of crystalline phases with which the liquids are in equilibrium. Light dash curves are used to indicate how the Mn_3O_4—SiO_2 join is swung up to the Mn_2O_3—SiO_2 join for projection purposes, as explained in the text.

gradient at the hot spot did not exceed 2°C over 1 inch at 1300°C. Temperatures on the strip furnace were measured with an optical pyrometer calibrated at melting points defined as follows: $CaSiO_3$, 1544°C; 10 CaO 90 wt. % SiO_2, 1708°C; Pt, 1769°C.

Examination of Quenched Samples.—Phase identification in the liquidus temperature region was most easily accomplished with the microscope, using transmitted as well as reflected light techniques. The examination of polished sections in reflected light was particularly useful for distinguishing primary crystals from quench crystals in the manganese oxide rich part of the system. The identity of the phases was further confirmed by x-ray techniques, using Fe radiation with a Norelco spectrometer unit. The x-ray technique was also used for determination of compositions of solid solution crystalline phases in the subsolidus temperature region.

In order to determine the compositions of liquids at liquidus temperatures it was necessary to carry out chemical analysis of quenched samples. After crushing of these samples, suitable amounts (~0.2 g) were weighed and transferred to a platinum container. Excess standard ferrous ammonium sulfate solution was added together with 5 ml concentrated H_2SO_4, and the solution was boiled for a couple of minutes. After cooling, 10 ml of HF was added, a cover was put on the crucible and the solution boiled until the sample was completely dissolved, which usually required a period of approximately 10 minutes. The crucible was plunged into a 600 ml beaker containing 250 ml water and 10 ml 1:1 H_2SO_4. After saturation with boric acid, the solution was titrated with 0.05 – n $KMnO_4$.

RESULTS

Results of quenching experiments are listed in table 1 and illustrated graphically in figure 1. This figure consists of 2 diagrams. The upper diagram with the appearance of a binary system shows phases present as a function of temperature. Because the compositions of all condensed phases cannot be represented in terms of the two chosen components, a supplementary diagram is presented in the lower half of the figure. This ternary diagram shows true compositions of condensed phases in equilibrium along boundary curves in the upper diagram.

The most important features of the diagrams are as follows: liquidus temperatures are high at both ends of the system, 1567 and 1723°C being the melting temperatures in air of manganese oxide and cristobalite, respectively. In the silica rich end of the system, liquidus temperatures remain high (~1700°C) until a composition of 50 Wt.% manganese oxide is reached, corresponding to the maximum extent of liquid immiscibility. As the manganese oxide content increases above this value, liquidus temperatures fall off sharply. The $MnO{\cdot}SiO_2$(ss)-tridymite boundary curve is crossed by the 0.21 atm. O_2 isobar at 1272°C in what appears as a peritectic situation in the upper diagram of figure 1. The lowest liquidus temperature in air is 1206°C, with $MnO{\cdot}SiO_2$(ss) and tephroite coexisting with a liquid containing 66 Wt.% manganese oxide and 34 Wt.% SiO_2. As the manganese oxide content increases above this level, liquidus temperatures start rising, and another "peritectic"

situation prevails at 1230°C, with tephroite and Mn_3O_4 as the crystalline phases present in equilibrium with liquid. In the composition range between 67 and 100 Wt.% Mn_3O_4, cubic Mn_3O_4 is the primary crystalline phase.

Tephroite is stable in air in the temperature interval 1204-1230°C. At the upper temperature limit of stability it decomposes incongruently to Mn_3O_4 and liquid; at the lower temperature limit of stability it decomposes to Mn_3O_4 and $MnO \cdot SiO_2$(ss). The phases Mn_3O_4 and $MnO \cdot SiO_2$(ss) coexist in equilibrium down to 1168°C in air. At this temperature Mn_2O_3(ss) becomes stable and the condensed phases present are either Mn_3O_4 + Mn_2O_3(ss) or Mn_2O_3(ss) + $MnO \cdot SiO_2$(ss) at temperatures below 1168°C, depending on the SiO_2 content of the mixture. The $MnO \cdot SiO_2$(ss) phase exists in stable equilibrium in air down to 1048°C. Below this temperature it decomposes to Mn_2O_3(ss) and tridymite. Tetragonal Mn_3O_4 exists as an equilibrium phase in air down to a minimum temperature of 877°C. Below this temperature pure Mn_3O_4 is oxidized to Mn_2O_3; this transformation temperature increases to a maximum of 1168°C as the SiO_2 content of the mixture increases.

A summary of "invariant" situations in the system manganese oxide—SiO_2 in air is presented in table 2, and powder x-ray diffraction data for manganese oxide containing crystalline phases are listed in table 3.

DISCUSSION

The most interesting feature of the phase relations in this system is the stable existence of a SiO_2-containing solid solution phase with α–Mn_2O_3 structure. The large increase in the transformation temperature of Mn_2O_3 to Mn_3O_4 as SiO_2 is added to manganese oxide shows conclusively that SiO_2 enters the structure of the latter. The phase formed is termed Mn_2O_3(ss) in this paper, leaving the question open as to the exact nature of the solid solution. The x-ray patterns show no appreciable shift in the d-spacings of the main lines of Mn_2O_3 as SiO_2 content increases, but some weak extra lines appear, indicating some degree of ordered substitution rather than a completely random distribution of the cations.

The Mn_2O_3(ss) phase appears to be identical to the naturally occurring mineral braunite, which has been described and studied by a large number of investigators in the past. Structure determinations by x-ray diffraction studies have been reported by Aminoff (1931) and by Byström and Mason (1943). The structures as well as d-spacings are very similar to those for the pure Mn_2O_3 end member, which has a C-type sesquioxide structure according to studies carried out by Zachariasen (1928) and by Pauling and Shappell (1930).

The way in which Si^{4+} ions are accommodated in the Mn_2O_3 structure in the mineral braunite has been the subject of a great deal of speculation and some investigations. In natural occurrences the composition of this mineral seems to be close to the formula $3Mn_2O_3 \cdot MnSiO_3$, corresponding to approximately 10 Wt.% SiO_2, although slight variations in this ratio as well as presence of other oxides in the structure are often encountered. Analytical data for this mineral are summarized in Dana's System of Mineralogy (1944). The authors of this book are careful to point out that the exact mechanism of the

substitution is unknown. Goldschmidt (1954), however, states categorically that "braunite is not contaminated manganese sesquioxide but the compound $3Mn_2O_3 \cdot MnSiO_3$".

Some recent magnetic and chemical studies have shed new light on this problem. Fyfe (1949) has developed a chemical test for the presence of trivalent manganese, based on the formation of a stable complex ion with acetylacetone. He found that α–Mn_2O_3 gives the reaction of $Mn^{2+} + Mn^{4+}$, whereas γ–Mn_2O_3, studied for comparison, reacts as 2 Mn^{3+}. Krishnan and Banerjee (1939) have made magnetic measurements on natural braunites to determine the oxidation state of manganese in this phase. Magnetic susceptibility measurements were non-conclusive, because the magnetic moment of Mn^{3+}, 4.90 Bohr magnetons, is almost midway between the moments of Mn^{2+} and Mn^{4+}, 5.92 and 3.87 Bohr magnetons, respectively. However, measurements of the magnetic anisotropy of the braunite revealed that the manganese was present as $Mn^{2+} + Mn^{4+}$ rather than as Mn^{3+}. Krishnan and Banerjee therefore suggest that the formula for braunite be written $3MnMnO_3 \cdot MnSiO_3$ as against the usual formula $3Mn_2O_3 \cdot MnSiO_3$.

The present investigation definitely establishes that a wide range of compositions is possible in braunite, from pure Mn_2O_3 as one end member to a silica content of at least 40 Wt.% SiO_2. It appears likely that the mechanism

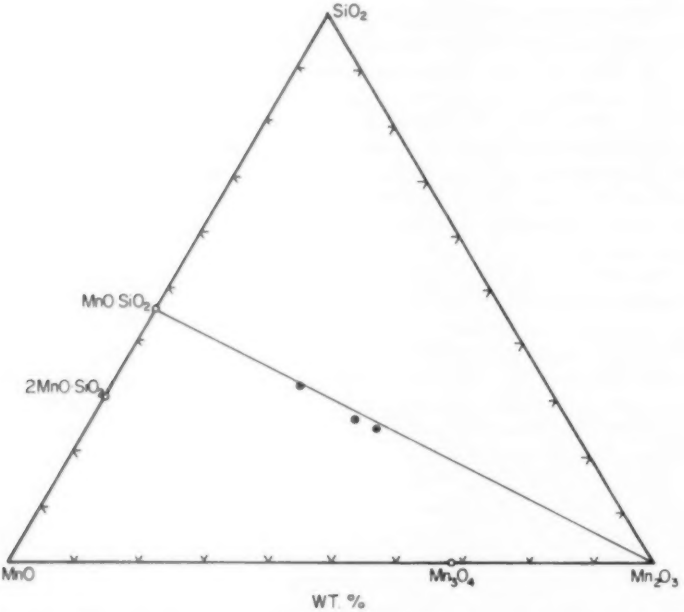

Fig. 2. Diagram showing compositions of Mn_2O_3(ss) crystals in air at 1000°C (solid dots). The light straight lines is the join $MnO \cdot SiO_2$—Mn_2O_3 (compare discussion in text).

for the solid solution formation is a substitution of Si^{4+} for Mn^{4+} in the Mn_2O_3 lattice. The present data give strong support for the assumption that Mn_2O_3 consists of divalent and tetravalent manganese rather than trivalent manganese, for the continuous and extensive solid solution established for Mn_2O_3(ss) is most likely explained by assuming the formula $Mn^{2+}\,Mn^{4+}\,O_3$.

A further support of the assumption that the Mn_2O_3(ss) crystals can be considered a solid solution $Mn^{2+}(Mn^{4+}Si^{4+})O_3$ is offered by the results of chemical analysis shown in figure 2. Compositions of Mn_2O_3(ss) crystals (solid dots) prepared by heating manganese oxide—SiO_2 mixtures in air for 200 hours at 1000°C fall close to the join $MnO \cdot SiO_2$—Mn_2O_3 as predicted by the mechanism of substitution suggested above.

The crystalline phases tephroite ($2MnO \cdot SiO_2$), tridymite (SiO_2), cristobalite (SiO_2) and Mn_3O_4 appear to be pure phases corresponding to the chemical formulas written above, as closely as could be determined with the experimental techniques used (x-ray and microscopic examination as well as phase evidence). The phase designated $MnO \cdot SiO_2$(ss), after quenching to room temperature, is closely similar to the naturally occurring mineral rhodonite. A small excess of manganese over the stoichiometric 1:1 ratio is permitted in this structure, giving rise to a solid solution one-phase area (labeled $MnO \cdot SiO_2$(ss)) in the upper diagram in figure 1. No high temperature x-ray examination of this phase was carried out in the present investigation. In view of the complexity of the structure of metasilicates (compare for instance extensive studies of the magnesium analogue, $MgO \cdot SiO_2$ (Atlas, 1952)), an x-ray study of the $MnO \cdot SiO_2$(ss) phase as a function of O_2 partial pressure and thermal history is a research problem in itself. In the present paper the phase is referred to as $MnO \cdot SiO_2$(ss), leaving open the question as to the exact crystal structure of this phase.

Another notable feature of the phase relations in this system is the stable existence in air of tephroite as well as $MnO \cdot SiO_2$(ss) at liquidus temperatures, both phases containing essentially all manganese as Mn^{2+}. This situation is completely different from the one prevailing in the system iron oxide—SiO_2, where magnetite (Fe_3O_4) and silica (cristobalite or tridymite) are the only crystalline phases present in equilibrium at liquidus temperatures in air. In other words, Mn^{2+} is much more stable relative to the other valence states of manganese than Fe^{2+} is relative to Fe^{3+}. The extreme stability of Mn^{2+} in oxide phases is of course inherent in the numerical values listed in the free energy tables compiled by Coughlin (1954).

As temperature is lowered, a tendency for oxidation of Mn^{2+} to higher valence states prevails, because this is a strongly exothermic reaction. Tephroite oxidizes at temperatures only slightly below the lowest liquidus temperature in the system, first to Mn_3O_4 plus $MnO \cdot SiO_2$(ss), and subsequently to Mn_2O_3(ss). The $MnO \cdot SiO_2$(ss) phase persists in air down to a temperature of 1048°C before oxidation to Mn_2O_3(ss) and tridymite takes place.

The boundary curve between the fields of tridymite and cristobalite has been dashed at 1470°C in accordance with the "classical" picture of stability relations among the various modifications (Fenner, 1913), and assuming no solid solution in tridymite or cristobalite. No consistent data regarding the

relative stabilities of these phases in the present system were obtained in runs of 2 days duration. Tridymite always formed at temperatures below 1480°C and cristobalite above this temperature in a mixture containing 40 Wt.% manganese oxide, while cristobalite was the phase always forming in the temperature interval 1430-1475°C in a mixture containing 8 Wt.% manganese oxide.

The incongruent melting of tephroite in air as distinguished from the congruent melting found by Glasser (1958) for this phase under strongly reducing conditions is a noteworthy feature. It is probable that the discrepancies in previous literature regarding the melting relations of this phase are due to unsatisfactory methods for controlling and maintaining the desired level of O_2 pressures in the gas phase. These relations are likely to be better understood upon completion of studies of the system MnO—Mn_2O_3—SiO_2 at various O_2 partial pressures now in progress in our laboratories.

The extremely strong stabilizing effect of SiO_2 on Mn^{2+} relative to the higher valence states of manganese in melts becomes apparent by an inspection of the composition curve for the liquid in the lower half of figure 1. This curve is for liquids at liquidus temperatures in air, hence temperature is a variable in addition to composition (silica to manganese oxide ratio). The effect of temperature is simple: Because the oxidation of Mn^{2+} is exothermic, a decrease in temperature causes a decrease in the Mn^{2+}/Mn^{3+} ratio. Referring to figure 1 it will be noticed that a pure manganese oxide liquid in air at temperature slightly above the liquidus consists of approximately 40 Wt.% MnO and 60 Wt.% Mn_2O_3. As SiO_2 is added, liquidus temperatures decrease (see upper half of fig. 1). If temperature were the only factor determining the Mn^{2+}/Mn^{3+} equilibrium, this ratio would be expected to decrease as silica is added, corresponding to a curve originating at the 40 MnO 60 Wt.% Mn_2O_3 composition point and located on the Mn_2O_3 side of the straight line connecting this point with the SiO_2 corner of the triangle in figure 1. The actual curve, however, bends sharply to the opposite side of this straight line. This situation is a result of the strong effect of acidity[1] on the Mn^{2+}/Mn^{3+} equilibrium. As the acidity of the system increases with increasing SiO_2 content, the Mn^{2+} is stabilized relative to Mn^{3+}, and so strong is this stabilizing effect of SiO_2 that it completely overshadows the opposite effect on the Mn^{2+}/Mn^{3+} equilibrium of decreasing temperatures. Hence the 0.21 atm. O_2 isobar along the liquidus surface has the course represented by the heavy curve in the lower half of figure 1. The slope of this curve varies continuously, except where a boundary curve is crossed.

The composition of the silica-rich liquid in the region of equilibrium coexistence of two immiscible liquids was only estimated roughly. The refractive index of the glass was not significantly larger than that of pure SiO_2 glass, and the manganese oxide content is judged not to exceed 1 Wt.%.

The relation between a diagram drawn with the appearance of a binary system, such as the join Mn_3O_4—SiO_2 represented in the upper half of figure 1, and the ternary system MnO—Mn_2O_3—SiO_2 represented in the lower, tri-

[1] For a discussion of acid-base relations in silicate liquids, see for instance a recent paper by Weyl (1956).

angular diagram in figure 1, has been explained in detail in previous papers by this author dealing with phase equilibria in iron oxide containing silicate systems (Muan, 1955, 1957, 1958). The same methods described in those papers have been used for projecting composition points from the lower ternary system up to the "binary" join in figure 1. Straight lines are drawn through composition points with a direction toward the O corner of the triangle representing the system Mn—Si—O. These lines are "reaction lines" describing changes in total composition of condensed phases as these react with O_2 of the gas phase in response to temperature changes. The intersections between these reaction lines and the Mn_3O_4—SiO_2 join in the lower triangular diagram are taken to represent compositions of condensed phases in the upper simplified "binary" diagram. These points are projected to the upper, binary join by first swinging the Mn_3O_4—SiO_2 join in the triangle around the SiO_2 corner upward until it falls on the Mn_2O_3—SiO_2 join, and then displacing the points along vertical lines to the upper half of the figure.

When using and interpreting the "binary" phase diagram in the upper part of figure 1 it is important to keep in mind its relation to the ternary system. Although it is true that compositions of condensed phases cannot be expressed in terms of two chosen components, such as Mn_3O_4 and SiO_2, nevertheless this diagram can be treated like a binary system as far as path of crystallization is concerned. The oxygen of the atmosphere (air) reacts with the condensed phases to keep the liquid compositions along the 0.21 atm. O_2 isobaric curve regardless of the nature of the crystalline phases separating out. Hence an apparently invariant situation will exist where the 0.21 atm. O_2 isobar crosses a boundary curve. Only at one temperature, at the given O_2 partial pressure, can two crystalline phases and a liquid coexist in equilibrium, because one degree of freedom has been "used up" in choosing air as the atmosphere. Consequently, intersections between the 0.21 atm. O_2 isobar and univariant lines in the system Mn—Si—O appear as invariant situations in the upper "binary" system.

An extensive discussion of the application of phase equilibria in the system manganese oxide-silica to geochemical and technological problems must await results of studies presently in progress in our laboratories at various O_2 partial pressures. However, a few general remarks may be made. The relatively constant ratio of silica to manganese oxide in naturally occurring braunites is an interesting observation which may perhaps be used to infer some of the conditions existing during the formation of this phase in nature. The composition limits of braunite depend primarily on two parameters, temperature and O_2 partial pressure. As O_2 partial pressure is reduced, the Mn_2O_3 to Mn_3O_4 decomposition temperature decreases, and the two boundary curves in figure 1, representing compositions of braunite in equilibrium with Mn_3O_4 and $MnO \cdot SiO_2$(ss), respectively, move downward. Hence the "peak" at which these lines meet also moves downward with decreasing O_2 pressure, and the composition of the braunite phase in terms of silica to manganese oxide ratio at this peak may also vary. These relations are illustrated in the sketch in figure 3. If a naturally occurring braunite has been formed at a temperature close to the "peak" under the prevailing conditions of

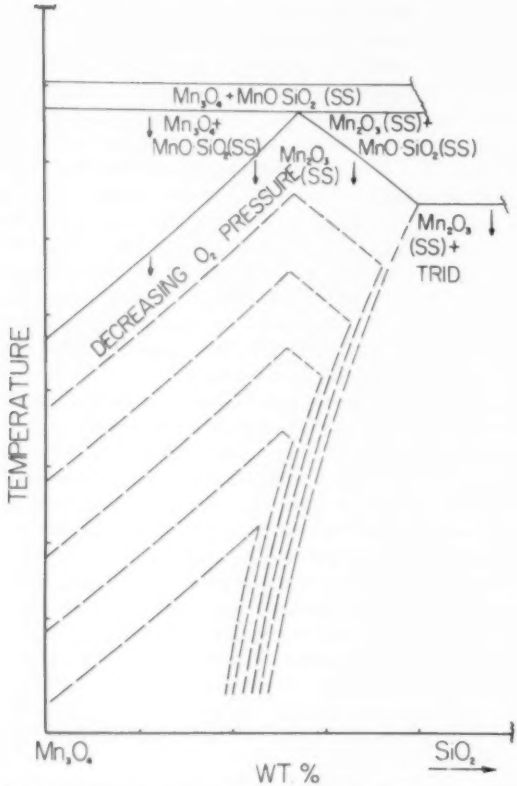

Fig. 3. Sketch presented in order to indicate probable changes in composition range of Mn_2O_3(ss) as O_2 partial pressure is decreased below that of air (compare discussion in text).

O_2 partial pressure, its composition range should be very narrow. Moreover, if the shift in the "peak" composition is known as a function of temperature and O_2 partial pressure from laboratory examinations, a close estimate of the values of these parameters at the time of formation of the mineral assemblage may be possible. Although slow reaction rates probably will prevent an experimental study of these reactions down to temperatures much below 1000°C, an attempt to map out the composition limits of the braunite phase volume seems like a worthwhile subject for future research.

SUMMARY

A start has been made on the investigation of phase equilibria in the system Mn—Si—O by working along the 0.21 atm. O_2 isobaric section through this system at a total pressure of 1 atm. The phase relations are

represented in an *apparently* binary diagram (Mn_3O_4—SiO_2) showing phases present as a function of temperature, and a supplementary diagram showing true compositions of condensed phases. Intersections between the 0.21 atm. O_2 isobar and boundary curves on the liquidus surface correspond to liquidus univariant situations in the ternary system characterized by the equilibrium coexistence of two crystalline, one liquid and a gas phase, or one crystalline, two liquid and a gas phase. However, because the O_2 partial pressure of the latter has been chosen, the existing degree of freedom has been "used up", and the presence of these phases in equilibrium appears as invariant situations in the system drawn as the "binary" system Mn_3O_4—SiO_3 for sake of simplification. Similarly, subsolidus ternary univariant situations in the system Mn—Si—O, with 3 crystalline phases and gas existing together in equilibrium, appear as invariant situations in the simplified "binary" diagram.

The "binary" system and the "invariant" situations are characterized as follows: manganese oxide melts at 1567°C in air, cubic Mn_3O_4 being the primary crystalline phase. Liquidus temperatures decrease sharply as SiO_2 is added A "peritectic" situation exists at 1230°C with Mn_3O_4, tephroite and a liquid of composition $54MnO$, $13Mn_2O_3$, 33 Wt.% SiO_2 present together in equilibrium with the gas. At 1206°C tephroite, $MnO \cdot SiO_2$(ss) (rhodonite), a liquid of composition $54MnO$, $12Mn_2O_3$, 34 Wt.% SiO_2 and gas coexist in equilibrium in what appears to be an eutectic situation. With SiO_2 contents increasing above 34 Wt.%, liquidus temperatures start rising, $MnO \cdot SiO_2$(ss) being the primary crystalline phase in the composition range 34-42 Wt.% SiO_2. At 1272°C another apparently peritectic sitaution prevails, with $MnO \cdot SiO_2$(ss), tridymite and liquid of composition $53MnO$, $5Mn_2O_3$, 42 Wt.% SiO_2 existing together in equilibrium in air. As SiO_2 content increases still farther, liquidus temperatures rise very steeply toward a plateau at 1700°C caused by the presence of two immiscible liquids over the composition range 55-99 Wt.% SiO_2 at liquidus temperatures. The melting point of pure SiO_2 (cristobalite) is 1723°C. Phase transformation in Mn_3O_4 and oxidation-reduction equilibria give rise to four apparently invariant situations in the subsolidus region of the system in the temperature range investigated. At 1204°C Mn_3O_4, tephroite and $MnO \cdot SiO_2$(ss) coexist in equilibrium in air. At 1168°C the following crystalline phases exist together in equilibrium: cubic Mn_3O_4, Mn_2O_3(ss) and $MnO \cdot SiO_2$(ss). At 1160°C another "invariant" situation exists as the tetragonal and cubic forms of Mn_3O_4 are present together with Mn_2O_3(ss) and gas. The phase $MnO \cdot SiO_2$(ss) is stable in air down to 1048°C. At this temperature it decomposes to Mn_2O_3(ss) and tridymite in an apparently eutectoid situation.

The presence of tephroite and $MnO \cdot SiO_2$(ss) as the equilibrium phases at liquidus temperatures in air shows the extreme stability of the Mn^{2+} ion and accounts for its occurrence almost to the exclusion of manganese ions of higher valence states in igneous minerals and rocks. The Mn_2O_3(ss) crystals appearing as one of the equilibrium phases in the subsolidus temperature region seem to be the synthetic analogues of the naturally occurring mineral braunite, "$3Mn_2O_3 \cdot MnSiO_3$". A large range of manganese oxide to silica ratios in this phase has been found in the present investigation, strongly sug-

gesting a subsitution of Si^{4+} for Mn^{4+} in the lattice of α–Mn_2O_3. In accordance with this observation and previous evidence from chemical as well as magnetic tests the α-form of Mn_2O_3 is probably best represented by the formula $(Mn^{2+}\ Mn^{4+})O_3$, and the braunite formula should be written more appropriately $Mn^{2+}(Mn^{4+}, Si^{4+})O_3$. Compositions of natural braunites should depend mainly on temperature and O_2 partial pressure existing during formation of the mineral. Further laboratory work on composition limits for the Mn_2O_3(ss) phase as a function of temperature and O_2 partial pressure, combined with chemical and petrographic analyses of braunite in manganese deposits, may shed some new light on the conditions of formation of these deposits.

ACKNOWLEDGMENTS

The assistance of T. Ranganathan and A. M. Byström in carrying out and supervising the chemical analysis, respectively, is gratefully acknowledged. This work was carried out as part of a research project sponsored by the American Iron and Steel Institute following the recommendation of the Research Subcommittee of the Refractories Committee. The author wishes to acknowledge the many helpful suggestions made by E. F. Osborn during the preparation of this manuscript.

TABLE 1

Results of Quenching Experiments

Temp. of Quenching Run (°C)	Phases Present*	Temp. of Run for Anal. (°C)	Initial Comp. (Wt.%) Mn_3O_4	Initial Comp. (Wt.%) SiO_2	Comp. After Equilibration (Wt.%) MnO	Comp. After Equilibration (Wt.%) Mn_2O_3	Comp. After Equilibration (Wt.%) SiO_2
1571	Liq.	1577	100	0			
1565	Mn_3O_4						
1565	Liq.	1574	99	1	38	61	1
1559	Mn_3O_4 + Liq.						
1256	Mn_3O_4 + Liq.						
1213	Mn_3O_4 + Teph.						
1194	Mn_3O_4 + $MnO \cdot SiO_2$(ss)						
1096	Mn_3O_4 + Mn_2O_3(ss)						
1557	Liq.	1566	98	2	44	54	2
1547	Mn_3O_4 + Liq.						
1539	Liq.	1551	95	5	51	44	5
1534	Mn_3O_4 + Liq.						
1234	Mn_3O_4 + Liq.						
1225	Mn_3O_4 + Teph.						
1208	Mn_3O_4 + Teph.						
1201	Mn_3O_4 + $MnO \cdot SiO_2$(ss)						
1508	Liq.	1515	90	10	45	45	10
1500	Mn_3O_4 (tr.) + Liq.						
1488	Mn_3O_4 + Liq.						
1160	Mn_3O_4 + Mn_2O_3 (ss)						
1000	Mn_3O_4 + Mn_2O_3 (ss)						

TABLE 1 (Continued)

Temp. of Quenching Run (°C)	Phases Present*	Temp. of Run for Anal. (°C)	Initial Comp. (Wt.%) Mn_3O_4	SiO_2	Comp. After Equilibration (Wt.%) MnO	Mn_2O_3	SiO_2
1417	Liq.	1420	80	20	51	29	20
1412	Mn_3O_4 + Liq.						
1233	Mn_3O_4 + Liq.						
1223	Mn_3O_4 + Teph.						
1204	Mn_3O_4 + Teph. + $MnO \cdot SiO_2$(ss)						
1194	Mn_3O_4 + $MnO \cdot SiO_2$(ss)						
1170	Mn_3O_4 + $MnO \cdot SiO_2$(ss)						
1161	Mn_3O_4 + Mn_2O_3(ss)						
1094	Mn_3O_4 (tr.) + Mn_2O_3(ss)						
1070	Mn_2O_3(ss)						
1000	Mn_2O_3(ss)						
1070	Mn_2O_3(ss)		78	22			
1164	Mn_3O_4 + Mn_2O_3(ss)		76	24			
1144	Mn_3O_4 + Mn_2O_3(ss)						
1094	Mn_2O_3(ss)						
1164	Mn_3O_4 (tr.) + Mn_2O_3(ss)		74	26			
1144	Mn_2O_3(ss)						
1226	Mn_3O_4 + Teph.		72	28			
1164	Mn_2O_3(ss) + $MnO \cdot SiO_2$(ss) (tr.)						
1144	Mn_2O_3(ss)						
1170	Mn_3O_4 + $MnO \cdot SiO_2$(ss)	1315	71	29	58	13	29
1164	Mn_2O_3(ss) + $MnO \cdot SiO_2$(ss)						
1144	Mn_2O_3(ss)						
1292	Liq.	1297	70	30	59	11	30
1277	Mn_3O_4 + Liq.						
1232	Mn_3O_4 + Liq.						
1227	Teph. + Liq.						
1208	Teph. + Liq.						
1206	Teph. + $MnO \cdot SiO_2$(ss) + Liq.						
1204	Mn_3O_4 + Teph. + $MnO \cdot SiO_2$(ss)						
1194	Mn_3O_4 + $MnO \cdot SiO_2$(ss)						
1170	Mn_3O_4 + $MnO \cdot SiO_2$(ss)						
1160	Mn_2O_3(ss) + $MnO \cdot SiO_2$(ss)						
1094	Mn_2O_3(ss)						
1257	Liq.	1260	68	32	53	15	32
1249	Mn_3O_4 + Liq.						
1233	Mn_3O_4 + Liq.						
1223	Teph. + Liq.						
1164	Mn_2O_3(ss) + $MnO \cdot SiO_2$(ss)						
1220	$MnO \cdot SiO_2$(ss) (tr.) + Liq.		65	35			
1207	$MnO \cdot SiO_2$(ss) + Liq.						
1205	Teph. + $MnO \cdot SiO_2$(ss)						
1203	Mn_3O_4 + Teph. + $MnO \cdot SiO_2$(ss)						
1200	Mn_3O_4 + $MnO \cdot SiO_2$(ss)						
1160	Mn_2O_3(ss) + $MnO \cdot SiO_2$(ss)						
1107	Mn_2O_3(ss) + $MnO \cdot SiO_2$(ss)						
1094	Mn_2O_3(ss)						

TABLE 1 (Continued)

Temp. of Quenching Run (°C)	Phases Present*	Temp. of Run for Anal. (°C)	Initial Comp. (Wt.%) Mn_3O_4	Initial Comp. (Wt.%) SiO_2	Comp. After Equilibration (Wt.%) MnO	Comp. After Equilibration (Wt.%) Mn_2O_3	Comp. After Equilibration (Wt.%) SiO_2
1264	Liq.	1269	60	40	53.5	6.5	40
1255	$MnO \cdot SiO_2$(ss) + Liq.						
1160	Mn_2O_3(ss) + $MnO \cdot SiO_2$(ss)						
1060	Mn_2O_3(ss) + $MnO \cdot SiO_2$(ss)						
1040	Mn_2O_3(ss) + Trid.						
1025	Mn_2O_3(ss) + Trid.						
1280	Liq.		58	42			
1270	$MnO \cdot SiO_2$(ss) (tr.) + Liq.						
1264	$MnO \cdot SiO_2$(ss) + Liq.						
1220	$MnO \cdot SiO_2$(ss) + Liq.						
1211	$MnO \cdot SiO_2$(ss)						
1240	$MnO \cdot SiO_2$(ss) + Liq.		57.4	42.6			
1217	$MnO \cdot SiO_2$(ss)						
1180	$MnO \cdot SiO_2$(ss)						
1094	Mn_2O_3(ss) + $MnO \cdot SiO_2$(ss)						
1308	Liq.	1311	56.7	43.3	52	4	44
1298	Trid. (tr.) + Liq.						
1277	Trid. + Liq.						
1271	$MnO \cdot SiO_2$(ss) + Liq.						
1250	$MnO \cdot SiO_2$(ss) + Liq. (tr.)						
1220	$MnO \cdot SiO_2$(ss)						
1180	$MnO \cdot SiO_2$(ss)						
1094	$MnO \cdot SiO_2$(ss)						
1259	$MnO \cdot SiO_2$(ss) + Liq. (tr.)		55.7	44.3			
1220	$MnO \cdot SiO_2$(ss)						
1180	$MnO \cdot SiO_2$(ss)						
1094	$MnO \cdot SiO_2$(ss)						
1404	Liq.	1381	55	45	51	4	45
1366	Trid. (tr.) + Liq.						
1342	Trid. + Liq.						
1277	Trid. + Liq.						
1269	$MnO \cdot SiO_2$(ss)						
1160	$MnO \cdot SiO_2$(ss) + Trid. (tr.)						
1080	$MnO \cdot SiO_2$(ss) + Trid. (tr.)						
1051	$MnO \cdot SiO_2$(ss) + Trid. (tr.)						
1045	Mn_2O_3(ss) + Trid.						
990	Mn_2O_3(ss) + Trid.						
1760	Liq.		50.8	49.2			
1488	Liq.						
1471	Trid. (tr.) + Liq.						
1760	Liq.		45	55			
1710	$Liq._1$ + $Liq._2$ (tr.)						
1660	Crist. + Liq.						
1518	Crist. + Liq.						
1400	Trid. + Liq.						
1056	Trid. + $MnO \cdot SiO_2$(ss)						
1042	Trid. + Mn_2O_3(ss)						
1496	Trid. + Crist. + Liq.		40.6	59.4			
1461	Trid. + Liq.						

TABLE 1 (Continued)

Temp. of Quenching Run (°C)	Phases Present*	Temp. of Run for Anal. (°C)	Initial Comp. (Wt.%) Mn_3O_4	SiO_2	Comp. After Equilibration (Wt.%) MnO	Mn_2O_3	SiO_2
1760	$Liq._1 + Liq._2$		35	65			
1708	$Liq._1 + Liq._2$						
1692	Crist. + Liq.						
1620	Crist. + Liq.						
1496	Trid. + Liq.						
1710	$Liq._1 + Liq._2$		12	88			
1690	Crist. + Liq.						
1475	Crist. + Liq.						
1430	Crist. + Liq.						

* Abbreviations used in this and succeeding tables have the following meanings: Teph. = crystals of tephroite ($2MnO \cdot SiO_2$); Crist. = crystals of cristobalite; Trid. = crystals of tridymite; Liq. = liquid; tr. = trace; (ss) = solid solution.

Summary of "Invariant"* Situations in the System Manganese Oxide—SiO_2 in Air

Phases Present	Comp. of Liquid (Wt.%) MnO	Mn_2O_3	SiO_2	Temperature (°C)
Mn_3O_4(cubic) + Liq.	40	60		1567
Mn_3O_4(cubic) + Mn_3O_4(tetr.)**				1160
Mn_3O_4(tetr.) + Mn_2O_3**				877
Mn_3O_4(cubic) + Teph. + Liq.	54	13	33	1230
Teph. + $MnO \cdot SiO_2$(ss) + Liq.	54	12	34	1206
Mn_3O_4(cubic) + Teph. + $MnO \cdot SiO_2$(ss)				1204
Mn_3O_4(cubic) + Mn_2O_3(ss) + $MnO \cdot SiO_2$(ss)				1168
$MnO \cdot SiO_2$(ss) + Trid. + Liq.	53	5	42	1272
Mn_2O_3(ss) + $MnO \cdot SiO_2$(ss) + Trid.				1048
Trid. + Crist. + Liq.	49	2	49	1470
Crist. + $Liq._1$ + $Liq._2$	44 1	1	55 99	1700
Trid. + Crist.**				1470
Crist. + Liq.**			100	1723

* The phase assemblages listed in reality represent univariant situations in the ternary system Mn—Si—O. However, the existing degree of freedom has been "used up" in choosing the O_2 partial pressure of the gas phase, and hence the situations may be considered "invariant".

** "Invariant" situations marked with double asterisk are based on data available in the literature, as follows:

Mn_3O_4(cubic) + Mn_3O_4(tetr.)	Van Hook and Keith, 1958
Mn_3O_4 + Mn_2O_3	Hahn and Muan, in press.
Trid. + Crist.	Sosman, 1955
Crist. + Liq.	Sosman, 1955

Powder X-ray Diffraction Data for Manganese Oxide Containing Crystalline Phases
(Fe Kα Radiation)

Mn_3O_4		Mn_2O_3(ss)		$2MnO \cdot SiO_2$		$MnO \cdot SiO_2$(ss)	
d	I/I_0	d	I/I_0	d	I/I_0	d	I/I_0
4.94	0.3	3.47	0.1	5.34	0.1	3.54	0.3
3.09	0.4	3.33	0.1	4.03	0.3	3.33	0.4
2.88	0.1	2.96	0.1	3.87	0.1	3.13	0.6
2.77	0.9	2.72	1.0	3.63	0.5	3.06	1.0
2.49	1.0	2.36	0.2	3.14	0.3	2.95	0.9
2.37	0.3	2.15	0.2	2.86	0.8	2.75	0.8
2.04	0.3	1.664	0.4	2.70	0.2	2.60	0.5
1.800	0.2			2.61	0.7	2.50	0.2
1.702	0.1			2.56	1.0	2.44	0.1
1.587	0.3			2.45	0.3	2.37	0.2
1.556	0.5			1.893	0.1	2.23	0.2
1.442	0.2			1.824	0.9	2.19	0.2
				1.735	0.2	2.12	0.1
				1.697	0.2	2.08	0.2
				1.570	0.4	1.892	0.1
				1.543	0.3	1.831	0.1
						1.730	0.1

References

Aminoff, G., 1931, Lattice dimensions and space group of braunite: Kungl. Sven. Vetenskapsakad. Hand., v. 9, p. 14-22.

Atlas, Leon, 1952, Polymorphism of $MgSiO_3$ and solid-state equilibria in the system $MgSiO_3$—$CaMgSi_2O_6$: Jour. Geol., v. 60, p. 125-147.

Byström, Anders and Mason, Brian, 1943, The crystal structure of braunite, $3Mn_2O_3 \cdot MnSiO_3$: Arkiv Kemi, Mineral., Geol., v. 16 B, p. 1-8.

Corruccini, R. J., 1949, Differences between the international temperature scales of 1948 and 1927: Jour. Research Natl. Bur. Standards, v. 43, p. 133-146.

Coughlin, J. P., 1954, Contributions to the data on theoretical metallurgy, XII—Heats and free energies of formation of inorganic oxides: U. S. Bur. Mines, Bull. 542.

Dana, J. D., and Dana, E. S., 1944, The system of mineralogy; rewritten by Palache, Charles; Berman, Harry and Frondel, Clifford: New York, John Wiley and Sons, Inc., 7th ed., v. 1., 834 p.

Doerinckel, F., 1911, Untersuchungen über das System Manganoxydul—Kieselsäure: Metallurgie, v. 8, p. 201-211.

Dubois, Pierre, 1934, Hydrate et variétés allotropiques du sesquioxyde de manganèse: Comptes Rendus, v. 199, p. 1416-1418.

Eitel, W., 1957, Structural anomalies in tridymite and cristobalite: Am. Ceram. Soc. Bull., v. 36, p. 142-148.

Fenner, C., 1913, The stability relations of the silica minerals: Am. Jour. Sci., v. 36, p. 331-384.

Flink, Gustav, 1926, Långban and its minerals: Am. Mineralogist, v. 11, p. 195-199.

Flörke, O. W., 1955, Strukturanomalien bei Tridymit und Kristobalit: Ber. deutsch. Keram. Ges., v. 32, p. 369-381.

Fyfe, W. S., 1949, State of manganese in manganese oxides: Nature, v. 164, p. 790.

Glaser, O., 1926, Thermische und mikroskopische Untersuchungen an den für die Kupolofenschlacke bedeutsamen Systemen: MnO—Al_2O_3—SiO_2, MnS—$MnSiO_3$ und CaS—$CaSiO_3$: Cent. für Mineral., Geol. und Palä., Abt. A: Min. und Petrog., p. 81-96.

Glasser, F. P., 1958, The system MnO—SiO_2: Am. Jour. Sci., v. 256, p. 398-412.

Goldschmidt, V. M., 1954, Geochemistry: London, Oxford Univ. Press, 730 p.

Hahn, W. C., and Muan, Arnulf, in press, Studies in the system Mn—O: Am. Jour. Sci.

Herty, C., 1930, Fundamental and applied research on the physical chemistry of steelmaking: Metals and Alloys, v. 1, p. 883-889.

Hill, V. G., and Roy, Rustum, in press, Silica structure studies, VI: On tridymites: Brit. Ceram. Soc. Trans., v. 57, p. 496-510.

Krishnan, K. S., and Banerjee, S., 1939, Magnetic studies on braunite, $3Mn_2O_3 \cdot MnSiO_3$: Zeitschr. Krist., v. 101, p. 507-511.

Magnusson, Nils H., 1924, The Långban minerals from a geological point of view: Geol. Fören. Stockholm Förhandl., p. 284-300.

Muan, Arnulf, 1955, Phase equilibria in the system FeO—Fe_2O_3—SiO_2: AIME Trans., v. 203, p. 965-976; Jour. Metals, Sept., 1955.

———, 1957, Phase equilibria at liquidus temperatures in the system iron oxide—Al_2O_3—SiO_2 in air atmosphere: Am. Ceram. Soc. Jour., v. 40, p. 121-133.

———, 1958, Phase equilibria at high temperatures in oxide systems involving changes in oxidation states: Am. Jour. Sci., v. 256, p. 171-207.

Palache, Charles, 1929, A comparison of the ore deposits of Långban, Sweden, with those of Franklin, New Jersey: Am. Mineralogist, v. 14, p. 43-47.

Pauling, L., and Shappell, M. D., 1930, The crystal structure of bixbyite and the C-modification of the sesquioxides: Zeitschr. Krist., v. 75, p. 128-142.

Roberts, H. S., and Morey, G. W., 1930, Micro-furnace for temperatures above 1000°C: Rev. Sci. Instr., v. 1, p. 576-579.

Sosman, R. B., 1952, Temperature scales and silicate research: Am. Jour. Sci., Bowen Volume, p. 517-528.

Sosman, R. B., 1955, New and old phases of silica: Brit. Ceram. Soc. Trans., v. 54, p. 655-670.

Van Hook, H. J., and Keith, M. L., 1958, The system Fe_2O_3—Mn_3O_4: Am. Mineralogist, v. 43, p. 69-83.

Weyl, W. A., 1956, Acid-base relationship in glass systems. A new acid-base concept applicable to aqueous systems, fused salts, glasses, and solids: The Glass Industry, v. 37, p. 264-269, 286, 288, 325-331, 336, 344, 346, 350.

White, J., Howat, D., and Hay, R., 1934, The binary system MnO—SiO_2: Roy. Tech. Coll. Jour. (Glasgow), v. 3, p. 231-240.

Zachariasen, W., 1928, Über die Kristallstruktur von Bixbyit, sowie vom künstlichen Mn_2O_3: Zeitschr. Krist., v. 67, p. 455-464.

[American Journal of Science, Vol. 257, April 1959, P. 316-320]

THE ANALCIME-JADEITE PHASE BOUNDARY: SOME INDIRECT DEDUCTIONS

W. S. FYFE and G. W. VALPY

Chemistry Dept., University of Otago, Dunedin, New Zealand

ABSTRACT. From a consideration of phase changes involving analcime some estimates have been made of the equilibrium pressures of the reaction: analcime = jadeite + H_2O. The results, although subject to large uncertainties, suggest that equilibrium pressures from existing experimental data are too high, particularly at the low temperature end of the system. Entropy and volume data for analcime confirm this conclusion and indicate that the boundary should have positive slope at low temperatures.

Over the past few years there has been a steady stream of papers concerned with the stability of mineral assemblages with total compositions corresponding to $Na_2O.Al_2O_3.4SiO_2$ and $Na_2O.Al_2O_3.6SiO_2$. These compositions are involved in the reactions:

$$\text{nepheline} + \text{albite} = 2 \text{ jadeite}$$
$$\text{albite} = \text{jadeite} + \text{quartz}.$$

In a hydrous system the place of the zeolite analcime must be considered, and from phase relations involving this phase it is possible to make an estimate of the conditions of the reaction:

$$\text{analcime} = \text{jadeite} + \text{water}.$$

At the present time calorimetric data exists for the phases albite, jadeite, nepheline and quartz but only entropy data is available for analcime. However, estimates of the necessary quantities can be obtained from phase relations.

The analcime = nepheline + albite + water phase boundary and an estimate of the analcime = jadeite equilibrium pressure at 535°C.—From studies in this laboratory (Valpy, 1958) it is considered that at 535°C (± 10°) the equilibrium pressure of the reaction:

$$\text{analcime} = \tfrac{1}{2} \text{ nepheline} + \tfrac{1}{2} \text{ albite} + H_2O \qquad (1)$$

is 1000 atmospheres. This value is in good agreement with that of Yoder (1954). At this point we then have the condition that the free energy change of reaction (1) is zero. From calorimetric and volume data the free energy of the reaction:

$$\tfrac{1}{2} \text{ nepheline} + \tfrac{1}{2} \text{ albite} = \text{jadeite} \qquad (2)$$

may be estimated at 535°C and 1000 atmospheres and hence under these conditions the free energy of reaction (2) is identical with the free energy of the reaction:

$$\text{analcime} = \text{jadeite} + H_2O \qquad (3)$$

From the data summarized by Kelley, et al. (1953) the free energy of reaction (3) at 535°C and 1000 atmospheres is approximately 3,400 calories. (All figures are rounded to the nearest 100 calories as errors involved in the figures themselves and approximations in the subsequent calculations do not justify greater accuracy.) As analcime is a phase of low density, at any moderate pressure the ΔV of reaction (3) is large and negative. In fact, if the density of water is unity, then the ΔV of reaction (3) is larger than that of reaction (2).

To evaluate the equilibrium pressure of reaction (3) at 535°C we require data on the molar volume of water between 1000 atmospheres and this pressure. We have attempted to estimate this by extrapolation of Kennedy's data (1950) making use of the linear character of constant density, pressure-temperature plots. With this data the equilibrium pressure estimated is 10,700 atmospheres. The average water density in the range was taken as 0.82 with an average ΔV of -14.43 cm^3. The density of analcime was taken as 2.267 from Hartwig (1930). Other densities were taken from Robertson, Birch and MacDonald (1957). Although the water density is difficult to estimate and may be considerably in error the ΔV due to this uncertainty should not be more than 15 percent and hence the estimated pressure should be within $\pm$ 1500 atmospheres. The ΔV of reaction (2) is -16.8 cm^3, only slightly greater than ΔV of (3), and hence the transition pressure of (3) should not be much greater than that of (2). In these calculations thermal expansion and compressibility of all solid phases is ignored.

The analcime + quartz = albite + water phase boundary and an estimate of the analcime = jadeite + water equilibrium pressure at 285°C.—The above reasoning may now be applied to the reaction:

$$\text{analcime} + \text{quartz} = \text{albite} + H_2O \qquad (4)$$

which we consider to be in equilibrium at 285°C ($\pm$ 15°) and 1000 atmospheres (Ellis, 1958; Valpy, 1958). From Kelley, et al. (1953) thermodynamic data is available for the reaction:

$$\text{albite} = \text{jadeite} + \text{quartz} \qquad (5)$$

and as the free energy change of reaction (4) is zero at 285° and 1000 atmospheres the free energy change of reaction (5) will be identical under these conditions with that of the reaction:

$$\text{analcime} + \text{quartz} = \text{jadeite} + \text{quartz} + H_2O \qquad (6)$$

The free energy change of (6) is thus approximately 4.200 calories. This free energy is greater than that of reaction (3) at 535° and 1000 atmospheres but at 285°C the ΔV will be greater due to the smaller molar volume of water. In this region extrapolation of Kennedy's data was subject to considerable uncertainties and an average water density of unity was assumed. This figure is possibly a little high but should not introduce more than 10 percent error in ΔV. The average ΔV of reaction (6) used was -18.4 cm^3 and the equilibrium pressure of reaction (6) is thus 10,500 atmospheres. The pressure is very similar to that estimated at 535°C and indicates that reaction (3) (or (6), which is of course, identical) has a very small entropy change.

The equilibrium pressure of the reaction: analcime = jadeite + water at 25°C.—To obtain an estimate of the transition pressure of analcime to jadeite at 25°C it is necessary to have data on the entropy of analcime. This is available from the measurements of King (1955) who gives a value of 56.0 cals/mol./degree at 25°C. This is an abnormally high entropy. Following Latimer (1951) it might be expected that the entropy would be close to that given by $\frac{1}{2}\ S_{ab} + \frac{1}{2}\ S_{neph.} + S_{ice} = 49.5$ cals./mol./degree. In this calculation S_{ice} is taken as 9.6 cals./mol., a value obtained from consideration of a large number of hydrates. The entropy is thus 6.5 cals./mol. too large. In general,

there is a good correlation between entropy and molar volume (see Fyfe, Turner and Verhoogen, 1958) and relative to nepheline, albite and ice, the molar volume of analcime is similar. This suggests that the large entropy may be associated with randomness of the cation arrangement in the analcime structure. The entropy and molar volume of jadeite are lower than that one would estimate by summing values for nepheline and albite. It may be noted further that there is a general correlation between the entropy contribution of water to a solid and the apparent volume of water in the solid, (this is taken as the difference in the volume of hydrate and anhydrous phase). In many cases the apparent molar volume of water is in the range 13-17 cm^3 with entropy contributions ranging from 8-11 cals./mol. With analcime the apparent molar volume of water is 20.3 cm^3 and a high entropy contribution would be expected. A further confirmation of the high entropy of analcime can be obtained from the temperature interval between the curves of reactions (4) and (1).

At 535°C and a thousand bars the free energy of reaction (4) is identical with that of the reaction:

$$\tfrac{1}{2} \text{ nepheline} + \text{quartz} = \tfrac{1}{2} \text{ albite} \qquad (7)$$

at 535°C. The free energy of (7) is available from Kelley, et al. (1953). If we assume that ΔC_p for reaction (4) is small, then $\Delta T\,\Delta S = \Delta G$ where ΔT is the difference in boundary temperatures of reactions (1) and (4), 250°C, and ΔS is the average entropy of reaction (4) between 285° and 535°C. From this argument ΔS is 11.6 cals./mol. This is a low value for a dehydration reaction in the region 285-535°C (see Fyfe, Turner and Verhoogen, 1958). From data in Kelley (1949) and from estimates of the entropy of water by Fyfe, Turner and Verhoogen, we may compare this value with those for the reactions brucite to periclase + vapor and boehmite to corundum + vapor. The average ΔS for these reactions is near 14 cals./mol. Using 56.0 cals./mol. for the entropy of analcime the entropy change of reaction (3) at 25°C is −7.35 cals./mol./degree. The volume change is certainly negative so that the low temperature

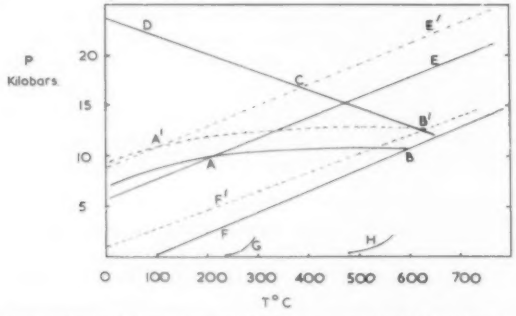

Fig. 1. Some estimated boundary relations concerned with jadeite. F-B and A-E are the calculated curves for reactions (2) and (5). A-B is the estimated curve for reaction (3). D-C is the boundary for (3) reported by Griggs and Kennedy. H and G represent the experimental boundaries for reactions (1) and (4) from Ellis, 1958, and Valpy, 1958. Dotted lines represent approximate corrections from data of Robertson, Birch and MacDonald (1957).

boundary should have positive slope. This conclusion is not changed by consideration of the compressibility of analcime (Yoder, 1955).

We may now proceed to estimate the free energy change of reaction (4) at 25°C. A "normal" ΔS of hydration in the range 25-285°C would be around 8 cals./mol. (Fyfe, Turner, Verhoogen, 1958) and for analcime it is more likely to be around 2-3 cals./mol. The entropy of reaction (4) at 25°C has the remarkably small value of +1cal./mol. These values lead to a free energy change at 25°C and 1000 bars for reaction (4) of 780 cals./mol. and for reaction (3) a free energy change of 2,900 cals./mol. Assuming a water density of unity the equilibrium pressure would be 7,600 atmospheres and allowing for the compression of water (Dorsey, 1940), is more likely to be around 7000 atmospheres. In figure 1, data for all calculated boundaries are summarized. From the ΔS and ΔV values the positive slope of the analcime-jadeite boundary should be around 15 atmospheres/°C at 25°C.

It should perhaps be mentioned that a similar value at 25°C is obtained simply by taking an average entropy of reaction (1) from 535-25°C assuming that the entropy of analcime at 25°C is 56 cals./mol./degree. This then frees the calculations from any use of data from reaction (5).

DISCUSSION

The only experimental boundary between the phases analcime and jadeite is that in Griggs and Kennedy (1956). This boundary is shown in figure 1 line C-D. Obviously there is enormous departure from the present estimated curve A-B in the low temperature region. Although there are great uncertainties in the estimated curve it is difficult to account for a three-fold error. The experimental results of Robertson, Birch and MacDonald (1957) on jadeite stability suggest that the calculated boundaries A-E and B-F are about 2000 bars too low and if these are raised the analcime-jadeite boundary will be increased by a similar amount. This would lead to close agreement with the published boundary at 600°C. and the position of the invariant point (B′) indicated by Robertson, Birch and MacDonald.

It will be noticed that the position of the second invariant point (A) suggests a large amount of back bending of the analcime-albite boundary. Such back bending must occur in this boundary because ΔV of the reaction will change sign at high pressures but it is difficult to estimate the extent. On the other hand, if line C-D was correct then the invariant point would be at C and there would be little scope for the required reversal of slope which once more suggests that this boundary is too high. It is also possible that the observed analcime-albite boundary is too high, it certainly represents an upper limit of analcime rather than a lower limit of albite as will be discussed in a later paper.

Features of petrogenetic interest arise from the predicted flat analcime-jadeite boundary. There is some evidence that jadeite is formed in a moderately low temperature environment. (e.g. Yoder and Chesterman, 1951; Coleman, 1954), with hydrous minerals. The formation of low temperature jadeite presents no problems if the total pressure in the environment is much greater than the partial pressure of water, but in the glaucophane schists of California, jadeite is associated with lawsonite, a mineral which, judging from present data of one of the authors (W.S.F.), requires a considerable partial pressure

of water to form. (A limited number of experiments indicate pressures greater than 5000 bars at 400°C.) Also lawsonite is unusual in that its molar volume is similar to that of anorthite so that differential pressure has little influence on the lawsonite-feldspar equilibrium. Thus high water pressures may exist in the region where jadeite forms in association with lawsonite. If the Griggs-Kennedy boundary was correct, the depth of burial required in a low temperature environment, where water and load pressures are equal, would be so great as to suggest that jadeite could not form in this region. But the predicted curve would possibly be attained in regions of lowest thermal gradients (see Birch, 1955), where at 30 kilometers the temperature might be less than 300°C.

All these remarks require experimental confirmation, particularly in view of possible effects of solid solutions. In general these will lower pressures necessary for the formation of impure jadeite.

References

Birch, F., 1955, Physics of the crust: Geol. Soc. America Special Paper, no. 62, p. 101-117.

Coleman, R. G., 1954, Optical and chemical study of jadeite from California: Geol. Soc. America Bull., v. 65, p. 1241 (Abst.).

Dorsey, N. E., 1940, Properties of ordinary water substance: Am. Chem. Soc. Mon. no. 81, Reinhold, New York.

Ellis, A. J., 1958, Ph.D. Thesis: University of Otago, New Zealand.

Fyfe, W. S., Turner, F. J., and Verhoogen, J., 1958 Metamorphic reactions and metamorphic facies: Geol. Soc. America Mem. 73.

Griggs, D. T., and Kennedy, G. C., 1956, A simple apparatus for high pressures and temperatures: Am. Jour. Sci., v. 254, p. 722-735.

Hartwig, W., 1930, Zur strukturbestimmung des analcims: Min. Abs., v. 4, p. 369.

Kelley, K. K., 1949, Contributions to the data on theoretical metallurgy, Part X: U. S. Bur. Mines Bull. no. 476.

Kelley, K. K., Todd, S. S., Orr, R. L., King, E. G., and Bonnickson, K. R., 1953, Thermodynamic properties of sodium-aluminium and potassium-aluminium silicates: U. S. Bur. Mines Rept. Inv. no. 4955.

Kennedy, G. C., 1950, Pressure-volume-temperature relations in water at elevated temperatures and pressures: Am. Jour. Sci., v. 248, p. 540-564.

King, E. G., 1955, Low-temperature heat capacity and entropy at 298.16° K. of analcite: Am. Chem. Soc. Jour., v. 77, p. 2192-2193.

Latimer, W. M., 1951, Methods of estimating the entropy of solid compounds: Am. Chem. Soc. Jour., v. 73, p. 1480-1482.

Robertson, E. C., Birch, F., and Macdonald, G. J. F., 1957, Experimental determination of jadeite stability relations to 25,000 bars: Am. Jour. Sci., v. 255, p. 115-137.

Valpy, G. W., 1958, M.Sc. Thesis: University of Otago, New Zealand.

Yoder, H. S., 1954, Carnegie Institution of Washington Year Book No. 53, p. 121.

Yoder, H. S., and Chesterman, C. W., 1951, Jadeite of San Benito County, California: Calif. Div. Mines, Special Rept., 10-C.

Yoder, H. S., and Weir, C. E., 1955, Carnegie Institution of Washington Year Book No. 54, p. 98.

WILEY BOOKS

RESEARCHES in GEOCHEMISTRY

Edited by PHILIP HAUGE ABELSON, *Carnegie Institution of Washington. With 25 contributors.* This book provides a comprehensive view of current research in geochemistry. Written by authorities in their respective fields, each chapter reviews (briefly) the present status of research in the area of inquiry, describes (in detail) the authors' recent contributions, and contains an extensive selected bibliography. The major contributions in this volume that make it unique in its field include: a description of techniques that have been used to estimate temperatures of formation of numerous ore deposits; dating methods for the study of pre-Cambrian stratigraphy which have already been successfully employed to date events occurring early in the history of the earth; an important contribution to the geothermometry of silicates and carbonates; and the use of tritium which could be very important in determining the water resources of this country, particularly in the arid west.

1959. 511 pages. $11.00.

ATLAS of LITHOFACIES MAPS

By L. L. SLOSS, E. C. DAPPLES, W. C. KRUMBEIN, *all of Northwestern University.* The authors show the distribution, thickness, and lithologic aspects of approximately 150 selected rock and time stratigraphic units (including maps of complete geologic systems) in the United States and Canada. By means of contours and two-color patterns the maps show patterns and thickness of strata, their lithologic aspect, and their surface and subsurface distribution. Based on ten years of research, the book represents a valuable tool in the interpretation of geologic history and the location of mineral deposits related to sedimentary rock.

1959. In press.

Send for examination copies.

JOHN WILEY & SONS, Inc.

440 Fourth Avenue New York 16, N. Y.

VOL. 257 No. 4, 1959

American Journal of Science

APRIL 1959

CONTENTS

Some Mineralogical Equilibria in the System K_2O—Al_2O_3—SiO_2—H_2O
J. Julian Hemley 241

The Magnetic Field in a Primary Meteorite Body .....*John F. Lovering* 271

Petrofabric Study of Conestoga Limestone from Hanover, Pennsylvania
Richard P. Nickelsen and Gerardo W. Gross 276

The System Na_2CO_3—$NaHCO_3$—CO_2—H_2O at Temperatures up to 200°
A. J. Ellis 287

Phase Equilibria in the System Manganese Oxide—SiO_2 in Air
Arnulf Muan 297

The Analcime-Jadeite Phase Boundary: Some Indirect Deductions
W. S. Fyfe and G. W. Valpy 316